Department of Precision and Microsystems Engineering

Membrane fouling: Study on fouling inside an Organ on a Chip

M. Looman

Report no : 2018.014
Coach : Dr. L. Sasso
Professor : Dr. Ir M. Tichem
Specialisation : Micro- and Nano Engineering
Type of report : Thesis work
Date : Monday June 25

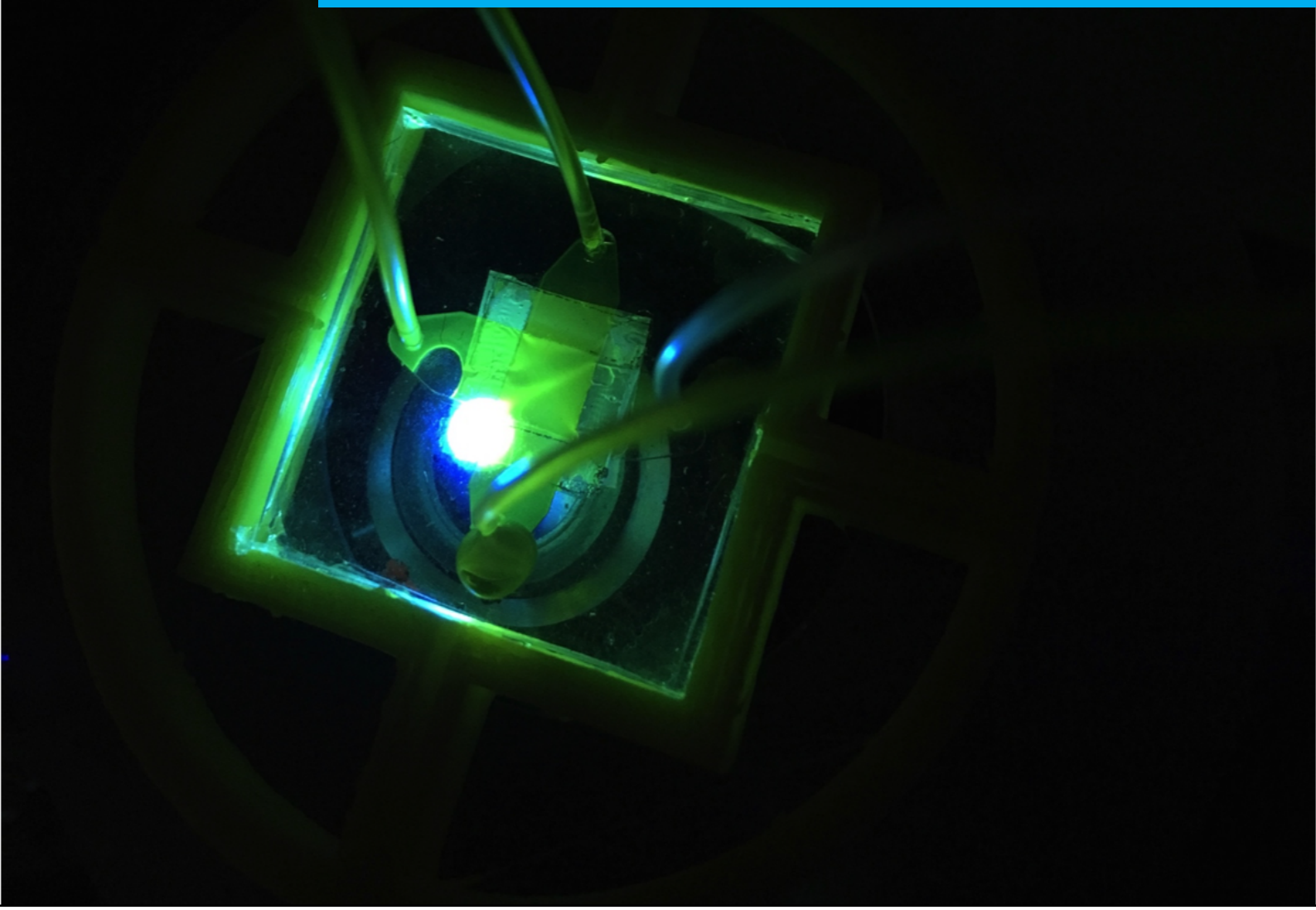

TU Delft Delft University of Technology

Challenge the future

Membrane fouling

Study on fouling inside an Organ on a Chip

by

M. Looman

to obtain the degree of Master of Science
at the Delft University of Technology,
to be defended publicly on Monday July 9, 2018 at 09:30 AM.

Student number: 4154282

Dr. L. Sasso,	TU Delft, Supervisor
Dr. Ir. M. Tichem,	TU Delft, Associate professor
Dr. P. Boukany	TU Delft, External member of the committee

TU Delft

Preface

The main topic in this thesis is the membrane and fouling of this membrane inside an Organ on a Chip (OoC). This thesis work is providing a research that is done within the department of Precision and Microsystems Engineering (PME) with a Micro and Nano Engineering (MNE) specialisation. This thesis report has several goals:

1. Inform about the importance of membrane fouling.
2. Give information about the causes of membrane fouling.
3. Summarize which procedures are undertaken to elongate the life time of a membrane. (State of the Art)
4. Explain the research problem and the approach taken.
5. Provide the results in form of a self-explaining, ready to be submitted paper.
6. Provide detailed information and further discussion on analysis methods.
7. Reflect on the experimental process.

The first Chapter covers point 1 to 4, describing all definitions and the motivation to get to the objective (Section 1.1), explaining the fouling parameters (Section 1.2), providing State of the Art information about the models that are developed in order to understand and predict fouling and the research that is executed to reduce the amount of fouling (Section 1.3) and explaining the planning with milestones and deliverables, accompanied by a risk mitigation. Chapter 2 covers point 5 and includes a paper, describing the main achievements in this research and Chapter 3 gives extra information on the analysis methods and the drawn conclusions. In the end, a Chapter is added which contains a reflection on the experimental process and personal experiences on the research.

During this thesis work, two types of fouling are found to occur during membrane fouling in a static situation. The susceptibility to fouling and dominant mechanisms are dependent on foulant particle and membrane pore size.

The thesis committee consists of Luigi Sasso, my daily supervisor and mentor, Marcel Tichem, associate proffessor within the MNE department; and Pouyan Boukany from the Faculty of Applied Sciences (TNW), which is the external member of the committee.

For all achievements during this thesis work I would first of all like to thank Luigi Sasso and Paola Fanzio for their guiding and stimulation and for having trust in me. Further, I would like to thank Richard Pleeging for his comments and support and Ineke van der Aar for her hugs.

I wish you a lot of pleasure and new insights while reading this thesis work.

M. Looman
Delft, January 2013

Contents

1 Introduction

1.1. Objective

The definition of fouling and the environment in which the membranes are applied are of big importance for the comprehension of the problem. These are explained in this section.

1.1.1. Definition of fouling

Membrane fouling (also known as clogging) is a phenomenon that can be explained in multiple ways. In this report the definition of fouling is formulated as the following:
Membrane fouling is the phenomenon in which solute particles stick in the membrane pores or onto the membrane surface and are not removed by the applied cross-flow, resulting in decline of particles permeating through the membrane.

1.1.2. Application of membranes in Organ on Chip systems

A fundamental form of the OoC system is cell culturing executed in a petri dish (Figure 1.1a). Cells can be grown on the bottom and are fed through the medium that is pipetted into the petri dish. This form of cell culturing enabled researchers to test the effect of medicine or other chemicals on cells without interactions in the human body. More advanced equipment developed for cell culturing incorporates a membrane (Figure 1.1b). This way, a cell can be fed from both top and bottom, approximating an *in vivo* situation.

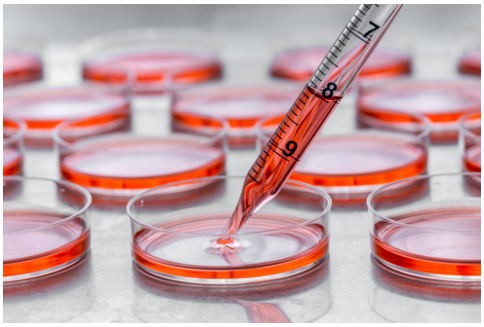

(a) Cell culturing in petri dishes.

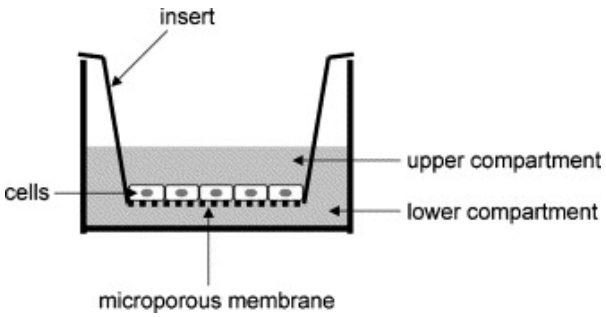

(b) Scheme of transwell membrane system [42].

Figure 1.1: Different cell culturing set-ups.

From the original cell culturing application, a large amount of functionalities is added to reach to the Organ-on-Chip (OoC), which enables studies on organs and tissue *in vitro* and provides fast analysis compared to systems on macro scale due to its small diffusion length. Additional to culturing medium with nutrients, mechanical factors can be applied to achieve conditions comparable to the conditions inside a human body. Figure 1.2a is an example of an OoC in which the membrane is used.

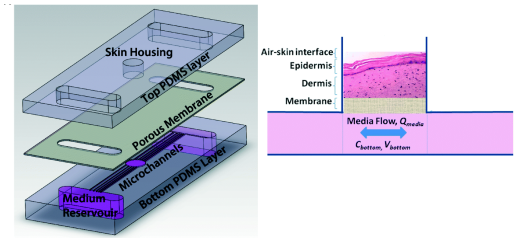

(a) Representation of the microfluidic system and transport model of an HSE-on-a-Chip.

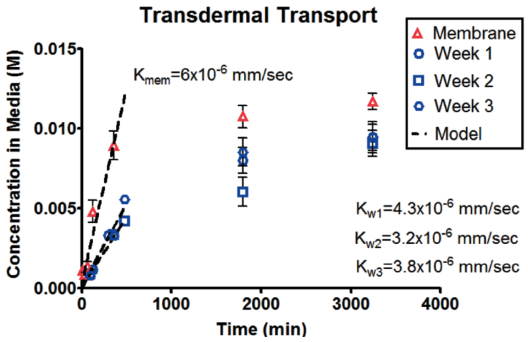

(b) Transdermal transport of FAM-tagged oligonucleotides through HSE-on-a-Chip in comparison to polycarbonate membrane. The overall permeability coefficients, Kp, of the HSEs were estimated using the transport model to evaluate the skin barrier function throughout 3 weeks.

Figure 1.2: Research on a human skin equivalent (HSE) on a chip by Abaci et al. [1].

1.1.3. Motivation

Fouling is a serious problem in cell culturing with membranes. Clogging of the pores results in a lower feed diffusion through the membrane, limiting the efficiency of culturing due to a decrease in cell viability: Research of Abaci et al. shows that as a result of fouling the viability of skin cells decreased to zero after 3 weeks [1]. This is reflected in Figure 1.2b, a graph with measurements of the OoC system that was visible in Figure 1.2a, which shows the permeability of the membrane in the red triangles. The permeability coefficient (slope) decreases and approximates zero.

Therefore it is important to analyse the fouling mechanisms apparent in an OoC system and to explore correlations between fouling and environmental factors in an OoC.

1.2. Membrane fouling parameters

There is a large amount of factors which influence fouling. Table 1.1 shows an oversight of the suspected relations of several factors with fouling. These factors are more elaborately described in the next sections.

Table 1.1: Expected correlation of several factors with fouling

Factor	Correlation with fouling (F)
Cross-flow speed	F ~ 1/V
Temperature	F ~ T
Pressure	F ~ P
Hydrophobicity	F ~ H
Surface roughness	F ~ SR
Pore size	F ~ 1/PS
Surface charge	F ~ SC
Pore tortuosity	F ~ τ
Particle nature	-
Solute size	F ~ SS
Particle concentration	F ~ PC

1.2.1. Hydrodynamics

Fluidic configuration and flow speed have a large effect on the severity of fouling. Zhu [83] defined two structures coupling membranes with a microchannel for gas/water separation; cross flow and dead-end composition, visible in Figure 1.3. When applying a cross-flow, the feed is flowing tangent to the membrane whereas dead end configuration is characterized by a feed flow perpendicular to the membrane.

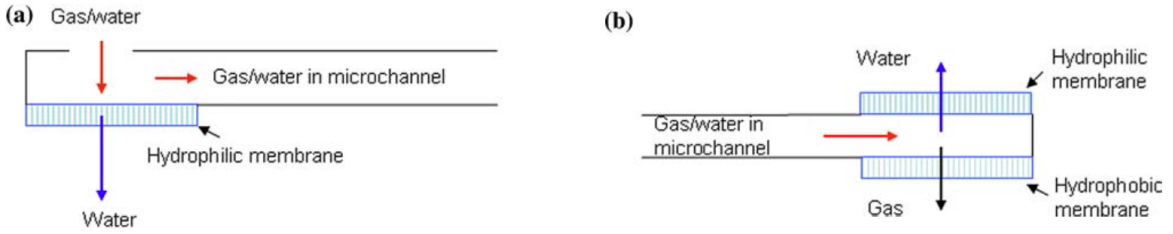

Figure 1.3: Structures coupling membranes with a micro channel for gas/ water separation: (a) the cross-flow mode; (b) the dead-end mode [83]

When particles are loosely attached to the surface of a membrane, a cross-flow configuration is much more effective to remove the particles. A dead-end configuration forces the particles into the membrane, causing more severe fouling. A considerable amount of research is done on fouling of Micro Filtration (MF) membranes [14, 15, 34, 39, 49]. Because filtering is the most effective in dead-end configuration, a lot of research is done in the dead-end field and there is a lack of information for fouling in cross-flow configuration. This is unfortunate as OoCs apply membranes in a cross-flow configuration.

1.2.2. Operating conditions

Temperature Temperature as well as temperature difference over the membrane can have an influence on membrane fouling, because the liquid medium can have a different phase, surface tension, rate of solute and diffusion coefficient at inconstant temperature. Steinhauer et al. study the temperature dependence on protein fouling and conclude that for β-lactoglobulin, fouling is enhanced at temperatures above 30 °C [76]. The temperature range for cell culturing is narrow and around body temperature, so an effect of temperature on fouling must be considered. All predictions and conclusions of this thesis are for a situation at room temperature (20 ± 0.5 °C), but for cell-culturing, an elevated amount of fouling must be considered.

Pressure The trans-membrane pressure difference, which can be associated with the force at particles towards the membrane is playing a role. Loh et al. [54] measures a positive correlation between applied pressure and flux through the membrane, which results in a higher amount of fouling . In the thesis research, the trans-membrane pressure is kept as low as possible.

1.2.3. Membrane properties

Many papers concerning the fouling of membranes with respect to their characteristics have been published [79]. Among them is Singh [72]: "like PS membranes, PVDF membranes have high chemical and thermal stability but are sensitive to fouling" . Singh claims that the reason for this is its hydrophobicity.

Hydrophobicity Hydrophobic membranes do not have the tendency to form a liquid film on their surface. Therefore, hydrophobic particles in the liquid are inclined to attach to the membrane, causing clogging.

Razmjou [64] states that superhydrophobicity could diminish the interaction between the feed water solution and membrane surface, thus reducing fouling tendency. Unfortunately, fouling is not fully removed by a change in hydrophobicity.

Surface roughness Surface roughness is another membrane characteristic claimed to have an effect on membrane fouling. Elimelech et al. [28] claims that colloidal fouling of Reverse Osmosis (RO) membranes is markedly influenced by membrane surface morphology . Lee et al. [50] compare the roughness of four membranes with their clogging behaviour and conclude that roughness is a presumably important influential factor affecting flux decline. Their research also states that membrane clogging is much more heavily occurring at microfiltration than ultrafiltration, which can be associated with roughness.

Pore size Building on the research of Lee et al. [50], it can also be stated that the pore dimensions of a membrane play a big role in fouling. Especially when filtrating with a dead-end composition, pores are easily clogged by particles that are bigger in size than the pore size itself. The combination of membrane pore size and solute size determines the different phases of fouling, which are described more elaborately in Section 1.2.4.

Surface charge Surface charge is a material characteristic which' effect on fouling is not extensively researched. Buonomenna [17] states that fouling depends more on the charge of the compound than on its molecular weight. Boussu [13] claims that both high hydrophobicity and a high surface charge are favourable when preventing membrane fouling. This is, however, highly dependent on the sort of particle in the feed.

Pore tortuosity Pore tortuosity is a factor that indicates the pore length in comparison with the membrane thickness. Pore tortuosity is extremely difficult to measure and therefore must be determined experimentally for each flow regime [27]. Baker [6] characterizes microporous membranes by their tortuosity (τ) and states that tortuous membranes have a higher adsorption rate within the membrane. This is why it is preferred to have a membrane with tortuosity close to 1 when minimizing fouling.

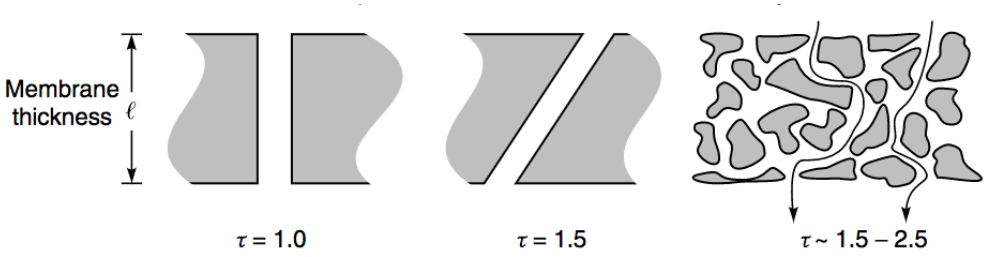

Figure 1.4: Cross-sections of porous membranes of different tortuosity [6].

Nowadays, manufacturers are able to produce membrane with a tortuosity close to 1 by using track-etch production techniques. However, filtration membranes are the most effective when catching particles both at the surface and interior, thus need a high tortuosity, which is difficult to measure. References take the pore tortuosity as a constant factor and use this to calculate the effective porosity $\epsilon_{\text{eff}} = \frac{\epsilon}{\delta\tau}$ with porosity ϵ, tortuosity τ and a constrictivity factor δ.

1.2.4. Feed properties

Fouling is caused by solute particles in the feed that adhere to the membrane. As can be read in the further paragraphs, different fouling behaviours and severities of fouling appear for different combinations of membranes and particles in the feed. The most important feed characteristics are further described.

Particle nature To begin with, the material of the particle or solute is important for fouling. Fouling can be caused by growth of bacteria on the membrane surface, a vast concentration of salt or minerals and the presence of particulate or colloidal species in the process liquid. Each category behaves differently for each membrane. Rana [63] states that humic macromolecules are more favourably adsorbed onto hydrophobic membranes. Qu [62] studies fouling by extracellular organic matter . Esfahani et al. [31] compares the fouling and flux recovering behaviour of Humic Acid (HA) and proteins on a polysulfone membrane and conclude that HA creates a reversible form of fouling when its concentration is enlarged and that proteins create the most severe form of fouling.
Feed culturing medium contains amino acids and proteins to stimulate for cell growth. For research, amino acids (building blocks for proteins) are most often used to graft on membranes with the intention to prevent fouling [70]. Several studies on protein fouling are undertaken [14, 15, 23, 25, 31, 39]. The model protein that is used within these researches is BSA. BSA is found to adhere more to hydrophilic surfaces [43] and to cause irreversible fouling on microfiltration membranes[40]. The effect of DNA, a chain of proteins, on fouling is researched under the name of biofouling [84]. The effects of DNA specifically on fouling are not found.

Particle size A change in fouling behaviour of solute particles is experienced with a changing particle size. Lee et al. [50] states that particle shape and size are presumably important parameters effecting fouling. Solute particle sizes (r_s) which are small compared to the pore size (r_p) tend to cause pore narrowing inside the pores, while solute with a relatively large r_s tend to form a 'cake layer' which is a less harmful way of clogging and can often be rinsed away [68].

As becomes clear in Figure 1.5, the different types of clogging correspond to the ratio r_s/r_p. Complete blocking occurs when a particle is blocking some pore or pores with no superposition of particles. Standard

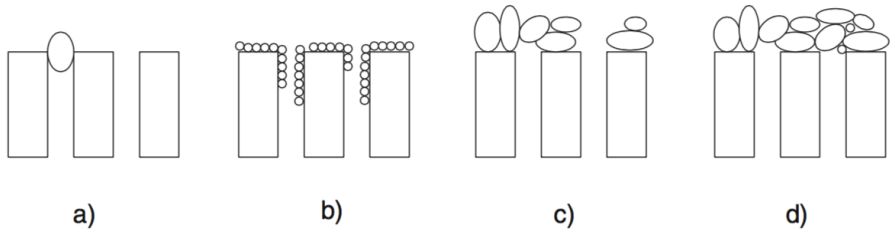

Figure 1.5: Different types of clogging initiated by different particle sizes. a, complete blocking. b, standard blocking. c, intermediate blocking. d, cake filtration[68].

blocking happens when a particle is deposited onto the internal pore walls leading to a decrease in pore volume. Intermediate blocking takes place when each particle settles on another particle previously arrived or directly blocks some pores. Cake filtration is the end phase in which each particle locates on others already arrived and already blocking some pores.

In Table 1.2 the four types of fouling are ordered with corresponding r_s/r_p ratio and severity.

Table 1.2: The four types of fouling with corresponding r_s/r_p ratio and severity.

Fouling type	$\mathbf{r_s/r_p}$	**severity of fouling**
Standard blocking	$\ll 1$	Very high
Complete blocking	1	Medium
Intermediate blocking	> 1	Low
Cake layer filtration	end phase	Very low

Research on particle size is done, but a relation between fouling with amino acids, proteins and DNA - which are built out of the same components but deviate in molecular weight- is not found. The combination of dependency of fouling on both molecular size and pore size is therefore a suitable research topic.

Particle concentration Particle concentration does also play a great role on pore clogging. The higher the concentration of particles in the liquid, the higher the risk on clogging. Khayet and Mengual [46] describe the effect of salt concentration when executing membrane distillation with humic acid. As explained in Section 1.2.4 some particles form bigger chains when being at higher concentrations and cause a different type of fouling.

1.3. State of the Art

As membrane fouling is frequently experienced, research is done to characterize, model and prevent it. This chapter contains information on all the named topics respectively.

1.3.1. Characterization/detection of fouling

In literature, membrane fouling analysis is executed on two elements of the system: The membrane itself and the outgoing feed.

Analysis on membrane only There are a lot of methods to analyse the membrane. The membrane is used to analyse the location of the fouling and the amount of particles. This is done with Scanning Electron Microscopy (SEM) [19, 20] (ESEM), optical microscopy [20], Fourier transform infrared Spectroscopy (FTIR) [20], Attenuated total reflection spectroscopy (ATR) [20] and many more. A method that is frequently used in the last years is confocal scanning laser microscopy (CSLM) [32]. With this method of analysis, 3D imaging can be done and one can look at multiple layers of the membrane and fouling inside pores.

SEM Morphological characterisation of fouling is often done using SEM. SEM is able to image the surface of a membrane and the size of the pores. Brink et al. [15] use the SEM to successfully image the decrease in pore size and inner pore accumulation of particles of track etched membranes . Cho and Fane image a change in porosity and structure after 17 and 42 hours of filtering with a biomass solution [18].

Table 1.3: Values for α and β determined by [14]

	α	β
Complete blocking	$K_A u_0$	2
Standard blocking	$(2K_B/A_0^{1/2})u_0^{1/2}$	3/2
Intermediate blocking	K_A/A_0	1
Cake filtration	$(R_r K_C/A_0^2)u_0^{-1}$	0

Analysis *in situ* The most commonly used method to analyse membrane fouling with feed is to apply the feed with a certain pressure and record the amount of feed permeating through the membrane. This is done with a weighing scale by Bowen et al. [14] or can be done with flow meters [19]. These methods are used to analyse permeate flow, but in the OoC this flow will be minimal, so another way of measuring must be chosen for determining the diffusion of feed particles through the membrane.

1.3.2. Models made to predict fouling

Research is done to become aware of variables influencing fouling [13, 61, 69, 78] and to predict different fouling mechanisms [14]. Loh et al. [54] divides the factors of fouling in a table with categories (Figure 1.6).

IMPACT FACTOR	MEMBRANE	PROTEIN	OPERATING CONDITIONS
ELECTROSTATIC INTERACTIONS	**surface chemistry**	**pI**, sequence	**pH**, ionic strength
HYDROPHOBIC INTERACTIONS	**surface chemistry**	**hydrophobicity parameter**	temperature
MECHANISM/ RATE OF FOULING	**porosity, morphology**	MW, structure, conformational flexibility	**concentration,** pressure velocity, **process volume**

Figure 1.6: Correspondence of membrane properties, protein properties, and operating conditions on the impacts to protein–membrane interactions and mechanisms and rates of fouling. Properties and operating conditions in bold indicate those that were manipulated purposefully in the study of Loh.[54]

As described in Section 1.2.4, the relation between particle/solute size r_s and membrane pore size r_p is of great influence on the existing fouling mechanisms. In 1995 Bowen et al. [14] described fouling, using the 4 fouling mechanisms. With the characteristic equation he defined for the fouling mechanisms (Equation 1.1), it is possible to analyse the dominating fouling mechanism.

$$\frac{d^2t}{dV^2} = \alpha\left(\frac{dt}{dV}\right)^{\beta} \tag{1.1}$$

In this equation, V is the total permeate volume and t is time. The values of α and β are determined by Bowen et al. and shown in Table 1.3.

In this Table u_0 is the initial mean velocity of the fluid through the membrane, which can be derived from the initial flux through the membrane. A_0 is the area of the clean membrane and K_A, K_B and K_C are constant factors indicating the blocked surface area of the membrane per unit of permeate volume, decrease in the cross section area of the pores per unit of permeate volume and area of the cake per unit of permeate volume respectively. Further, R_r is the ratio of the cake resistance over the clean membrane resistance.

Using the table and the characteristic equations, an integral analysis can be done to determine the fouling mechanism and K and R values experimentally (Figure 1.7).

More extensive models to describe fouling are developed by Bolton [12] who incorporates the effects of adsorption of material into the membrane and is able to predict both flow rate with constant pressure and pressure with a constant flow rate due to fouling. Just as Bolton, many researchers describe the factors affecting fouling for filtering objectives. The dead end configuration is therefore the most common point of view. Cell culturing is done with a cross-flow configuration, in which the fouling mechanism is slightly different. Field et al. [33] reformulate the characteristic equations which makes it directly applicable to permeating flux (Equation 1.2 and 1.3) and expand the existing models for membrane fouling to fit both fouling in cross-flow and dead end configuration.

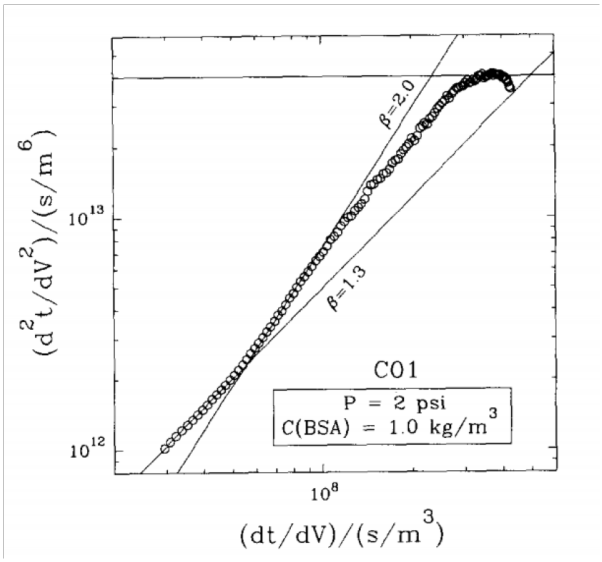

Figure 1.7: d^2t/dV^2 versus dt/dV curves for an applied pressure of 2 psi, a 1.0 kg/m3 solution of BSA and the C01 membrane. Some values of β are shown [14].

$$-\frac{dJ}{dt} = K_\beta A^{2-\beta} J^{3-\beta} \tag{1.2}$$

$$J = J_0 \cdot (1 + K_n \cdot (2-n)(A \cdot J_0)^{(2-n)} \cdot t)^{\frac{1}{n-2}} \tag{1.3}$$

The equations created by Field et al. include the effect of transversal flow delivering shear stress on the fouling, resulting in fouling removal. If there is fouling removal, the equations stated below apply.

$$-\frac{dJ}{dt} = K_\beta (J - J_{s\beta}) \cdot J^{2-\beta} \tag{1.4}$$

This first equation introduces J_s, which is the flux at long/infinite time. J_s is dependent on the shear stress when intermediate blocking and cake filtration apply, for $\beta = 0$ and $\beta = 1$.

$$J \longrightarrow J_{s2} = \frac{C_2^+ \tau \epsilon_0}{J_0 2\sigma} [\sqrt{1 + 4\sigma J_0^2/(C_2^+ \tau \epsilon_0)} - 1] \tag{1.5}$$

$$J_{s1} = J_1^* = \sqrt{C_1^+ \tau/\sigma} \tag{1.6}$$

$$J_{s0} = J_0^* = \sqrt{C_0^+ \tau/k_c} \tag{1.7}$$

$$-\frac{dJ}{dt} = \frac{J_0 \sigma}{\epsilon_0} [J^2 + \frac{C_1^+ \tau \epsilon_0}{J_0 \sigma} \cdot J - \frac{C_1^+ \tau \epsilon_0}{\sigma}] \cdot J^{-1} \tag{1.8}$$

As can be seen in the equations, fouling is assumed to be dependent on initial volumetric flux through the membrane J_0 , constants in original cross-flow fouling equation C_n, shear stress at the membrane surface τ, fractional free area at membrane surface ϵ_0, area blocked per unit passage of filtrate σ and another constant in a cross-flow fouling equation κ_c.

1.3.3. Use of cross-flow to prevent fouling

The equations defined in the last section assume that the shear stress caused by a cross-flow is creating a decrease in fouling. The effect of cross flow velocity on fouling is studied by several references [20] [21].

Figure 1.8 shows that the resistance due to reversible fouling (R_{rf}) created by intermediate blocking and cake filtration is decreasing with increasing cross-flow velocity. This is an interesting test result, but as OoC systems only incorporate relatively low flow rates, cross-flow velocities in the order of 1 m/s will not be reached.

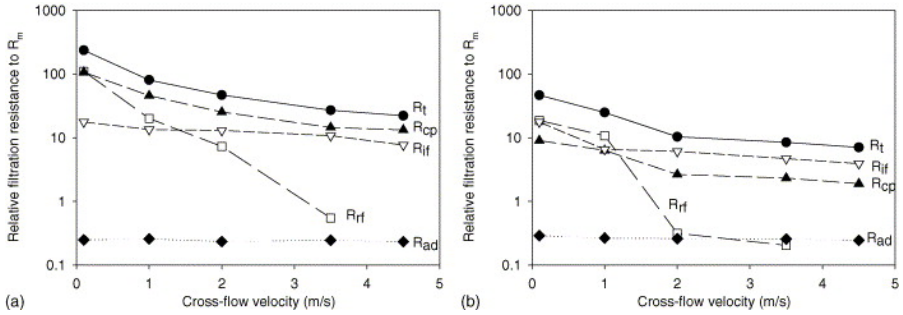

Figure 1.8: Various filtration resistances after 4 h of filtration at different cross-flow velocities [21] (a) Micro Filtration (MF). (b) Ultra Filtration (UF) .

1.3.4. Surface treatments of membranes to prevent fouling

In order to reduce the interaction of commercially available membranes with possible foulants, the surface chemistry of the membrane can be modified. This is done through surface grafting with hydrophilic polymers, amino groups, zwitterionic polymers and surface plasma treatments.
Because different solvents in the feed respond differently to each surface chemistry, surface treatment is an extensively researched topic. Next paragraphs give an insight in the different membrane treatments that are commonly used to improve fouling behaviour.

Addition of hydrophilic polymers Reduction of fouling through the addition of hydrophilic polymers is first done in the 1970's and since then has been of high interest. One of the first researchers on this topic, Shimomura [71], finds that the water flux and salt rejection improves highly when executing a surface plasma treatment on PAN films. Buonomenna et al. [17] attain rejection of positively charged particles by introducing amino groups to the surface.

Hashim et al. [37] add PVDF-g-PEGMA to a PVDF membrane to accomplish a 100% fouling recovery rate, but do not accomplish the fouling itself to reduce. Other researchers do accomplish fouling rejection: Kang and Asatekin[5, 45] use the addition of PAN-g-PEO molecules to a PAN porous membrane to reduce fouling and Koh et al. [48] add P(VDF-co-CTFE)-g-POEM to PVDF membranes and accomplish full BSA rejection. The last three researchers state that the improved fouling conditions are only obtained within a certain concentration range of the additives.

Li et al. and Zhao et al.[51, 82] use zwitterionic copolymers (PVDF-g-PSBMA) and (MPDSAH) respectively to increase the surface hydrophilicity of commercial membranes and find an improvement in fouling behaviour. Balta et al. [7] increase the hydrophilicity of a PES membrane with ZnO nanoparticles and find an increasing rejection performance for an increasing nano particle concentration. Liu [52] grafts the copolymer PVDF-g-PACMO on a PVDF surface and reaches a better antifouling performance and a higher fouling rejection rate. For these researches, no maximum concentration of zwitterionic copolymers or ZnO nanoparticles is found.

Very little research is done on anti-fouling membrane modification of polycarbonate (PC) membranes. This can be because most of the materials tested are more hydrophobic and therefore need an anti-fouling treatment.

1.3.5. Production of anti-fouling membranes

Prevention of fouling is not only done by adjustments on existing membranes, but also by producing new, anti-fouling membranes. Bengani et al. [8] produce a fouling resistant membrane through self-assembly of zwitterionic groups, whereas Wang et al.[80] use surface layer-by-layer assembly to create a thin film composite membrane with a low contact angle and salt rejection of 99.5%. Noteworthy is that the membranes described are not physically but chemically improved to decrease fouling.

1.3.6. Processes to recover the membrane from fouling (Life time expansion)

Next to fouling prevention, fouling and flow rate recovery is a frequently researched topic. The next paragraphs describe forms of cleaning that are implemented to expand the life time of membranes.

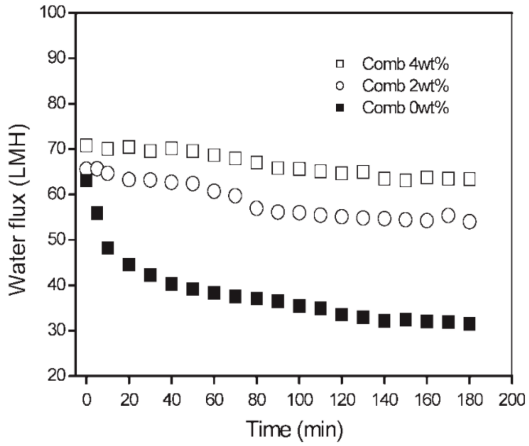

Figure 1.9: Flux of PVDF membranes with different concentrations of P(VDF-co-CTFE)-g-POEM comb polymer. [48]

Physical cleaning Physical cleaning is the most easy accessible form of cleaning and can be done in multiple ways. Back-flushing in which the flow is reversed, is mainly used for applications incorporating a dead-end flow. Further, some researchers apply a flow with bubbles to diminish fouling. Mi and Elimelech [58] analyse different cross-flow cleaning treatments and conclude that cleaning with deionized (DI) water and bubbles is one of the possible ways to remove 100% of organic (Sodium Algenate) fouling .

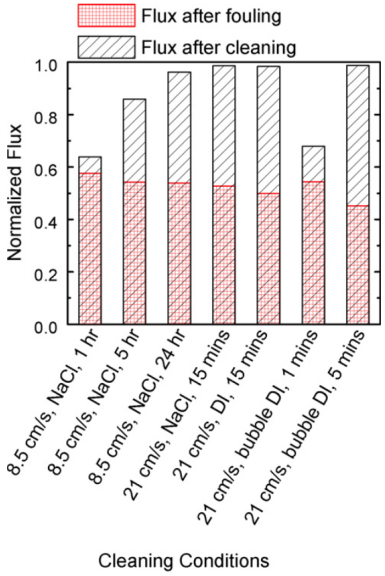

Figure 1.10: Cleaning efficiency of alginate-fouled FO membranes at various cleaning conditions [58].

Chemical cleaning Ang et al. [4] perform an analysis to rate chemical cleaning in a cross-flow configuration with NaOH (pH 11), SDS, and EDTA. The maximum cleaning efficiency (100%) is reached with a 2 mM solution of EDTA when cleaning a SRNOM fouled membrane for one hour. According to Ang et al. NaOH is not reactive enough with Ca^{+} to thoroughly clean a fouled membrane. Ang et al. also state that the cross-flow velocity applied during the cleaning cycle is influencing its efficiency, but the flow has to be combined with a chemical to react and break bonds with the rest of the fouling layer. Bio-compatibility after cleaning is not taken into account by Ang et al.

Membrane modifications to maximize cleaning effectivity Several surface treatments that are done to decrease fouling are also usable for cleaning objectives [8, 37, 45, 51, 52]. Furthermore, researches are done to

Table 1.4: Surface treatments for membranes used in research

Material	Treatment	Solute particle	Reference	Salt rejection	Flux decline	Flux recovery	Relative flux
PAN	Surface plasma treatment	NaCl	[71]	98%			
PAN	Surface coating with PAN-g-PEO	BSA, molecular dies	[5]		15% over 24h (BSA)		
PVDF	Addition of PVDF-g-PEGMA	BSA (model protein)	[37]	66% (BSA)	10% over 0.5h	100%	
PVDF	Addition of P(VDF-co-CTFE)-g-POEM	BSA	[48]		11% over 3h		
PVDF	Addition of PVDF-g-PSBMA	BSA	[51]		44.5% over 2.5h	81%	55.5% over 2.5h
PVDF	Adittion of amino groups	Methylene blue Congo red	[17]	100 %			 95% (Congo red)
PAN	Surface coating with PAN-g-PEO	BSA	[45]	20 %		100% (with NaCl)	
PES	Enhancement of membranes using ZnO nanoparticles	HA, molecular dies	[7]		12% over 24 h (HA)		
PVDF	Grafting of PVDF with PVDF-g-PACMO	BSA	[52]		11% over 1h	89%	
PP	grafting zwitterionic polymer (MPDSAH)	BSA	[82]		54% over 2h	90%	
PTFE	Synthesis of PMMA-r-SBMA and PAN-r-SBMA copolymers	Vitamins Several dies	[8]		4% over 50h	99% (with DI water)	
PES	Surface modificating molecules	Different molecular weights	[59]		65% over 140h		
Polyamide	Layer by layer assembly of poly acrylic acid and potent anti-microbial agent to- bramycin	BSA, Ecoli, bacteria sodium alginate solution	[80]	99.5%	35% over 5h		
PSF	cross-linked PVCL-co-PSF copolymer (smart membrane)	HA BSA	[73] [73]		63% over 2h 78% over 2h	95% 93%	

increase the flux recovery of fouled membranes. Xie [81] uses the adsorption of Tween 20 onto a propylene microporous membrane to improve the recovery of membranes with respect to fouling. After adsorption of Tween 20 on the surface, foulants are easily removed with 5% NaOH and 0.05%NaClO washing.

Smart gating membranes for self-cleaning Recent research points out the great amount of possibilities created with smart gating membranes. Smart gating membranes with tunable surface properties create opportunities to achieve self-cleaning functionality for reducing membrane fouling while retaining the permeability. Upon adding a stimulus, the shrunken and hydrophobic gates become swollen and hydrophilic; such transitions weaken the interactions between the foulant and membrane surface for foulant detachment [53]. This process is visualised by Liu et al.[53] in Figure 1.11

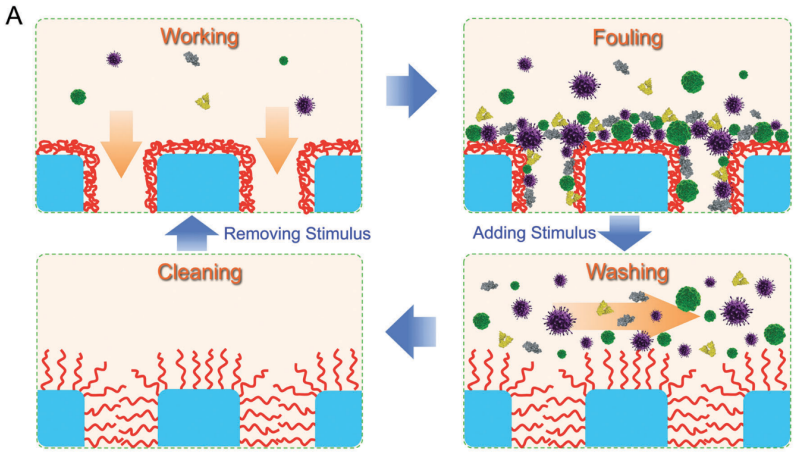

Figure 1.11: Schematic illustration of the self-cleaning principle with smart gating membranes through easily adding/removing a simple environmental stimulus, e.g., temperature decrease for PNIPAM gates [53].

The possibility for cell culturing on smart gating membranes, however, is not researched yet. Table 1.4 contains information on several treatments that are tested to prevent fouling. As can be seen, no surface treatments are executed on Polycarbonate (PC), a material that is often used for membranes in OoC's.

1.4. Relevance of State of the Art membrane fouling research on this project

1.4.1. Models

Most of the research on membrane fouling is focused on the field of filtering systems and bioreactors. From the models created by Field et al. [33], fouling inside a cross-flow filtering system is easily predicted. The models made for filtering systems cannot be used in this thesis work because the liquid flux in OoCs is assumed zero. However, whenever a decrease in particle flux appears, the fouling mechanisms can be compared and

Table 1.5: Test variables used in the thesis

Part	Variable	Value
Membrane	Pore size [μ]	0.4 1 3 5
Feed	Molecular Weight [Da]	$\sim 10^2$ (Glycine) $\sim 10^4$ (BSA) $\sim 10^7$ (λ-DNA)

the share of the dominant mechanisms in the diffusion decrease can be compared with the share of each fouling mechanism in liquid flux decrease seen in the State of the Art.

1.4.2. Fouling in membranes

Knowledge on every possible factor playing a role in fouling in microfiltration is researched. Because the flow rates used are much lower, the prevailing way of particle transport is most likely diffusion and therefore the fouling effect is expected to be less severe. However, the influence of each factor described in Chapter 1.2 is expected to be similar. This research validates the similarities between fouling behaviour inside filtering systems and the OoC.

1.4.3. Fouling reduction

Much effort is done to reduce membrane fouling. An implementation that is effective in preventing fouling is applying a surface treatment to decrease interactions of membrane and particles in the feed. In OoC systems a membrane surface treatment could inhibit cell attachment to the membrane which can lead to a lower cell viability. Because the time span of this research does not allow to test for both cell attachment and anti-fouling behaviour for new surface treatments next to the exploration of applicant fouling mechanisms, this research focuses only on the observation of fouling on commercial membranes.

The configuration of the OoC has similarities to filtering systems with a cross-flow configuration (Figure 1.3a), due to the fluidic flow direction parallel to the membrane. In filtering systems, a high cross-flow has the ability to remove cake layer fouling. A possible next step, which is not reached in this research, is to study this for OoC systems within the range of flow rates used for OoC systems.

1.4.4. Analysis methods

An imaging method that is frequently used in the State of the Art to envision fouling mechanisms is the SEM. The SEM is also used in this research to distinguish dominant fouling mechanisms on fouled membranes. The dynamic analysis done on filtering systems cannot be used in this work. Either flow meters or weighing scales would perceive a minimal, probably unmeasurable effect of differences in particle concentration.

1.5. Research and Planning

The topics described in the preceding sections are of big importance when defining a research plan. The thesis must have an added value and therefore next sections explain the research goal and conclude with a research plan and milestones.

1.5.1. Research goal

This research is focused on recognising fouling mechanisms appearing in the OoC with use of the fouling mechanisms distinguished during fouling studies of a filtering system (Section 1.3.2). As the fouling mechanisms appear for different rates of r_s/r_p, the tests are done for membranes with different pore sizes and feed in different solute particle sizes. Table 1.5 shows an overview of the variables chosen for the test.

The major part of human cells has a size between 10 and 15 μm, so membranes with pore size smaller than 10 μm are chosen. Polycarbonate (PC) membranes with pore sizes ranging from 0.2 to 8 μm are the most commonly used for cell culturing, so these are used as a standard for the tests.

A standard feed for cell culture is Dulbecco's Modified Eagle's Medium (DMEM), which contains amino acids, vitamins, inorganic salts, glucose and phenol red. All of these components can behave differently in the fouling process. Out of these components amino acids are chosen to be studied. Because studies need to be done on increasing particle size, the amino acid Glycine, the model protein BSA and λ-DNA, all consistent out of the same components, but with increasing size are chosen for the experiments. Because BSA was not obtainable with a fluorescein(FITC) label, Ovalbumin, which is very similar to BSA [56, 77], is used as a substitute.

During this research it is important to analyse the fouling mechanisms apparent in a semi-static situation and to explore the correlations between fouling with pore size and feed size.

1.5.2. Approach

Two ways of analysis will take place during this thesis: a static fouling analysis in which the fouling mechanism is studied and a dynamic fouling analysis in which the decrease in particle diffusion is recorded.

Static fouling During the qualitative tests a 1 µl droplet of deionized water is pipetted into a petri dish. Then, the membrane is placed onto the droplet and a 1 µl droplet of tested feed is deposited onto the membrane. Reference membranes are immersed in water without feed particles. The membranes are removed after immersion for one hour, one day and one week and are then dried for two days. The whole procedure is illustrated in Figure 1.12 and the protocol used is in Appendix C.

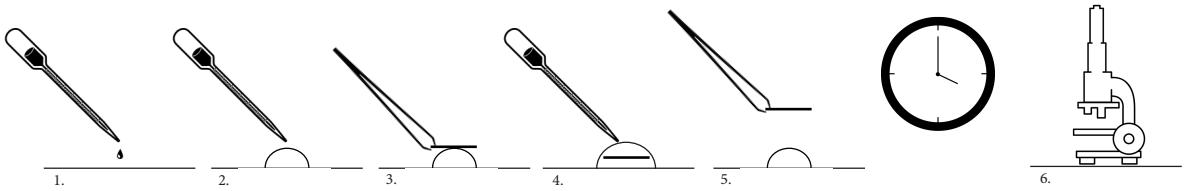

Figure 1.12: Illustrations of the static fouling test.

The membranes are imaged with the SEM, compared in order to validate which kind of fouling is dominating, processed with Fiji to distinguish the remaining pore size and amount of pores and analysed for relations between pore size and feed size with fouling. Image processing with Fiji is explained in Chapter 3.1.2.

Dynamic fouling During the dynamic fouling analysis, the two fluorescent labeled feed materials, Glycine and BSA, are analysed for fouling over different membranes. The dynamic fouling analysis is done to determine the amount diffusion through the membrane in the same configuration as in an OoC system. The change in diffusion of particles indicates the amount of fouling. A microfluidic flow cell is produced to facilitate measurements on two channels in contact through a membrane (Figure 1.13). The top channel is used to inject the fluorescent feed particle and the bottom channel is used for measurements. Optical transparency of PDMS allows to visually analyse the path of the feed and amount of particles diffusing through the membrane. The concentration of particles in the measurement channel is measured at time intervals of 30 seconds to 2 minutes at the measurement area indicated in Figure 1.13.

Measurements are done with an inverted fluorescence microscope of Zeiss with a 38HE filter. The light emission of the particles is measured over an area set by the frame at a measuring point just after the membrane. Light intensities measured by the microscope, are converted to values for the concentration of particles at the measurement area and are processed to calculate the amount of fouling on the membrane.

Production of the test device A microfluidic flow cell is designed and produced to execute dynamic fouling experiments. To facilitate two channels separated by a membrane, the flow cell is built up out of two PDMS layers, clamping a membrane with help of adhesive layers. The production process is visualised in Figure 1.13a. The PDMS layers are produced by replication molding, which enables fast and 'medium scale' production. Schematic drawings of the molds including dimensions are shown in Appendix B. A HTM140 mold is produced with a high resolution 3D printer. Then PDMS and its curing agent are mixed at 10:1 and

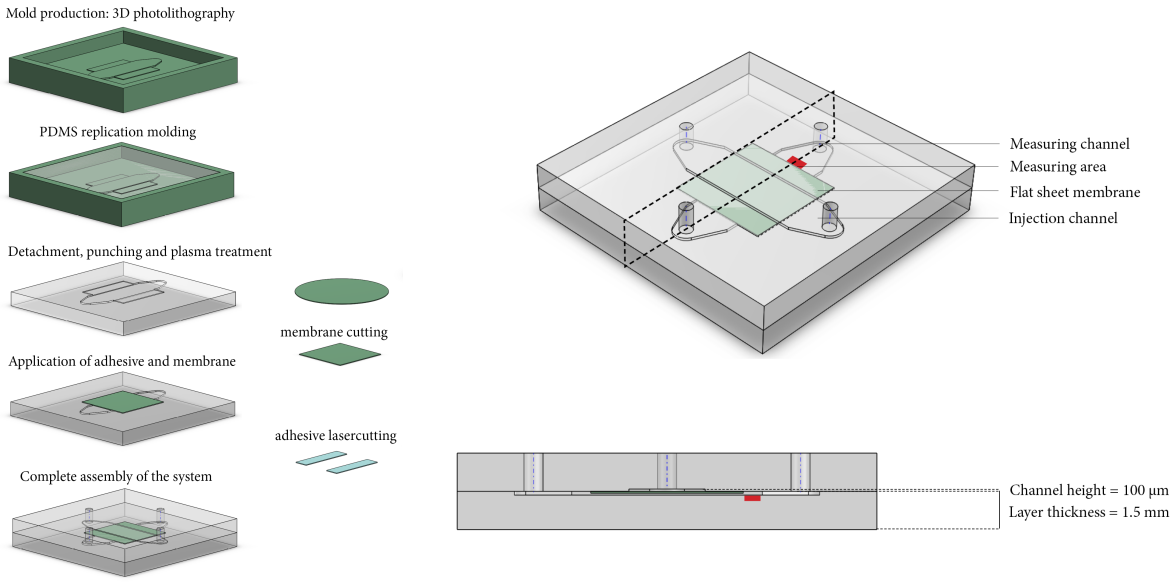

(a) Production process

(b) 3D-view and main functionalities

Figure 1.13: Schematic illustration of the inverted microscope compatible microfluidic flow cell.

the PDMS is baked at 70 °C for 1 hour. After detaching the PDMS from the mold, holes are punched to create in- and outlets in the device. Optimal settings are researched to bond the PDMS layers with air plasma. This way, the PDMS, which is naturally hydrophobic, is made more hydrophilic and is less prone to fouling [11] and gas nucleation [65]. A detailed description and protocol for every production step can be found in Appendix C and the optimization of the bonding protocol is described in Appendix E.

1.5.3. Planning

The goals of this thesis must be achieved within a defined amount of time, stated in ECTs: 35. This results in a narrow time frame and a tight planning for the research. The planning that is followed to execute this research is visible in the Gantt chart with deliverables and milestones in Figure 1.14. For each phase a risk mitigation is composed.

Preparation During the preparation, trainings are done for the devices used during the thesis, components are ordered for the production. One big risk during this phase is that delivery times may be long (Table 1.6). Therefore the ordering is done in two phases in which first components for the microfluidic device are ordered and later components for analyses. The preparation phase is built in to prevent long waiting periods when the research is started.

Table 1.6: Risk mitigation of the preparation

Risk	Mitigation
Long delivery times	Order in batches
Waiting time for a training	Plan in advance

Flow cell production The flow cell production consists of the design and dimensioning in SolidWorks and the production of the device as a whole. Flow cell production is a very time consuming phase as optimized production settings need to be determined. The risks involved in flow cell production and a mitigation are summed in Table 1.7.

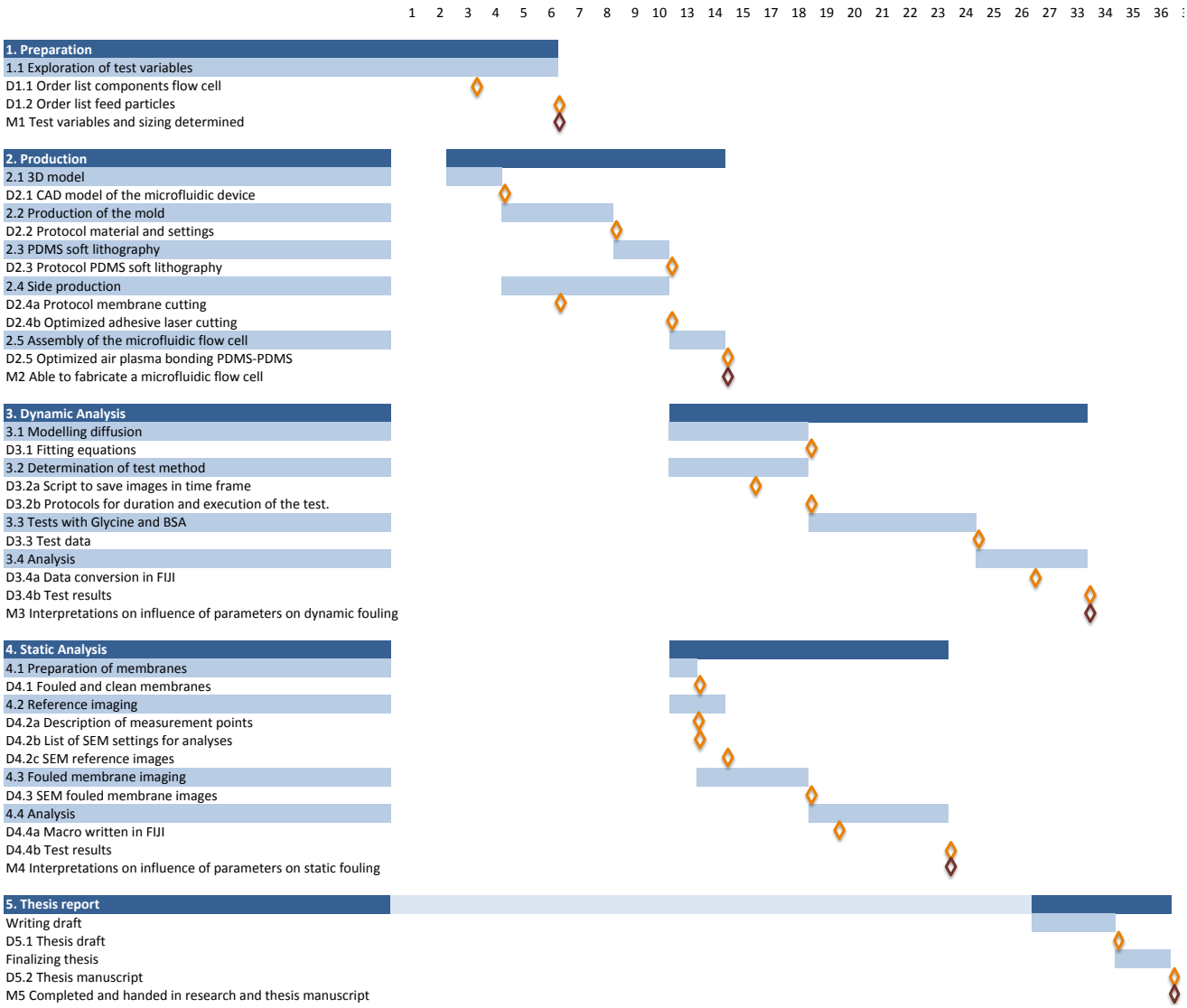

Figure 1.14: Gantt chart followed during the thesis.

Table 1.7: Risk mitigation of the flow cell production

Risk	**Mitigation**
Bubbles inside the mold	Degas HTM140 before use
	Pipet bubbles out of the resin
Bubbles inside the PDMS	Degas for a longer period
Membrane does not stick well	Other adhesive (e.g. UV curable [60])
	Change fluidic chip design
Channels collapse	Change dimensions

Dynamic analysis During the dynamic analysis, modelling is done and the flow cell produced is tested. Figure 1.14 shows an overlap for the production and dynamic analysis. Due to leakages in the microfluidic device during the pilot tests, adjustments in the production needed to be done. Therefore, the most important perceived risk is a leakage in the flow cell (Table 1.8).

Table 1.8: Risk mitigation of dynamic analysis

Risk	Mitigation
Modelling time consuming	Make assumptions
Leakages within flow cell	Back to Milestone 2
Bubbles inside test system	Degas fluids before use
Long duration of experiments	Only test the most important selection of the test variables
Fouling on PDMS	Coating the PDMS channels (Milestone 2)
	Use other material for flow cell (Milestone 2)
Depth of focus of microscope is exceeded	Change thickness of the PDMS layers
	Use lower magnification (larger depth of focus)
Weak diffusion pattern measured	Use higher concentration of feed

Static analysis The static analysis is providing a fast analysis to distinguish fouling mechanisms in time. Each membrane is immersed in a separate droplet to avoid membranes sticking onto each other. The risks and a mitigation is given in Table. 1.9.

Table 1.9: Risk mitigation

Risk	Mitigation
Membrane ruined after SEM analysis	Cut membrane in 4 pieces in case extra SEM imaging is needed
Fouling is inconstant over the membrane	Measuring at different locations
Outlying data	Execute multiple measurements
High deviation within measurement data	Interpret the results and reason how the deviation is prevented

Thesis report The last phase stated in the planning is the thesis report. Here, all information is gathered and written down. The only risk foreseen here, is a lack of time. Therefore writing is also done in intermediate steps throughout the other phases. As stated in Table 1.10, the first aim is to write down all information and the next step is to improve the writing. This way at least all information is provided.

Table 1.10: Risk mitigation

Risk	Mitigation
Lack of time	First make the structure, then improve writing

2

Paper

The fabrication of a microfluidic flow cell to study and understand fouling by diffusion in microfluidic systems resembling an Organ on a Chip system.

Miranda Looman

Delft, the Netherlands

Abstract

Organ on a Chip (OoC) systems are of high interest through its use for medicine testing in a small time scale without the need for animal testing. Membranes used in OoCs form a base to grow cells on and need to be suitable for cell-attachment and porous. Fouling is the 'Achilles heel' in membrane performance. Research shows that as a result of fouling the viability of the skin cells grown in the chip decreased to zero after 3 weeks. If research on organs is to extend and research on cell- or tissue growth will include longer time spans, the influence of membrane fouling with conditions similar to the OoC is an important factor to understand. In this research a microfluidic flow cell is produced and used to explore fouling within the OoC. Static and dynamic fouling experiments are executed on membranes having pore sizes ranging from 0.4 to 5 μm. Scanning electron microscope (SEM) images indicate that standard blocking and cake layer formation are dominating fouling mechanisms. Membranes with 1 μm pore size are the most susceptible to standard blocking. Further a decrease in pore area of 0%, 11% and 20% and a decrease in uncovered amount of pores of 27%, 34% and 80% for Glycine, BSA and λ-DNA respectively are measured after one week of fouling. Cake layer formation is seen after fouling for a shorter duration for BSA (one day) than for Glycine (one hour) and a higher concentration of BSA particles is permitted through all tested membranes than Glycine, therefore the conclusion is drawn that BSA causes less fouling than Glycine.

Keywords: Membrane, Fouling, Microfluidics, Flow cell, Fabrication, Diffusion
2018 MSC: code, code

1. Introduction

Being able to grow cells *in vitro* provided researchers an opportunity to test for medicines or study diseases without interferences in the human body with low volumes of consumables at relatively low time-scales compared to testing inside the human body. The analysis on living cells gives a more truthful result for the reactions of the human body than non-biological models or animal testing and therefore has been of high interest.

The initial way of cell culturing in petri dishes has evolved to microfluidic chips in which chemical and mechanical stimulae can be applied to mimic organs: the Organ on a Chip (OoC). A big advantage of OoC devices is their compatibility with imaging methods like microscopes so that experiments can be imaged *in situ*.
In the OoC the membrane is an essential component. Membranes are used as a base to grow cells on and therefore need to be bio-compatible, suitable for cell-attachment and porous. Membranes can be equipped with electrodes, enabling them to add stimulae to cells or respond to for instance temperature [1], glucose [2] or UV-light [3], evolving towards so-called 'smart membranes'.

As demonstrated by a considerable amount of research in the field of micro filtration (MF) [4–8] fouling is the 'Achilles heel' in membrane performance. The application of membranes in OoCs adds a new functionality, but besides the knowledge coming from research on fouling in filtering systems, little is known about fouling inside an OoC.

Abaci et al. [9] show a permeability decrease in time for a reference membrane inside a microfluidic chip. Membrane fouling can occur due to several compounds in a cell culturing medium, resulting in a lower feed diffusion through the membrane. This is limiting the efficiency of culturing and decreases cell viability, especially for systems in which compounds are exchanged through the membrane, e.g. a lung, gut or kidney on a chip. The research of Abaci et al. [9] shows that as a result of fouling the viability of the skin cells grown in the chip decreased to zero after 3 weeks. If research on organs is to extend and research on cell- or tissue growth will include longer time spans, the influence of membrane fouling with conditions similar to the OoC is an important factor to understand. Therefore, it is paramount that research must be done on fouling within an OoC system.

1.1. Fouling mechanism theory

Knowledge of the dependence of microfiltration membrane fouling on temperature [10], trans-membrane pressure [11], membrane hydrophobicity [12, 13], surface roughness [14, 15], surface charge [16, 17] , tortuosity [18] and particle nature [19–21], size [15, 22] and concentration [23] is very extensive. However, there is a gap in literature about the influence of these factors on fouling in OoC systems.

Sabia et al. [22] distinguished different fouling mechanisms for fouling in filtration systems that are used during the analysis to distinguish fouling phenomena by diffusion. For fouling by microfiltration certain solute size (r_s)/pore size (r_p) ratios result in different fouling mechanisms, visible in Figure 1.

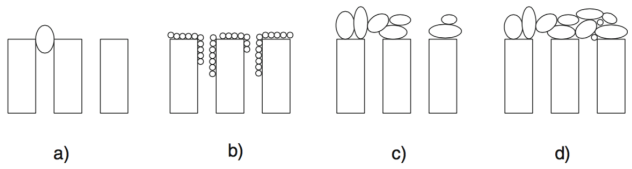

Figure 1: Different types of membrane fouling initiated by different particle sizes. a, complete blocking. b, standard blocking. c, intermediate blocking. d, cake filtration[22].

In Table 1 the four types of fouling are ordered with corresponding r_s/r_p ratio and severity.

Table 1: The four types of fouling with corresponding r_s/r_p ratio and severity.

Fouling type	$\mathbf{r_s/r_p}$	**severity of fouling**
Standard blocking	$\ll 1$	Very high
Complete blocking	1	Medium
Intermediate blocking	> 1	Low
Cake layer filtration	$\gg 1$	Very low

1.2. State of the art

The majority of research on membrane fouling is focused on the fields of filtering systems and bioreactors. Flow cells with cross-flow filtration systems in which solute particles flow parallel to the membrane are comparable to two-channel OoC systems. Research by Zhu et al. [24] points out the differences in fouling with a cross-flow and a dead-end configuration. Cross-flow configurations are proved to cause a lower amount of fouling and in filtering systems, a high cross-flow can even be used to remove cake layer fouling [6]. The models created by Field et al. [25] describe cross-flow fouling. However, research on cross-flow filtering systems assumes a liquid flux through the membrane, which does not apply in an OoC.
A significant amount of research is done to reduce membrane fouling [16, 26–35]. One of the most effective methods of decreasing interactions of membrane and solute particles is the application of a surface treatment. Possible drawbacks of membrane surface treatments in OoC systems is a reduction in cell attachment to the membrane and a decrease in cell viability. Because the time span of this research does not allow to test for cell attachment and anti-fouling behaviour for new surface treatments next to the exploration of applicant fouling mechanisms, this research focuses only on the observation of fouling on commercial membranes.

1.3. Aim of paper

The work described in this paper is aimed to understand fouling by diffusion in microfluidic systems resembling an Organ on a Chip system. Therefore it is important to analyse the fouling mechanisms apparent in a semi-static situation and to explore the correlations between fouling with pore size and feed size.

2. Materials and methods

2.1. Feed particles

Amino acid (Glycine) and protein (Obuvalmin) particles were bought with a Fluorescent FITC label (Thermo Fisher Scientific). Further, unlabelled λ-DNA was bought in a storage buffer of 10 mM Tris-HCl (pH 7.6) and 1 mM EDTA(Thermo Fisher Scientific). During the experiments the feed temperature was maintained at room temperature.

2.1.1. Preparation for analyses

Glycine and Obuvalmin were soluted in deionized (DI) water in a concentration of 10^{-7} [M] at room temperature. The solutions were sonicated for 30 minutes to prevent agglomerations in the solution. λ-DNA was defrosted for an hour in water at room temperature.

2.2. Membranes

Four track-etched polycarbonate membranes were provided by Sigma-Aldrich with different pore sizes ranging from 0.4 to 5 μm.

2.2.1. Preparation for static analysis

During the static analysis, membranes were tested for fouling under static conditions. The four membrane types were prepared in the same manner. Per solute type one membrane was immersed in the solution for a duration of one hour, one day and one week. The membranes were immersed simultaneously to ensure similar operating conditions (e.g. temperature). Of each membrane type a reference membrane was prepared by immersing it in DI water for an hour. The membranes were dried for two days and sputter coated with a 6.5 nm layer of gold.

2.2.2. Preparation for dynamic analysis

Membranes were cut by hand to obtain the measures to fit within a flow cell without leakages.

2.3. Microfluidic flow cell

HTM140 was provided by EnvisionTEC, PDMS (184 Silicone Elastomer) and a curing agent were provided by Down Corning; and a silicone transfer film adhesive between two polyester release liners (ARseal 8026) was provided by AdhesivesResearch.

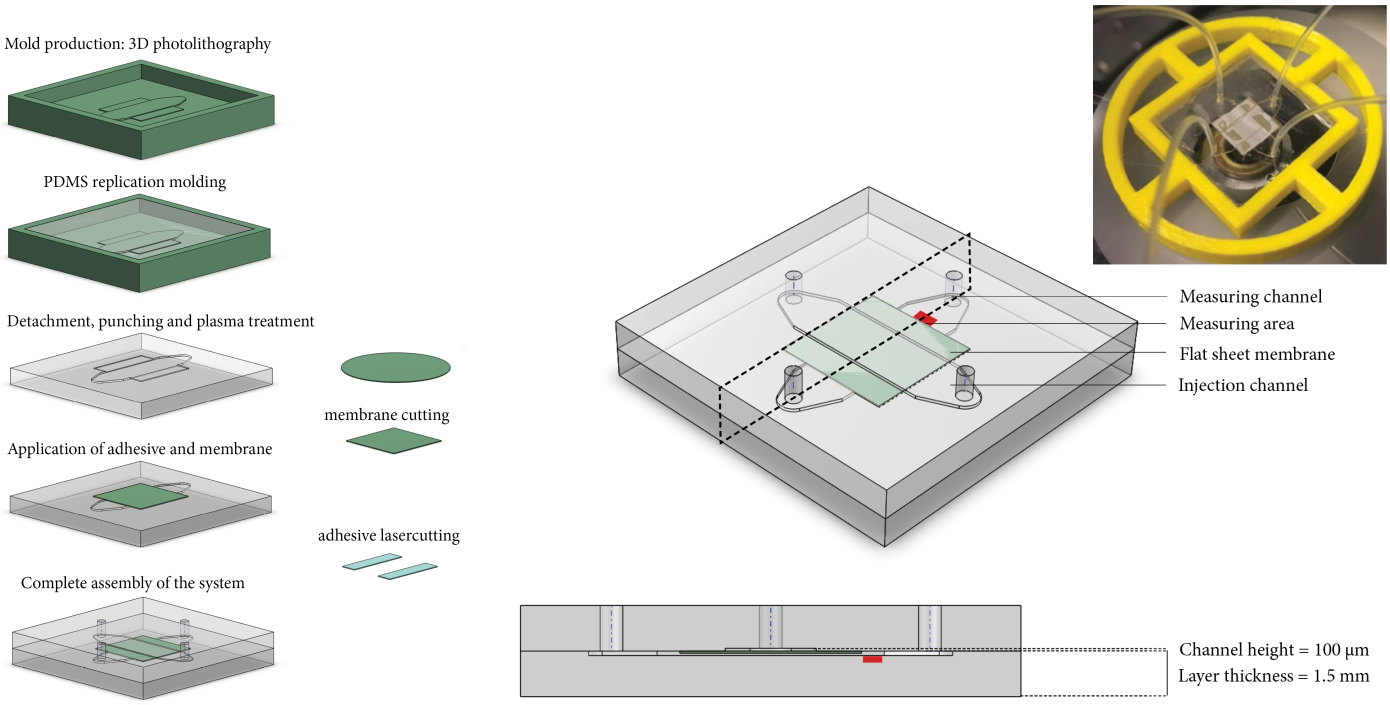

(a) Production process

(b) 3D-view and main functionalities

Figure 2: Schematic illustration and picture of the inverted microscope compatible microfluidic flow cell.

Production. The production flow chart is shown in Figure 2a. Production was done by replication molding, which enables fast and 'medium scale' production. During this process, firstly a HTM140 mold was produced with a high resolution 3D printer (EnvisionTEC). Then PDMS and its curing agent were mixed 10:1 and the PDMS was baked for 1 hour at 70 °C. After detaching the PDMS from the mold, holes were punched with a blunt end needle (64-1869, Warner Instruments) to create in- and outlets in the device. The silicone transfer film adhesive was cut with a laser etching machine (Optec).

The two PDMS layers were bonded with an air plasma treatment (Diener Femto).

2.4. Static membrane fouling studies

2.4.1. Morphological analysis

The prepared membranes were inspected with a scanning electron microscope (SEM) (Jeol JSM-6010LA) using 5-10 kV at magnifications of 1000, 4500 and 10000 and the images were analysed for fouling mechanisms.

2.4.2. Data processing

To be able to draw a well-based conclusion on appearing fouling mechanisms, images taken with the SEM were processed with FIJI and pore area of every pore within the image was measured. The area's and amount of pores were recorded and compared with the reference membrane before determining correlations with pore size and fouling particle. A more extensive description of this analysis is found in Chapter 3.

2.5. Dynamic membrane fouling studies

The microfluidic flow cell in Figure 2b was used to execute dynamic membrane fouling studies. The lower channel of the device was connected to a syringe pump (SP100iZ, World Precision Instruments, Inc.) and injected with DI water for an hour to fill the device and to wet the membrane. Next, the upper channel was connected to the pump to inject the desired feed. The dynamic fouling studies were performed at a constant flow rate of 1 µl/min. The microfluidic flow cell was used in combination with an inverted microscope. The measurement area is indicated with the red mark in Figure 2b. Imaging started at the moment that the fluorescent particles entered the injection channel ($t = 0$). Injection of the fluorescent fluids into the microfluidic system was stopped when an equilibrium was reached or after injecting for 4 hours. After each experiment, the lower measurement channel of the microfluidic device was injected with DI water for several hours.
The dynamic fouling study cycle was repeated 3 to 5 times with one microfluidic device to examine fouling.

2.5.1. Inverted fluorescence microscope

The diffusion of particles through the membrane over time was determined using Fluorescent Inverted Microscopy (Zeiss Axiovert 40 MAT, 50x magnification, Zeiss filterset 38 HE, frame time 200 ms, illuminated with a halogen lamp (Hall100) at 12V). Imaging was done with 30 to 120 seconds intervals at a fixed measuring spot right after the membrane in the measurement channel.

2.5.2. Data processing

The images taken with the fluorescence microscope were assembled for each test and mean intensity data over the duration of the measurement were created in Fiji. The curve with experimental values for intensity was converted to a curve of normalised concentration at each measuring frame.

2.5.3. Mathematical model

A mathematical model was composed to physically interpret the measurement data. As no flow permeates through the membrane in cell culturing systems, particles are assumed to travel by diffusion.

The diffusion towards the lower channel can be described by solving Fick's second law for diffusion (Equation 1). When simplifying the situation to free particle diffusion in 1D, assuming the upper side of the membrane as having a constant concentration C_0, and assuming a further 1D diffusion, resulting in boundary and initial conditions (Equation 2-4) , Fick's second law can be solved.

$$\frac{\partial C}{\partial t} = D\frac{\partial^2 C}{\partial x^2} \tag{1}$$

$$C(x = 0, t) = C_0 \tag{2}$$

$$C(x = \infty, t) = 0 \tag{3}$$

$$C(x, t = 0) = 0 \tag{4}$$

The resulting formula for the concentration at the lower side of the membrane is written down in Equation 5.

$$C(x, t) = C_0 \text{erfc}(\frac{x}{2\sqrt{Dt}}) \tag{5}$$

In Equation 5, D is the diffusion coefficient of a specific particle in a solution at a defined pressure and temperature. According to Grathwohl et al. D is replaced by D^* for particle diffusion through porous media [36].

$$D^* = \frac{\epsilon\delta}{\tau}D \tag{6}$$

With porosity ϵ, constrictivity factor δ and tortuosity τ.

2.5.4. Curve fitting

Combining Equation 5 and 6 and normalizing for injected feed concentration, Equation 7 was composed, which was used to fit the normalised experimental values of concentration.

$$\frac{C_1}{C_0}(x, t) = a \cdot \text{erfc}(b\frac{x}{2\sqrt{\frac{\epsilon\delta}{\tau}D * t}}) \tag{7}$$

where a and b are fitting values used to determine whether an effect of fouling could be distinguished. Further, the location of the measuring spot x, diffusion constant for a particle D, porosity of the membrane ϵ, tortuosity of the membrane τ and constrictivity factor δ are playing a role in the concentration measurement. Note that value b was affected by the change in effective diffusion coefficient after the membrane. Data up to the point where an equilibrium is reached was used for fitting. The best fit was determined by minimizing the sum of squared residuals (SSR), where the residual is equal to the difference between an experimental value and the model. The curve fit was analysed and a and b values were compared for consecutive measurement cycles within each flow cell. Further, the correlation of a and b with pore size and feed particle were analysed. Results that had a poor or physically impossible fit were omitted from the analysis.

Table 2: Settings used for laser-cutting to create a 'kiss-cut' in the adhesive layer.

Laser		**Process**	
Diode current (A)	6.44	Drill numbers	4
Speed (mm/s)	20	Drilling Step (um)	20
Jump Speed(mm/s)	200	Number of levels	1
Laser Firing Rate (KHz)	50	Z Step (um)	60
Laser Power (%)	20	Repetitions	75

3. Results and discussion

3.1. Microfluidic flow cell manufacturing

A microfluidic flow cell (Figure 2b) was fabricated to execute dynamic fouling experiments. PDMS was used for the flow cell because of its optical transparency and biocompatibility.

Dimensions and positioning. The flow cell facilitated two channels separated by a flat sheet membrane. The width of the channels was chosen to be 4 mm to create a relatively big diffusion area (4x4 mm) and a channel height of 100 µm is chosen with respect to measurements with the fluorescence microscope: due to the relatively small channel height the intensity of light emitted by the particles at the focus point is minimally affected by emission of particles at higher or lower height levels.

The cross-flow configuration of the flow cell is chosen from a measurement objective. With a 90 degree angle, the effect of scattering light on the measurements are minimised.

The membrane is attached to both PDMS layers with an adhesive layer along the boundaries of the channels. High precision alignment of the two PDMS layers and the membrane is essential for bonding of the membrane between the two layers. Wrong alignment can cause leakages within the device.

Optimization adhesive layer. The adhesive layer chosen is a silicone transfer film. This material is chosen for its biocompatibility and low auto-fluorescence. The settings used for laser cutting (Table 2) were optimized to create a 'kiss-cut'. This way, the rectangular shapes could easily be removed from the sheet with tweezers.

Optimization bonding process. The bonding process needed optimization to prevent leakages out of and within the device. Several combinations of PDMS curing and bonding settings were tried. A description of the bonding optimization is given

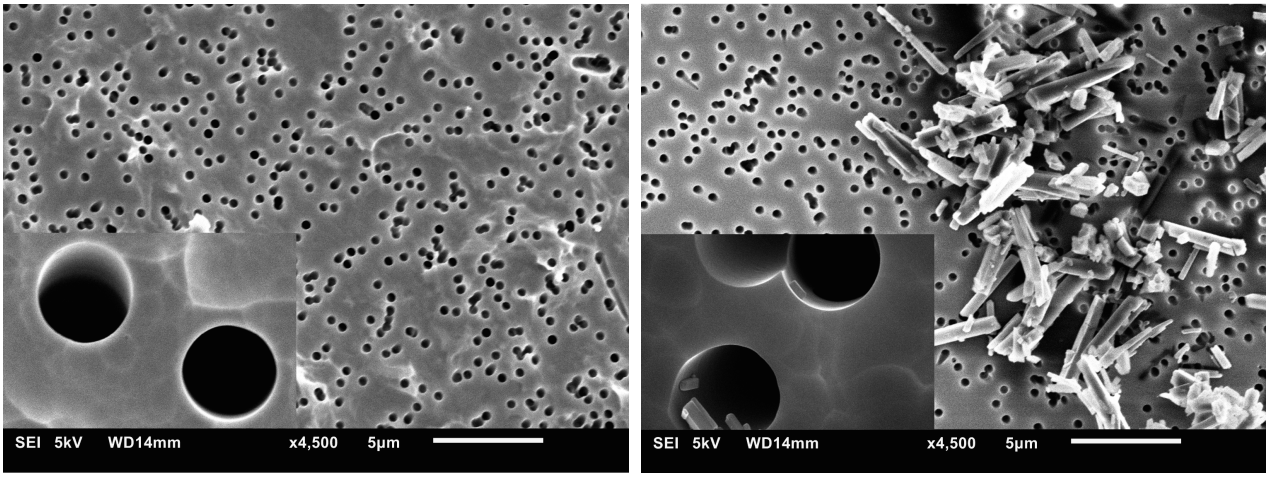

(a) Reference membrane

(b) Foulant: Glycine

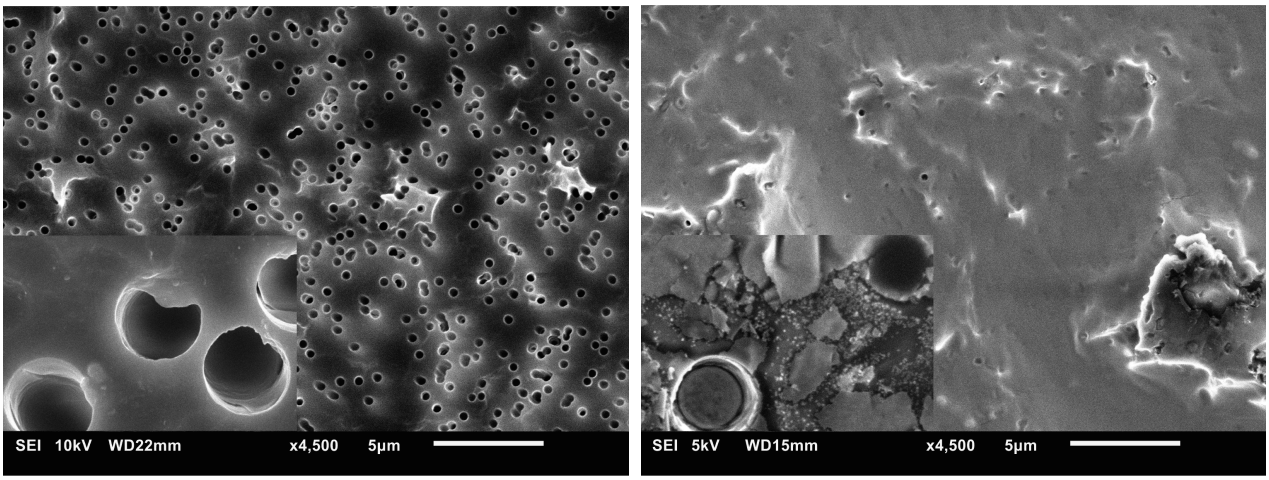

(c) Foulant: BSA

(d) Foulant: λ-DNA

Figure 3: SEM images of membranes that are fouled for one week. Each image shows a membrane with 0.4 µm pore size and the inset at the bottom left shows a membrane with 5 µm pore size fouled by the same foulant.

in Appendix E of the thesis report. A study on bonding undertaken by Bhattacharya et al. [37] points out that bonding strength is highly dependent on used plasma pressure. Therefore, plasma treatments were executed with the highest chamber pressure possible with the plasma cleaner. As a result of the bonding optimization, a PDMS curing process of 1 hour at 70 °C and an air plasma treatment of 2 minutes with a power of 60 Watt a chamber pressure of 3 mbar ensured for bonding without leakages. Note that bonding needed to be done within 15 minutes after the plasma treatment [38].

Due to the plasma treatment PDMS, which is naturally hydrophobic, became more hydrophilic making it less prone to fouling [39] and gas nucleation [40]. The microfluidic flow cell is used for dynamic testing after bonding.

3.2. Static membrane fouling studies

3.2.1. Fouling mechanisms

The first stage of the static membrane fouling studies was imaging of the membranes with SEM. Figures 3a to 3d show several SEM images that were made for analysis after fouling for one week. Each image presents a membrane with 0.4 µm pore size and the inset at the bottom left shows a membrane with 5 µm pore size fouled by the same foulant. Observing the images by eye, fouled membranes can be distinguished by layers of particles overlaying the pores. This analysis contains conclusions on fouling mechanisms seen for fouling for one hour, one day and one week.

Static fouling with Glycine (Figure 3b). The membrane surface was covered with a layer of crystals formed during the drying process. This layer indicates that cake layer formation is likely to be the dominant fouling mechanism (Figure 1). A difference in fouling mechanisms was seen for larger pore sizes: membranes with a pore size of 3 and 5 µm showed crystals inside the pores, which is an indication of standard blocking (Figure 1). This can be a result of the drying process: As the last part of the water evaporates from the pores, crystals can be locally formed there.

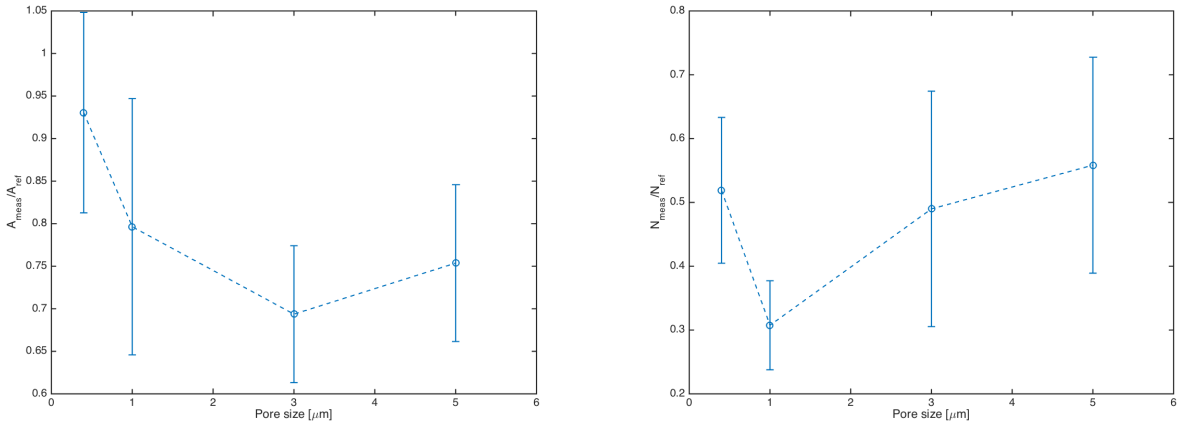

(a) (b)

Figure 4: Membrane fouling with several feed components for one week: mean measurement values of a) pore area (A_{meas}/A_{ref}) and b) pore number (N_{meas}/N_{ref}) over membrane pore size for fouling with a range of feed particles. The values are normalised with values measured for a reference membrane. The error bars indicate the standard error of the mean and the dashed line is meant to guide the eye.

Static fouling with BSA (Figure 3c). The effects of fouling with BSA were distinctly less visible than for Glycine and λ-DNA. In some images, a foulant layer covering some pores was seen. Minor fouling effects could be seen by eye at a magnification of 10000x.

Static fouling with λ-DNA (Figure 3d). A thick layer of foulant was covering every type of membrane after a week of fouling with λ-DNA. When observing images taken for fouling for an hour and a day, also pore narrowing was seen, which is an indication of standard blocking (Figure 1).

The SEM analysis suggests that two fouling mechanisms contributed to the fouling during the static analysis: standard blocking and cake layer formation.

3.2.2. Correlation of pore size with fouling

The graphs in Figure 4 visualise the correlations of membrane pore size with fouled pore area aA_{meas} and number of pores N_{meas} measured after static fouling for one week. The graphs show the mean value measured for each pore size over three membranes each fouled with a different foulant. The error bars indicate the standard error of the mean and the dashed line is to guide the eye.

For a membrane with 0.4 µm pore size, the normalised pore size decreased to 0.93 with an uncertainty of 0.33 and normalised pore area decreased to 0.52 with an uncertainty of 0.069. No significant effect of fouling is visible in the change of pore size, but the pore number decreases significantly.

For a membrane with 1 µm pore size, the normalised pore size decreased to 0.80 with an uncertainty of 0.21 and normalised pore area decreased to 0.31 with an uncertainty of 0.22. A minimal effect of fouling is visible in the change of pore size, but the pore number shows a significant decrease.

For a membrane with 3 µm pore size, the normalised pore size decreased to 0.69 with an uncertainty of 0.37 and normalised pore area decreased to 0.49 with an uncertainty of 0.27. A significant effect of fouling is visible both in the change of pore size and pore number.

For a membrane with 5 µm pore size, the normalised pore size decreased to 0.75 with an uncertainty of 0.20 and normalised pore area decreased to 0.56 with an uncertainty of 0.20. A significant effect of fouling is visible both in the change of pore size and pore number.

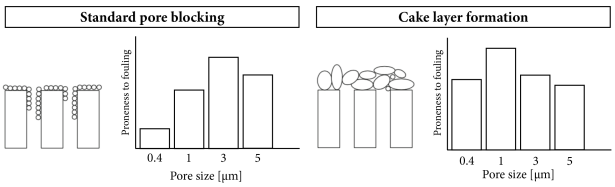

Figure 5: Assumed affinities for fouling mechanisms for each membrane [µm].

Overall, the membrane with a pore size of 3 µm shows the largest decrease in pore area after one week of fouling, which physically indicates that a membrane with a pore size of 3 µm has the highest susceptibility for standard blocking. For all membranes a significantly large decrease in pore number is measured after fouling for one week. This is an indication of cake layer formation. The decrease in pore number is the highest for membranes with a 1 µm pore size. This indicates that membranes with a 1 µm pore size are highly susceptible to cake layer formation. On this basis, Figure 5 classifies the pore size [µm] in suspected susceptibility of fouling. This susceptibility is not quantified.

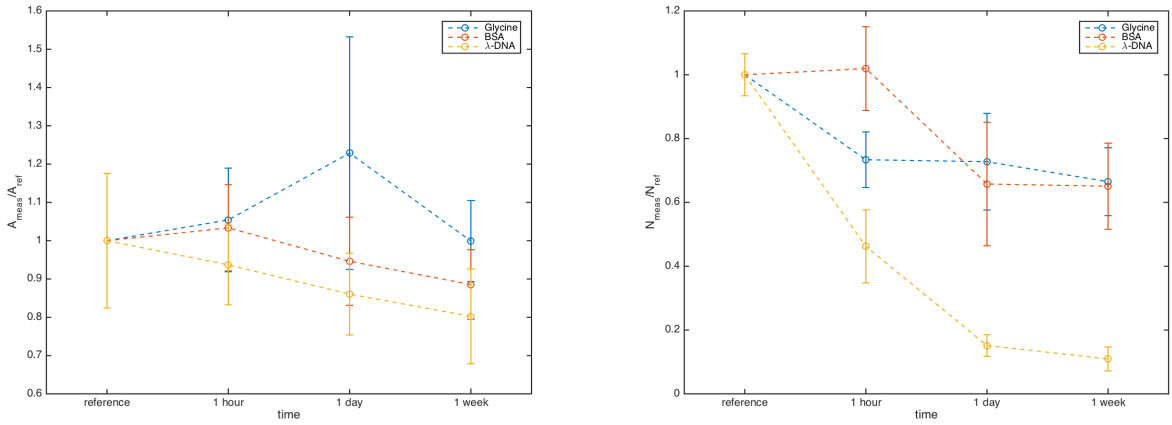

(a) (b)

Figure 6: Membrane fouling with Glycine, BSA and λ-DNA over time: mean values of a) pore area and b) number of pores measured for fouling with Glycine, BSA and λ-DNA. The mean value is calculated for membranes with pore sizes ranging from 0.4 to 5 µm. The values are normalised with values measured for a reference membrane. The error bars indicate the standard error of the mean and the dashed line is meant to guide the eye.

3.2.3. Correlation of feed properties with fouling

Figure 6a and 6b visualise the measurement data for fouled pore area A_{meas} and number of pores N_{meas} for static fouling over time with different feed particles. When looking at fouling independent of membrane pore size, a mean and standard error of the mean can be calculated over the measurements with 4 different pore sizes.

Fouling with Glycine did not result in a pore size decrease as the pore size measured after one week of fouling was 1.0 with an uncertainty of 0.11. Pore number decreased to 0.73 with an uncertainty of 0.087 after fouling for one hour and stayed at a similar level for the rest of the fouling duration.

Fouling with BSA resulted in a minor pore size decrease as the pore size measured after one week of fouling was 0.89 with an uncertainty of 0.091. Pore number decreased to 0.66 with an uncertainty of 0.19 after fouling for one day and stayed at a similar level for the rest of the fouling duration.

Fouling with λ-DNA resulted in a relatively high pore size decrease compared to the other fouling types as the pore size measured after one week of fouling was 0.80 with an uncertainty of 0.12. Pore number decreased to 0.11 with an uncertainty of 0.037 after fouling for one week, decreasing gradually over the whole fouling duration. During the last period of fouling the decrease in measured pore number was less. In this situation the amount of pores counted was maximally 20% of the amount counted for the reference membrane, so a big part was likely to be covered with a cake layer. Therefore, a constant value for pore number in this last fouling phase does not intrinsically indicate that cake layer formation (Figure 1) was less, but it is possible that foulant particles adhered to other particles covering the membrane and did not cover extra pores.

Summing the results, for both BSA and λ-DNA a trend was seen for pore area and fouling time, but as the standard error of the mean was high, the trend is not supported by the statistics. A significant decrease in N_{meas} was found for fouling with Glycine after one hour, BSA after one day and DNA over the whole fouling duration. Figure 7 shows two of the fouling mechanisms defined by Sabia et al. [22] and the feed particles ranged for susceptibility for the fouling mechanism. This susceptibility is not quantified.

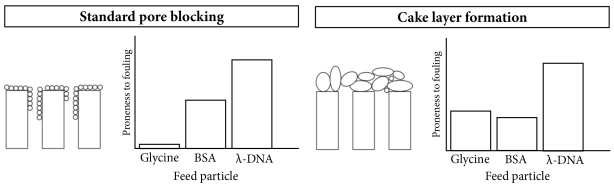

Figure 7: Assumed affinities for fouling mechanisms for each feed particle.

Feed characteristics . The results indicate that fouling in the form of direct blocking is occurring more for BSA and λ-DNA than Glycine. Cake layer formation seems similar for BSA and Glycine but occurs later for BSA. For λ-DNA, cake layer formation is the suggested dominant fouling mechanism. (Figure 7). The types of feed are chosen and classified by differences in molecular weight (MW). The trends seen for different types of feed could be attributed to molecular weight. BSA suggest to be less prone to cake layer formation than Glycine, which is not an intrinsic effect of MW. The chosen particle types vary in structure, surface tension and molecular charge, which can all be of influence on membrane fouling. An explanation of BSA being less prone to cake layer formation is due to its smooth form without side chains (Figure 8).

As research indicates that fouling in microfiltration systems is dependent on particle structure, surface tension and molecu-

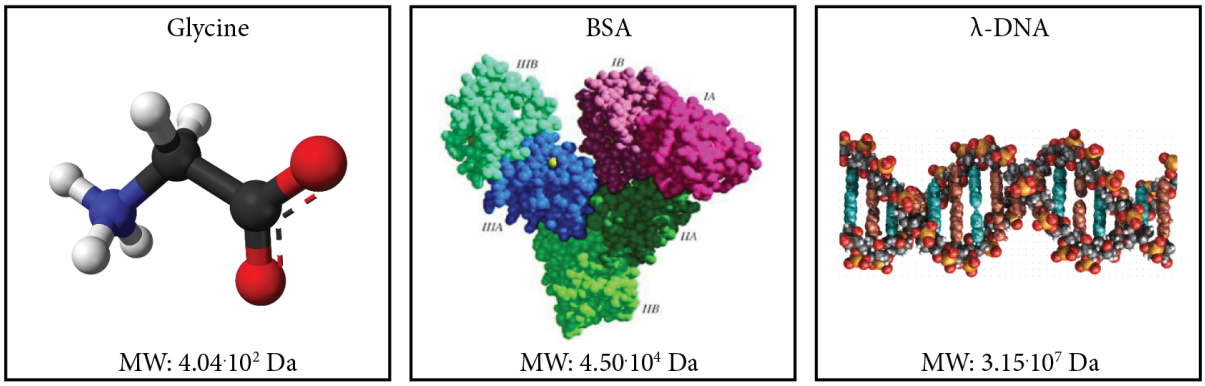

Figure 8: Structure and molecular weight of each molecule that is used in the fouling experiments. Images of the molecular structures are created by [41–43].

lar charge, these factors could also play a role in static fouling in an OoC. Noteworthy is that λ-DNA has a length of approximately 17 µm [44] is bought in a storage buffer of 10 mM Tris-HCl (pH 7.6) and 1 mM EDTA, which will have had an influence on the results.

3.2.4. Explanation of high standard deviations

Processing of the acquired SEM images with FIJI has resulted in data for pore area measured by FIJI (A_{meas}) and pore number counted by FIJI (N_{meas}) with a standard deviation. A normalised measure for the experimental data is calculated dividing the data with the mean area and number of pores counted in FIJI for the reference membranes A_{ref}, N_{ref} .

For all membranes independent of feed particle a decrease in pore size and pore number in time is seen. The standard deviations of both A_{meas} and N_{meas} are too high to draw a conclusion on the contribution of standard blocking or cake layer formation. This work shows a standard deviation up to 44% for the reference membrane. The conversion of images into data is of large influence on this high deviation. Several factors are playing a role:

Deformations in the membrane. As the membranes are flat sheets, small deformations are inevitable. This can result in a tilted image of certain pores. The measured area of a tilted pore can decrease with a factor 0.8. An explanation is given in Chapter 3 of the thesis report.

A difference in brightness and contrast of the image. Images made with the SEM can have a different brightness and contrast between pores and membrane surface due to quality of focus. When this contrast is high, pores can be measured accurately. When the contrast is low, different boundaries are measured and a pore that has a size similar to the mean can be measured smaller or bigger.

Differences due to settings of the SEM. Use of consistent settings for imaging is one of the most easy ways to avoid deviations in measured pore size. A difference in stage height of 5 mm combined with a difference in spot size of 3 can lead to a different magnification of the pores. Based on experimental observations, this can lead to a difference in pore area measurement up to a factor 4.

3.3. Dynamic membrane fouling studies

3.3.1. Interpretation of fitted parameters(a,b) with respect to fouling

The fouling model composed in Equation 7 was physically interpreted for differences in fitted parameters a and b.

Variable a. In theory, variable a is equal to the measured concentration after full diffusion normalised for the injected concentration (Equation 7) and has the value 1 in the ideal situation.

A cause of a becoming smaller can be photo-bleaching or in case of a close to 0 intensity an air bubble can be positioned in front of the measuring area. A lower value of a can also mean that part of the particles is blocked at the membrane surface. This is an interesting phenomenon to study during further research.

When the fitting value of a is larger than 1, this physically means that the concentration at the measuring area is higher than the injected concentration. An explanation for a larger a value is that the measurement area contains more densely packed particles in the form of an agglomeration. Furthermore, deviations in fitting values for a could be explained in the following ways:

Fluorescein is a fluorescent particle that is known for its proneness to photobleaching [45]. For this reason, any contact with light may cause a decrease in emission intensity, thus a decrease in fitted a. The effect of photo bleaching is studied in Chapter 3 of the thesis report and is proved to apply in this research.

Background light is a factor which can raise the light intensity that is recorded. Because of a filter used inside the fluorescence microscope, the excitation light will not be playing a role in the measured intensity. Further, all experiments are done in a dark room with all lights turned off. Despite all precautions

and warning signs, noise coming from background light must still be considered.

Variable b. The relation of variable b with the diffusion coefficient is $b \sim \frac{1}{\sqrt{D^*}}$. This means that diffusion of particles through the membrane is happening quadratically faster for a b smaller than 1 and quadratically more slow for a b larger than 1.

When variable b gets higher, this physically means that the diffusion propagates slower with a factor b^2. A higher value for b can be caused by a situation in which the particles are agglomerating, affecting the permeability through the membrane. A higher value for b can also be an indicator of fouling as $D^* = \frac{\epsilon\delta}{\tau}D$ and a lower value for porosity ϵ is the key indicator of fouling.

When variable b becomes lower than 1, this physically means that the diffusion propagates faster than expected. The reason for this can be that diffusion is not the only way of particle propagation. The pressure in the system may be elevated when injecting the fluorescent particles, resulting in fluid flow through the membrane and in direction of the measurement area.

Furthermore, frequently outlying fitting values for b could be explained in the following ways:

1. The used diffusion constant for the fluorescent particle is incorrect.
2. The diffusion factor is taken as a constant factor over the whole length of diffusion, while actually a small part of the diffusion takes place through the membrane.
3. The shape of the diffusing particle is not taken into account in the diffusion equation. Whenever the shape is affecting the difficulty of diffusing through the membrane, the b value is influenced.

A more extensive physical interpretation of a and b values is given in Chapter 3 of the thesis report.

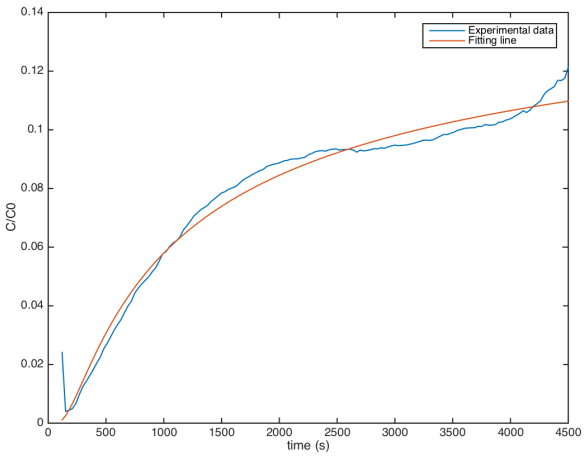

Figure 9: A plot of the measurement data and the curve fit calculated by fitting the data to Equation 7 by minimizing the sum of squared residuals.

3.3.2. *Extraction of a and b value out of measurements*

The first stage of the dynamic membrane fouling studies was the fitting of the measured and converted normalised concentration values. Figure 9 and Table 3 are examples of this preliminary result. The graph in Figure 9 shows the experimental data fitted by Equation 7 and Table 3 shows the corresponding fitting values, the squared residual and the weighted squared residual that is calculated by resnorm/a^2.

Table 3: Values for a and b and the squared residual of the norm fitting the data to Equation 7 minimizing the sum of squared residuals.

	Value
a	0.17
b	0.34
resnorm	0.0024
weighted resnorm	0.086

Equation 7 fitted the data accurately, albeit a small sinusoidal error was observed in 11 of the 20 fits (55%). This error could be attributed to a periodic difference in pressure delivered by the syringe pump.

Further, noise peeks were seen when looking at the error of the fit in 17 of the 20 fits (85%). The noise peeks could be caused by agglomerations of feed particles diffusing through the measurement area of the microscope.

The data for a and b in the preliminary result of Table 3 show that following the fitted curve, the final concentration at the measurement area would be 17% of the injected value and the propagation of the particles is $\frac{1}{0.34^2} = 8.6$ times the particle propagation by diffusion only. For every range of fits, the mean value of b lies beneath 1. This is due to the fact that Equation 7 takes the whole diffusion length as diffusion through a porous membrane. Therefore, a correction term needs to be added. The squared residual norm is 8.6% and is low enough to account for a good fit.

3.3.3. *Correlation of membrane properties with fouling*

To verify for correlations of membrane pore size with the measured data, mean a and b and a standard deviation of the mean were plotted over membrane pore size (Figure 10a and 10b). The dashed lines are intended to guide the eye.

When looking at the a value for fouling with Glycine, a positive trend was seen with pore size, but it was not supported by the statistics. The fitted b values for fouling with Glycine are more or less within the same uncertainty range so no conclusion can be drawn on a correlation of b with pore size.

No patterns can be distinguished for the mean a and b value for diffusion of BSA over pore size, nor is the standard deviation small enough to draw a significant conclusion on the correlation of value a and b and pore size of the membrane. No indication of fouling was distinguished out of the results.

To sum up the results, no correlations are drawn for either a or b with pore size due to high uncertainties and lack of distinguishable patterns. It could be that fouling is only slightly detectable due to the short duration and the deviation in patterns is

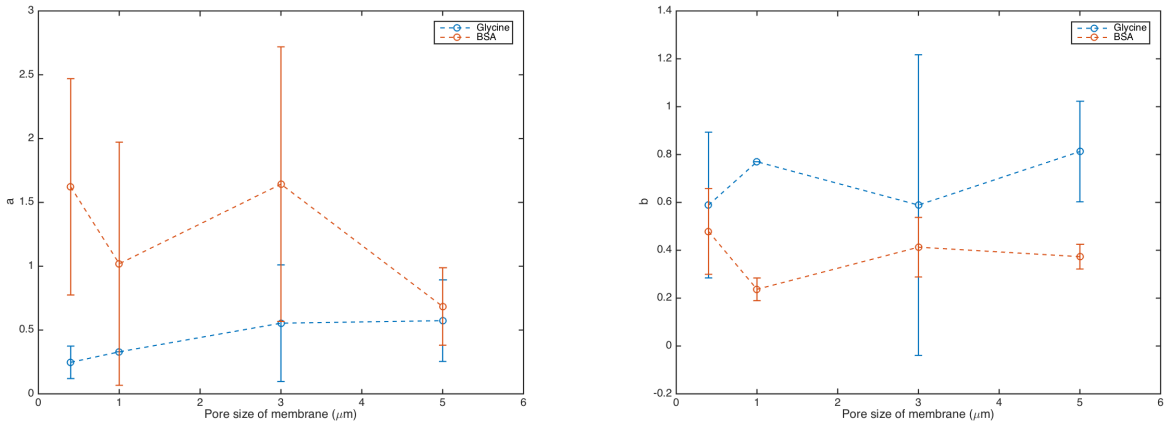

(a) (b)

Figure 10: Dynamic experiments for fouling with Glycine and BSA. The graphs show the mean fitting values over pore size. The error bars indicate the standard deviation of the mean and the dashed line is meant to guide the eye.

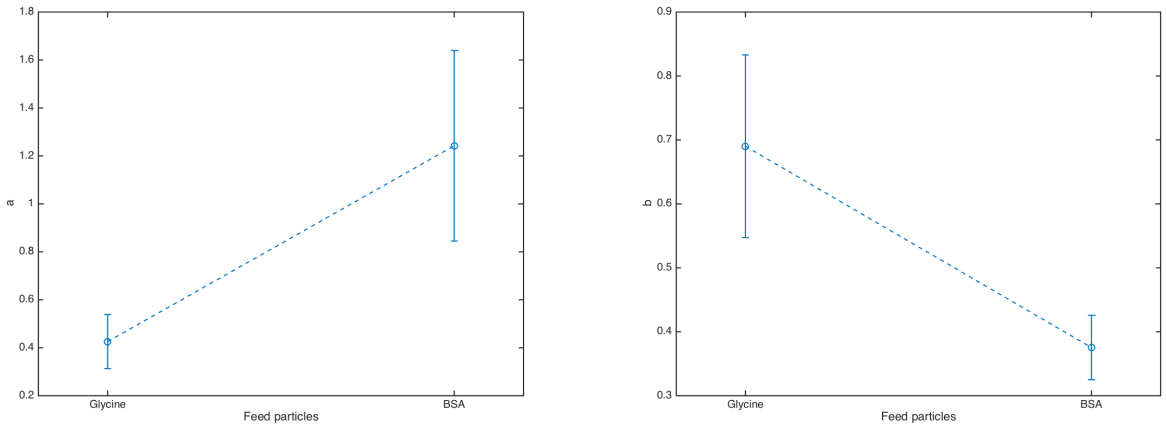

(a) (b)

Figure 11: Fouling of membranes with a pore size ranging from 0.4 to 5 µm during the dynamic analysis: mean fitting values of a and b for fouling with Glycine and BSA. The error bars indicate the standard error of the mean and the dashed line is meant to guide the eye.

too high to be able to distinguish effects of fouling. Therefore this experimental method is inadequate to use for fouling analysis. Fouling experiments in which two channels are injected as described in Appendix A would be suitable to instantly monitor a decrease in diffusion, but it must be certain that only diffusion plays part.

3.3.4. Correlation of feed properties with fouling

For every pore size, a has a larger value for BSA than for Glycine and b has a lower value for BSA than for Glycine (Figure 10). Figure 11a and 11b show graphs which indicate the dependence of a and b value on feed properties independently of membrane pore size. In these graphs, the error bars indicate the standard error of the mean taken over 4 test devices with different pore sizes.

The dynamic fouling analysis with Glycine results in a mean fitting value a of 0.43 with an uncertainty of 0.11 and a fitting value b of 0.43 with an uncertainty of 0.40.

The dynamic fouling analysis with BSA results in a mean fitting value a of 0.69 with an uncertainty of 0.14 and a fitting value b of 0.38 with an uncertainty of 0.050.

With significance, the value of a is increasing over molecular weight. This is not an indication of fouling, but it suggests that BSA particles permeate better through each membrane than Glycine particles. When looking at the a value of Glycine, which is significantly below 1 for all track-etched membranes, one could say that only part of the feed particles diffuse through the membrane and there are particles adhering to the membrane. The values of b are not significantly correlated during this thesis. The values of b for both Glycine and BSA, were significantly lower than 1, which suggests that a correction factor for Equation 7 needs to be applied (diffusion factor described in

Section 3.3.1).

4. Conclusion

In this study membrane fouling by diffusion of particles in a microfluidic device similar to an OoC was researched.

A flow cell was produced in which dynamic tests were executed. Air plasma treatments for bonding were optimally executed with a pressure of at least 3 mbar to account for good bonding without leakages. Leakages within the flow cell at the boundaries of the membrane were avoided through accurate alignment of the adhesive layer, membrane and channels within each layer. This way, the flow cell could withstand five measurement cycles while holding the membrane and channels in the desired configuration. Imaging with an inverted fluorescence microscope was possible as its focus depth was not exceeded when focussing on the measurement channel.

The experimental data for static fouling suggest that fouling occurs for all membranes with pore sizes ranging from 0.4 to 5 μm in combination with Glycine, BSA and λ-DNA. For both BSA and λ-DNA a trend was seen for measured pore area over fouling time, but as the standard error of the mean was high, the trend was not supported by the statistics. Further, a significant decrease in amount of pores is found for fouling with Glycine after one hour, BSA after one day and λ-DNA over the whole fouling duration. Cake layer formation (Figure 1d) is assumed to be a dominant fouling mechanism.

For execution of the dynamic fouling analysis a model was developed that showed a good fit on the measurement curve, besides having a small sinusoidal error and noise peaks. No distinct patterns were observed for follow up measurements. Diffusion decline could not be perceived with the used measurement method and fouling could not be distinguished during the dynamic fouling analysis. A conclusion that can be drawn is that diffusion through the membrane is higher for BSA than for Glycine, which is reinforced by the static fouling experiments showing that BSA fouling by cake layer occurs after a longer fouling duration than Glycine.

A comparison between static and dynamic analysis suggests an unexpected phenomenon: BSA was permeating better through every membrane than Glycine. This can be caused by a difference in structure and flexibility, but also by surface tension or molecular charge.

Summarized, it may be concluded from the static and dynamic fouling analyses, that fouling by diffusion is applying. After fouling in static situation for a day, it is seen that cake layer is formed at all membranes with all feed types. λ-DNA appears to be the most influential foulant and BSA appears to diffuse through the membrane more easily than Glycine. There is a dependency on pore size as standard pore blocking is also seen for larger pore sizes, which is supported by literature [22]. Further research should be done on a dynamic analysis to detect fouling *in situ* without the need for multiple cycles.

5. Acknowledgements

The author likes to thank Luigi Sasso and Paola Fanzio of the Technical University of Delft for their continuous guiding and stimulation. The author would also like to thank Guishan Wang of the Technical University of Delft for his help in programming an operation code to enable imaging in time intervals, AdhesivesResearch for supplying the adhesive, Sandro Meucci of Micronit for the introduction with the membrane; and Spiridon Veldhoven en Rob Luttjeboer for their patience and advice on production and analysis.

References

[1] T. Meng, R. Xie, Y.-C. Chen, C.-J. Cheng, P.-F. Li, X.-J. Ju, L.-Y. Chu, A thermo-responsive affinity membrane with nano-structured pores and grafted poly (n-isopropylacrylamide) surface layer for hydrophobic adsorption, Journal of Membrane Science 349 (2010) 258–267.

[2] L.-Y. Chu, Y. Li, J.-H. Zhu, H.-D. Wang, Y.-J. Liang, Control of pore size and permeability of a glucose-responsive gating membrane for insulin delivery, Journal of Controlled Release 97 (2004) 43–53.

[3] J. Deng, L. Wang, L. Liu, W. Yang, Developments and new applications of uv-induced surface graft polymerizations, Progress in Polymer Science 34 (2009) 156–193.

[4] L. Brink, S. Elbers, T. Robbertsen, P. Both, The anti-fouling action of polymers preadsorbed on ultrafiltration and microfiltration membranes, Journal of membrane science 76 (1993) 281–291.

[5] W. Bowen, J. Calvo, A. Hernandez, Steps of membrane blocking in flux decline during protein microfiltration, Journal of Membrane Science 101 (1995) 153–165.

[6] A. B. Koltuniewicz, R. Field, T. Arnot, Cross-flow and dead-end microfiltration of oily-water emulsion. part i: experimental study and analysis of flux decline, Journal of Membrane Science 102 (1995) 193–207.

[7] C.-C. Ho, A. L. Zydney, A combined pore blockage and cake filtration model for protein fouling during microfiltration, Journal of colloid and interface science 232 (2000) 389–399.

[8] S. Giglia, G. Straeffer, Combined mechanism fouling model and method for optimization of series microfiltration performance, Journal of membrane science 417 (2012) 144–153.

[9] H. E. Abaci, K. Gledhill, Z. Guo, A. M. Christiano, M. L. Shuler, Pumpless microfluidic platform for drug testing on human skin equivalents, Lab on a Chip 15 (2015) 882–888.

[10] T. Steinhauer, S. Hanély, K. Bogendörfer, U. Kulozik, Temperature dependent membrane fouling during filtration of whey and whey proteins, Journal of Membrane Science 492 (2015) 364–370.

[11] S. Loh, U. Beuscher, T. K. Poddar, A. G. Porter, J. M. Wingard, S. M. Husson, S. R. Wickramasinghe, Interplay among membrane properties, protein properties and operating conditions on protein fouling during normal-flow microfiltration, Journal of Membrane Science 332 (2009) 93–103.

[12] R. Singh, Hybrid Membrane Systems for Water Purification: Technology, Systems Design and Operations, Elsevier, 2006.

[13] A. Razmjou, E. Arifin, G. Dong, J. Mansouri, V. Chen, Superhydrophobic modification of tio 2 nanocomposite pvdf membranes for applications in membrane distillation, Journal of membrane science 415 (2012) 850–863.

[14] M. Elimelech, X. Zhu, A. E. Childress, S. Hong, Role of membrane surface morphology in colloidal fouling of cellulose acetate and composite aromatic polyamide reverse osmosis membranes, Journal of membrane science 127 (1997) 101–109.

[15] N. Lee, G. Amy, J.-P. Croue, H. Buisson, Identification and understanding of fouling in low-pressure membrane (mf/uf) filtration by natural organic matter (nom), Water research 38 (2004) 4511–4523.

[16] M. Buonomenna, L. Lopez, P. Favia, R. dAgostino, A. Gordano, E. Drioli, New pvdf membranes: the effect of plasma surface modification on retention in nanofiltration of aqueous solution containing organic compounds, Water research 41 (2007) 4309–4316.

[17] K. Boussu, C. Vandecasteele, B. Van der Bruggen, Relation between membrane characteristics and performance in nanofiltration, Journal of Membrane Science 310 (2008) 51–65.

[18] R. W. Baker, Membrane technology and applications, John Wiley & Sons, Ltd (2004) 96–103.
[19] D. Rana, T. Matsuura, Surface modifications for antifouling membranes, Chemical reviews 110 (2010) 2448–2471.
[20] M. R. Esfahani, H. A. Stretz, M. J. Wells, Comparing humic acid and protein fouling on polysulfone ultrafiltration membranes: Adsorption and reversibility, Journal of Water Process Engineering 6 (2015) 83–92.
[21] F. Qu, H. Liang, Z. Wang, H. Wang, H. Yu, G. Li, Ultrafiltration membrane fouling by extracellular organic matters (eom) of microcystis aeruginosa in stationary phase: influences of interfacial characteristics of foulants and fouling mechanisms, Water research 46 (2012) 1490–1500.
[22] G. Sabia, M. Ferraris, A. Spagni, Model-based analysis of the effect of different operating conditions on fouling mechanisms in a membrane bioreactor, Environmental Science and Pollution Research 23 (2016) 1598–1609.
[23] M. Khayet, J. Mengual, Effect of salt concentration during the treatment of humic acid solutions by membrane distillation, Desalination 168 (2004) 373–381.
[24] X. Zhu, Micro/nanoporous membrane based gas–water separation in microchannel, Microsystem technologies 15 (2009) 1459–1465.
[25] R. W. Field, J. J. Wu, Modelling of permeability loss in membrane filtration: Re-examination of fundamental fouling equations and their link to critical flux, Desalination 283 (2011) 68–74.
[26] H. Choi, K. Zhang, D. D. Dionysiou, D. B. Oerther, G. A. Sorial, Effect of permeate flux and tangential flow on membrane fouling for wastewater treatment, Separation and Purification Technology 45 (2005) 68–78.
[27] H. Choi, K. Zhang, D. D. Dionysiou, D. B. Oerther, G. A. Sorial, Influence of cross-flow velocity on membrane performance during filtration of biological suspension, Journal of membrane science 248 (2005) 189–199.
[28] T. Shimomura, M. Hirakawa, I. Murase, M. Sasaki, T. Sano, Preparation of polyacrylonitrile reverse osmosis membrane by plasma treatment, J. Appl. Polym. Sci 38 (1984) 173–183.
[29] N. A. Hashim, F. Liu, K. Li, A simplified method for preparation of hydrophilic pvdf membranes from an amphiphilic graft copolymer, Journal of Membrane Science 345 (2009) 134–141.
[30] J.-H. Li, M.-Z. Li, J. Miao, J.-B. Wang, X.-S. Shao, Q.-Q. Zhang, Improved surface property of pvdf membrane with amphiphilic zwitterionic copolymer as membrane additive, Applied Surface Science 258 (2012) 6398–6405.
[31] J. Zhao, Q. Shi, S. Luan, L. Song, H. Yang, H. Shi, J. Jin, X. Li, J. Yin, P. Stagnaro, Improved biocompatibility and antifouling property of polypropylene non-woven fabric membrane by surface grafting zwitterionic polymer, Journal of membrane science 369 (2011) 5–12.
[32] S. Balta, A. Sotto, P. Luis, L. Benea, B. Van der Bruggen, J. Kim, A new outlook on membrane enhancement with nanoparticles: the alternative of zno, Journal of membrane science 389 (2012) 155–161.
[33] P. Bengani, Y. Kou, A. Asatekin, Zwitterionic copolymer self-assembly for fouling resistant, high flux membranes with size-based small molecule selectivity, Journal of Membrane Science 493 (2015) 755–765.
[34] Y. Wang, Z. Wang, X. Han, J. Wang, S. Wang, Improved flux and antibiofouling performances of reverse osmosis membrane via surface layer-by-layer assembly, Journal of Membrane Science (2017).
[35] Z. Liu, W. Wang, R. Xie, X.-J. Ju, L.-Y. Chu, Stimuli-responsive smart gating membranes, Chemical Society Reviews 45 (2016) 460–475.
[36] P. Grathwohl, Diffusion in natural porous media: contaminant transport, sorption/desorption and dissolution kinetics, volume 1, Springer Science & Business Media, 2012.
[37] S. Bhattacharya, A. Datta, J. M. Berg, S. Gangopadhyay, Studies on surface wettability of poly (dimethyl) siloxane (pdms) and glass under oxygen-plasma treatment and correlation with bond strength, Journal of microelectromechanical systems 14 (2005) 590–597.
[38] B.-H. Jo, L. M. Van Lerberghe, K. M. Motsegood, D. J. Beebe, Three-dimensional micro-channel fabrication in polydimethylsiloxane (pdms) elastomer, Journal of microelectromechanical systems 9 (2000) 76–81.
[39] D. Bodas, C. Khan-Malek, Hydrophilization and hydrophobic recovery of pdms by oxygen plasma and chemical treatmentan sem investigation, Sensors and Actuators B: Chemical 123 (2007) 368–373.
[40] X. Ren, M. Bachman, C. Sims, G. Li, N. Allbritton, Electroosmotic properties of microfluidic channels composed of poly (dimethylsiloxane), Journal of Chromatography B: Biomedical Sciences and Applications 762 (2001) 117–125.
[41] P. D. Godfrey, R. D. Brown, Shape of glycine, Journal of The American Chemical Society 117 (1995) 2019–2023.
[42] K. M. Naik, D. B. Kolli, S. T. Nandibewoor, Elucidation of binding mechanism of hydroxyurea on serum albumins by different spectroscopic studies, SpringerPlus 3 (2014) 360.
[43] W. K. Purves, W. K. Purves, G. H. Orians, D. Sadava, H. C. Heller, Life: The Science of Biology: Volume III: Plants and Animals, volume 3, Macmillan, 2003.
[44] B. J. Kirby, Micro-and nanoscale fluid mechanics: transport in microfluidic devices, Cambridge university press, 2010.
[45] L. Song, E. Hennink, I. T. Young, H. J. Tanke, Photobleaching kinetics of fluorescein in quantitative fluorescence microscopy., Biophysical journal 68 (1995) 2588.

3

Extensive analyses description

The results described in the paper in Chapter 2 are achieved due to a great amount of work and analysis. In this chapter comments are given on the methods of analysis and data processing to explain the analysis in detail and to clarify which steps are taken to achieve repeatability in this research.

3.1. Stationary analysis

3.1.1. Imaging

Every treated membrane is imaged 9 times: at three locations (Figure 3.1) and with magnifications of 1000x, 4500x and 10000x to be sure that deviations for fouling on different places on the membrane and on imaging with different magnifications are taken into account.

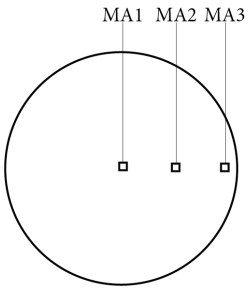

Figure 3.1: The positions of the imaging/measurement area's indicated with MA1, MA2 and MA3.

3.1.2. Image processing

Membrane surface images made with the SEM are analysed using ImageJ. The steps for analysis are as shown in Figure 3.2: First an image is imported in ImageJ. Then the scale (b) and a colour threshold(c) need to be set. The last step is to indicate which particle dimensions apply and then ImageJ gives pore area's as a result.

The amount of pores measured and the mean area of the pores are analysed in order to estimate what the fouling principles are. A decreasing pore area is seen as an indicator for standard blocking and a decreasing amount of pores is seen as an indicator for intermediate blocking and/or cake filtration.

Uncertainty As described in the paper, there are some disadvantages when analysing digitally: Because a membrane is a thin film, it is prone to deform and pores are then imaged under an angle. When using these images for analysis in ImageJ, the pores seem to be smaller, but in fact are not. The result of this tilt is visible in Figure 3.3

Further, a difference in brightness used for imaging can also affect the measured pore size.

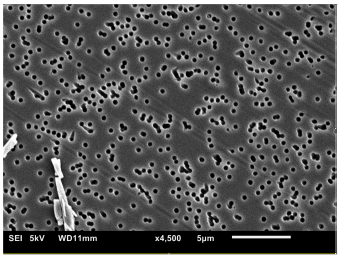

(a) Image made with the SEM.

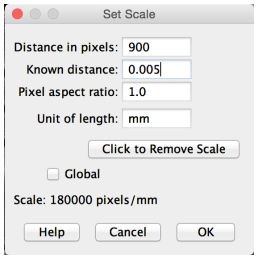

(b) Setting scale.

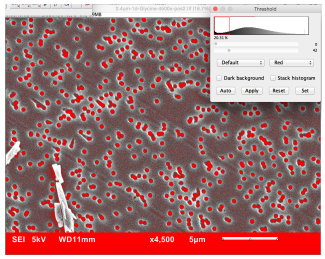

(c) Setting threshold.

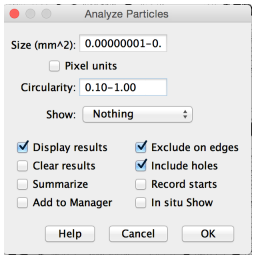

(d) Setting particle dimensions.

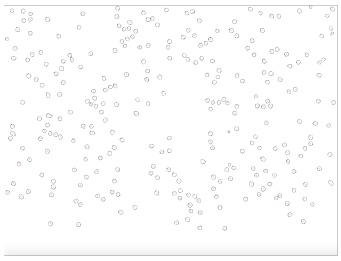

(e) Pores localised by ImageJ.

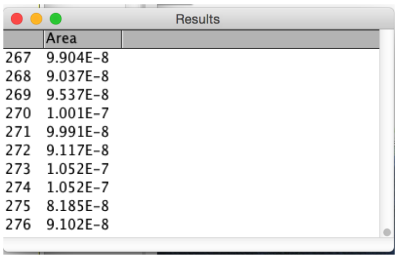

(f) List of area's per pore.

Figure 3.2: Steps and results of an analysis in ImageJ.

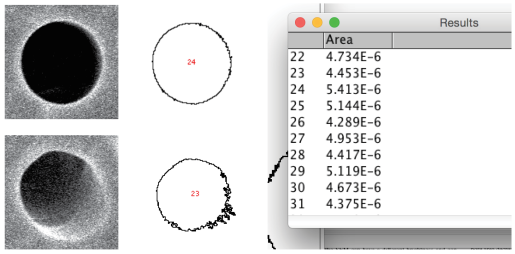

Figure 3.3: Differences in measured pore area caused by a pore tilt.

3.1.3. Results and discussion

The static analysis is executed to draw a conclusion on the fouling mechanisms appearing in a static situation. The outcomes for each combination of membrane pore size and foulant type over fouling time is given in Appendix F. The next paragraphs contain conclusions over all tested membranes per foulant particle. The static fouling experiments are executed with 4 different membranes and can be seen as 4 experiments. Therefore, the plots in the next paragraphs show the mean value over all pore sizes and the error bars indicate the standard error of the mean. The dashed lines are meant to guide the eye .

Glycine fouling, all membranes When looking at Glycine fouling, measured pore area is not a parameter which is significantly decreasing over all membranes. Only a membrane with a pore size of 3 µm has a decreased pore area that is significantly measured after 1 day of fouling. For all membranes, a correlation is seen for the normalised number of pores counted and duration of fouling. To verify the correlation independent of pore size, the mean is taken over all measurements done with glycine and a standard error of the mean is calculated. Figure 3.4a and 3.4b show the change in pore area and amount of pores respectively after fouling for 1 hour, 1 day and 1 week.
As was expected, still no conclusions can be drawn about correlation of pore area measured with duration of fouling by Glycine. For the correlation of amount of pores measured with duration of fouling by Glycine, there is already a significant decrease in amount of pores after one hour. This indicates that fouling for one hour already results in cake layer formation for all track-etched membranes.

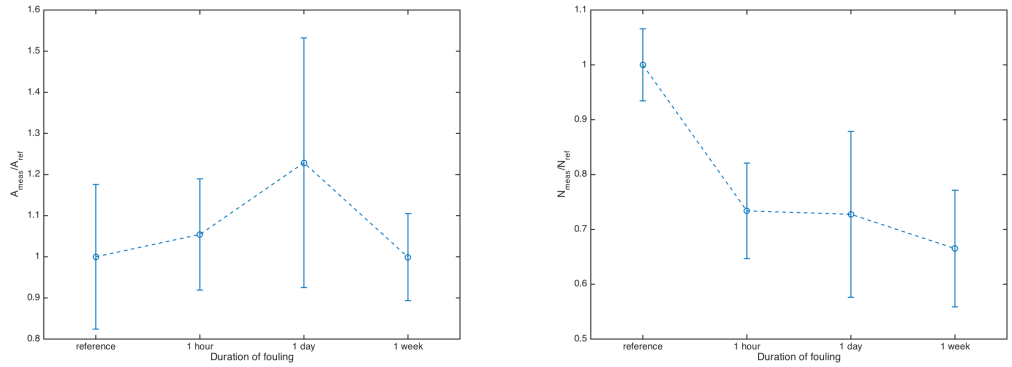

(a) (b)

Figure 3.4: Membrane fouling with Glycine: mean measurement values of a) pore area (A_{meas}/A_{ref}) and b) pore number (N_{meas}/N_{ref}) over time. The values are normalised with values measured for a reference membrane. The error bars indicate the standard error of the mean and the dashed line is meant to guide the eye.

BSA fouling, all membranes When looking at BSA fouling, the mean normalised pore area decreases over time for all membranes, but due to high standard deviation bars, the decrease is not significant for all membranes. Only a membrane with a pore size of 3 µm has a decreased pore area that is significant after one week of fouling. Further the number of pores decreases for all membranes after a certain duration of fouling. To verify the correlation independent of pore size, the mean is taken over all measurements done with BSA and a standard error of the mean is calculated. Figure 3.5a and 3.5b show the change in pore area and amount of pores respectively after fouling for 1 hour, 1 day and 1 week. The normalised pore area decrease insignificantly after one day of fouling for all track-etched membranes. The normalised number of pores decrease significantly after one day of fouling for all track-etched membranes.

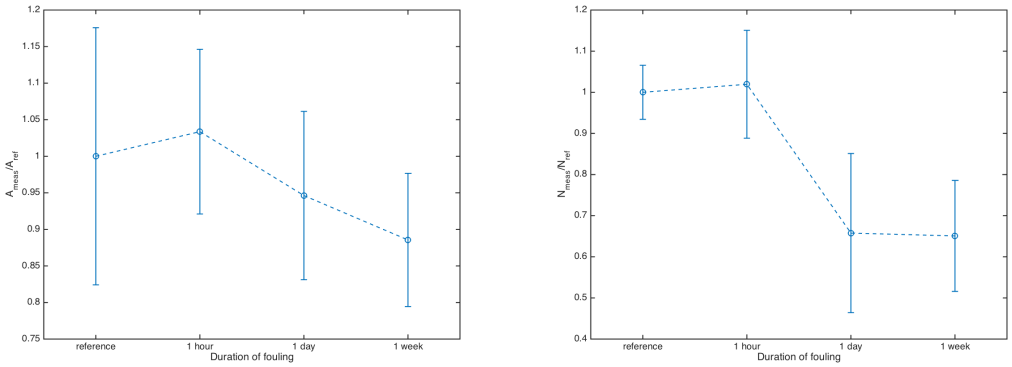

(a) (b)

Figure 3.5: Membrane fouling with BSA: mean measurement values of a) pore area (A_{meas}/A_{ref}) and b) pore number (N_{meas}/N_{ref}) over time. The values are normalised with values measured for a reference membrane. The error bars indicate the standard error of the mean and the dashed line is meant to guide the eye.

λ-DNA fouling, all track-etched membranes When looking at λ-DNA fouling, both mean normalised pore area and mean normalised amount of pores are decreasing over all membranes, but due to high standard deviation bars, the decrease is not significant for all membranes. To verify the correlation independent of pore size, the mean is taken over all measurements done with BSA and a standard error of the mean is calculated. Figure 3.6a and 3.6b shows the change in pore area and amount of pores respectively after fouling for 1 hour, 1 day and 1 week. The graphs show a mean normalised pore area that is decreasing, but the standard error of the mean is unfortunately still large. The normalised amount of pores is, however, significantly decreasing

over duration of fouling so the pore coverage is significantly increasing during the whole fouling experiment.

The decrease is more steep over the first period of time. This is due to feed particles depositing on a clean membrane but later being absorbed onto a deposited DNA-particle.

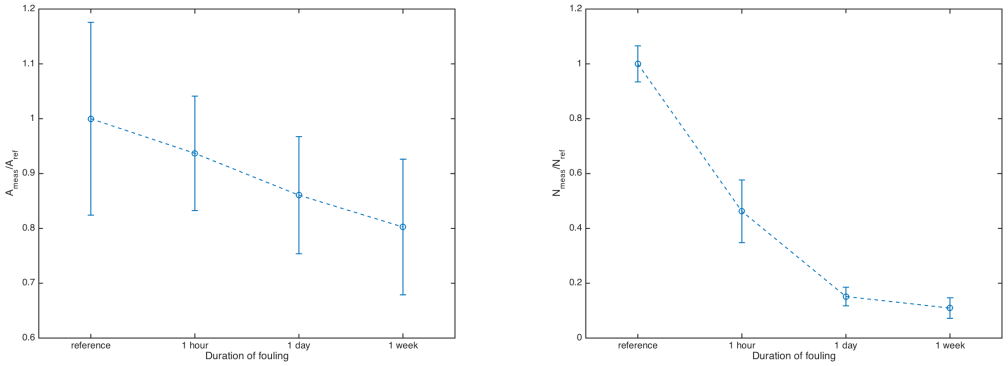

(a) (b)

Figure 3.6: Membrane fouling with λ-DNA: mean measurement values of a) pore area (A_{meas}/A_{ref}) and b) pore number (N_{meas}/N_{ref}) over time. The values are normalised with values measured for a reference membrane. The error bars indicate the standard error of the mean and the dashed line is meant to guide the eye.

Interpretations and conclusions The sections before showed the measurement results of the static fouling analysis. Overall, a negative correlation is seen for both pore area and amount of pores with duration of fouling. Table shows the oversight on decrease in pore area and amount of pores over all experiments. The conclusions for every feed particle for the previous section are:

- Glycine particles are not much resulting in direct fouling, but are significantly forming a cake layer after fouling for one hour.
- BSA particles seem to have a stronger partition in direct fouling, but the correlation is not significant. However, significant cake-layer formation happens after fouling for one day.
- λ-DNA particles have the strongest correlation with fouling, both for direct fouling and cake layer formation. After one week the cake-layer seems to have covered the whole surface.

The static analysis is executed in several steps. All of these steps can introduce discontinuities and errors. The goal, which was to execute each separate experiment minimally 4 times, was not succeeded. That is why the repeatability of the experiments is not validated and a standard error of the mean cannot be given for all graphs.

3.2. Dynamic analysis

3.2.1. Feed liquid

The Glycine and Obuvalmin are bought with a Fluorescent FITC label to enable fluorescent analysis. To verify the working principle of the dynamic analysis, first experiments are executed with Fluorescein, which has a molecular weight comparable to Glycine. The material properties needed are summed in Table 3.1. Molecular weight properties are obtained out of the ordering information.

Table 3.1: Material properties needed for the used feed

Feed particle	MW [Da]	Diffusion Coefficient $\times 10^6$ [cm^2/sec]
Fluorescein	$\sim 3.76 \cdot 10^2$	4.25 ± 0.01 [24]
Glycine-FITC	$\sim 4.04 \cdot 10^2$	10.55 [55]
Obuvalmin-FITC	$\sim 4.50 \cdot 10^4$	0.675 ± 0.006 / 0.813 ± 0.009 [24]

During the first experiments with Fluorescein, a change in measurement method has taken place. The initial experimental plan is described in Appendix A.

3.2.2. Dynamic Model

A model is made to physically interpret the test data. Following section describes which physical events take place during the experiment and the simplifications that apply in the model.

Physical events Time passes before the fluorescent liquid reaches the location where diffusion through the membrane takes place. From this moment the interface between upper channel and membrane is considered as a plane with a constant concentration.

Flow reaches membrane The top channel is assumed to contain a laminar flow because of the flow speed of 1 µl/min. To predict which amount of time passes before the diffusion through the membrane takes place, Equations 3.1 and 3.2 are used.

$$t_{\text{toD1}} = \frac{l_{\text{beginmembrane}} bh}{Q} = \frac{0.04 * 0.04 * 0.001}{10^{-6} * \frac{1}{60}} = 96\,\text{s} \tag{3.1}$$

$$t_{\text{toD2}} = \frac{l_{\text{endmembrane}} bh}{Q} = \frac{0.08 * 0.04 * 0.001}{10^{-6} * \frac{1}{60}} = 192\,\text{s} \tag{3.2}$$

In the equations above, the time to diffusion at the beginning of the membrane, t_{toD1} and at the end of the membrane, t_{toD2} are dependent on the distance from inlet to the membrane l, channel width b, channel height h and applied flowrate Q. The time to diffusion is 96-192 seconds.

Particles diffuse through membrane After the fluorescent fluid front has come into contact with the membrane, particles can diffuse through the membrane towards the lower channel. The diffusion towards the lower channel can be described solving Fick's second law for diffusion (Equation 3.3). When simplifying the situation to free particle diffusion in 1D, assuming the upper side of the membrane as having a constant concentration C_0, resulting in boundary and initial conditions (Equation 3.4-3.6) , Fick's second law can be solved.

$$\frac{\partial C}{\partial t} = D\frac{\partial^2 C}{\partial x^2} \tag{3.3}$$

$$C(x = 0, t) = C_0 \tag{3.4}$$

$$C(x = \infty, t) = 0 \tag{3.5}$$

$$C(x, t = 0) = 0 \tag{3.6}$$

The resulting formula for the concentration at the lower side of the membrane is written down in Equation 3.7.

$$C(x, t) = C_0 \text{erfc}(\frac{x}{2\sqrt{Dt}}) \tag{3.7}$$

In Equation 3.7, D is the diffusion coefficient of a specific particle in a solution at a defined pressure and temperature. According to Grathwohl et al. D is replaced by D^* for particle diffusion through porous media [36].

$$D^* = \frac{\epsilon\delta}{\tau} D \tag{3.8}$$

With porosity ϵ, constrictivity factor δ and tortuosity τ. This results in the following formula describing the particle concentration right after the membrane called C_1.

$$C_1 = 0 \qquad @t < t_{\text{todiffusion}} \tag{3.9}$$

$$C_1 = C_0 \text{erfc}(\frac{x}{2\sqrt{\frac{\epsilon\delta}{\tau} D(t - t_{\text{todiffusion}})}}) \qquad @t > t_{\text{todiffusion}} \tag{3.10}$$

Table 3.2: Membrane characteristics determined by research

Pore size membrane [µm]	Thickness [μm]	Porosity, ϵ [%]	Reference
0.4	11	2.52	[75]
1	8	6.28	[75]
3			
5	9	8	[38]

As there is only scarce information on the track-etched membranes provided by the manufacturers, values determined by [75] and [38] are assumed correct values for the used membranes.

Table 3.2 shows the values used for calculations with the different membranes. The graphs in Figures 3.7a and 3.7b show plots of the expected concentration curve right after the membrane over time. This curve is composed of Equation 3.10 and the parameters for a 0.4 µm pore size membrane and is plotted for several porosities.

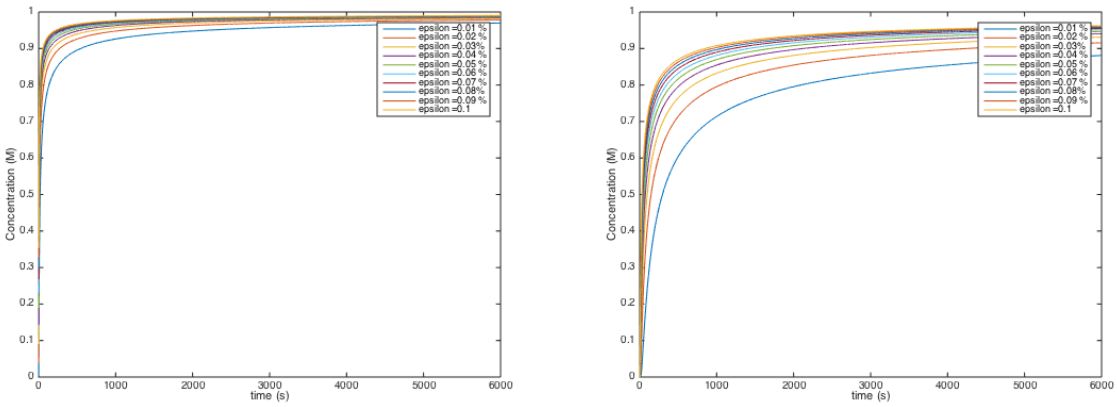

(a) Glycine.

(b) BSA.

Figure 3.7: Expected concentration curve right after the membrane over time. This curve is composed of Equation 3.10 and the parameters for a 10 µm thick 0.4 µm pore size membrane and is plotted for several porosities .

It is important to take a look onto the expected differences for different values of ϵ. For BSA, bigger differences are expected to show than for Glycine.

Particles diffuse through DI water After diffusing through the membrane, the solute particles experience free diffusion through deionized water. Both the diffusion through the membrane and water can be taken together and simplified to 1 dimension, showing in Figure 3.8.

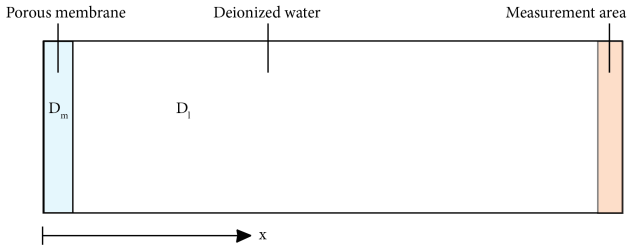

Figure 3.8: Simplified diffusion problem.

In this situation, Fick's law can again be applied. At $x = k$ (the thickness of the membrane) the boundary conditions are stated in Equation 3.11 to 3.13.

$$C_2(k,t) = C_1(k,t) = C_0 \text{erfc}\left(\frac{k}{2\sqrt{\frac{\epsilon\delta}{\tau} D(t - t_{\text{todiffusion}})}}\right) \qquad @t > t_{\text{todiffusion}} \tag{3.11}$$

$$D\frac{dC_2}{dx} = \frac{\epsilon\delta}{\tau} D\frac{dC_1}{dx} \tag{3.12}$$

$$\frac{dC_2}{dx} = \frac{\epsilon\delta}{\tau} C_0 e^{\frac{-k^2}{4\frac{\epsilon\delta}{\tau} D(t - t_{\text{todiffusion}}))}} \qquad @t > t_{\text{todiffusion}} \tag{3.13}$$

This problem was too difficult to solve analytically within the time frame of this research, thus the equation for the concentration at the measuring spot is assumed to be as follows:

$$C_2(x,t) = a \cdot C_0 \text{erfc}\left(b\frac{x}{2\sqrt{D^*(t - t_{\text{todiffusion}})}}\right) \qquad @t > t_{\text{todiffusion}} \tag{3.14}$$

This equation is normalised for the injected concentration of fluorescent particles and becomes:

$$\frac{C_2}{C_0}(x,t) = a \cdot \text{erfc}\left(b\frac{x}{2\sqrt{D^*(t - t_{\text{todiffusion}})}}\right) \qquad @t > t_{\text{todiffusion}} \tag{3.15}$$

In Equation 3.15, a and b are constants that have the value 1 in the ideal situation. This equation and constants a and b are used to fit the experimental data. The disadvantage when using this equation to fit with Matlab is that a fitting parameter for the time delay cannot be incorporated. This is due to the fact that a complementary error (erfc) function cannot be negative. As a result, time to diffusion cannot be incorporated as a variable in the fitting function. This can result in less accurate fitting values and a less significant fit.

Change in curve propagation for changing a and b Equation 3.15 is fitted with a Matlab script to compare the experimental values with the expected curve. The physical meaning of a deviation of a and b are described in Chapter 2 and the changes seen in curve behaviour for deviations of a and b from 1 are shown in Figure 3.9.

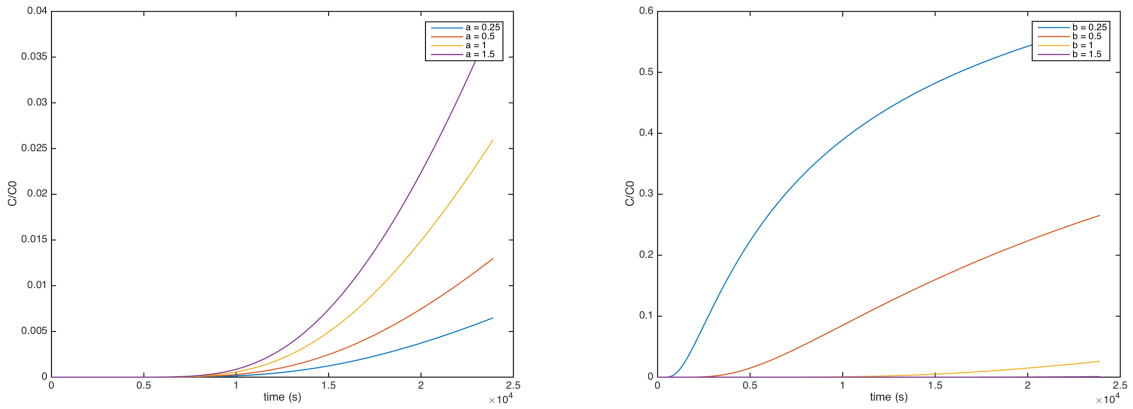

(a) Different values for a. b=1

(b) Different values for b. a=1

Figure 3.9: Change in the fitting curve (Equation 3.15) for normalised concentration at the measuring spot over time.

3.2.3. Image processing

The images acquired are imported in ImageJ and a table with mean intensity values is obtained and imported in an excel file. As the intensity data indicate a certain particle concentration, calibration of the intensity for several concentrations is done. A calibration equation is composed in Appendix D.

After processing, the values for measured concentration are fitted to the modelled equation for concentrations, Equation 3.15, and constants a and b are determined.

3.2.4. Results

Each dynamic experiment and belonging fitting curves are shown and discussed in Appendix G. Further, Appendix G contains graphs with the fitting values (a and b) over consecutive measurements with one measurement device. Next sections describe differences in fitting data and errors with the expected curve and describe correlations between fitted values for consecutive test cycles within one test flow cell.

Interpretations on fitting values and fitting errors The graphs of measurement can be divided in several propagation patterns: one similar to the fitting curve with a sinusoidal error term and one with a peak in concentration at the start and a slight decrease in time. These propagations are described and an explanation is given for deviant fitting values.

Close to 1 a and b value, sinusoidal error This is a set of measurements that is desired, because it can be compared with the fitting curve. If the error is examined, a sinusoidal term can be distinguished. The cause of this error could be a deviation in applied pressure caused by the syringe pump. It would be very interesting to research this behaviour more extensively and see whether the sinusoidal term is changing when using another (syringe) pump.

Negative b value A concentration propagation with a high peak followed by a gradual decrease can arise when the feed liquid is introducing a 'shock pressure' in which the feed is dispersing very fast with high pressure. This is fitted with a negative value for b in which the concentration of feed particles is at maximum at t=0 and slightly decreases. The assumption during this thesis is that particles diffuse from the high concentration channel towards the measuring area, so all measurements with a negative value for b are omitted. Further, situations containing a 'shock pressure' are not common in an OoC and can be excluded from the analysis.

Very low b value A b value that is below 0.1 indicates that particles are propagating towards the measuring channel more than a hundred times faster than is calculated. This can be an indication that the pressure could have induced liquid flow towards the measuring point and diffusion is no longer the dominating particle propagation process. This is an adverse phenomenon and therefore measurements with b values below 0.1 are not included in the analysis.

a value higher than 1 When the a value of a fit is higher than 1, this physically means that the concentration at the measuring point is expected to become higher than the concentration of the injected fluorescent fluid. This is not possible since the injected fluid is only in contact with water, thus a zero-concentration. A higher value of a can be the result of a fit with a measurement that is ascending steeply. This steep ascent can be the result of overpressure, creating fluid flow in the direction of the measuring area.

Measured concentration higher than injected concentration This phenomenon can be related to the paragraph described above. It is physically impossible to gain a higher concentration of particles in the measurement channel than is initially injected. A measuring value higher than the injected concentration can be caused by densely packed or agglomerated particles in front of the measuring area. Further it can mean that the measuring spot is positioned at an edge of the microfluidic device as the diffraction of light is different and this can be recorded with a relatively high value of intensity.

a value lower than 1 If the fitted a value is lower than one, this physically means that the concentration in the measurement channel will not reach the level of the injected concentration. This can be caused by a lower level of concentration or a lower level of fluorescent emission of each excited particle. A phenomenon known as fading or photo-bleaching causes a decrease in emission intensity in time. Photo bleaching is known to play a big role during research with Fluorescein. Thermofisher provides the graph in Figure 3.10a.

To verify the emission intensity decrease of Fluorescein a test is done in which the intensity emission of a known concentration of Fluorescein is recorded in time intervals of 30 seconds. The intensity decrease is exponential and can be seen in Figure 3.10b. In this research there is awareness on photobleaching, but as it is expected to happen for every particle, it is not assumed to elicit differences between measurements. An actual initiator of a lower concentration level in the measurement channel could be a high resistance

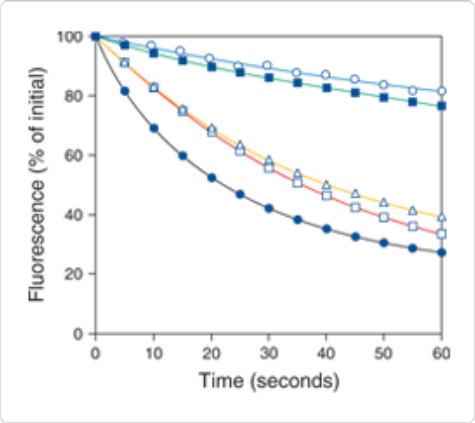

(a) Comparison of photostability of green-fluorescent antibody conjugates: Fluorescein (F2761, filled circle). [9, 16, 74].

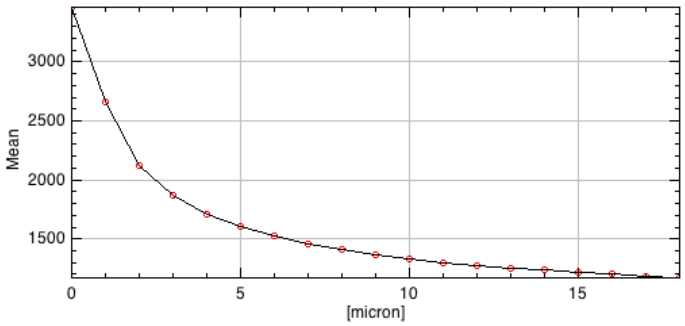

(b) Decrease of emission intensity over frames with a time frame of 50 ms, light source of 10 V and Flourescein concentration of 10^{-7} mol/l.

for particles to permeate through the membrane. A lower fitted a value could therefore be an indicator of membrane fouling.

Small peaks and dales at any place of the measurement curve Small peaks visible in the measurement curve cannot be ascribed to a certain behaviour. The unpredictable peaks look like noise and are most probably caused by small agglomerations of fluorescent particles passing the measurement area. Some measurements show more peaks over time. In this case, it is likely that the agglomerations are formed at the surface of the membrane and released when clotted together.

Non-zero concentration at the start of the experiment (t=0) When the test device is not properly flushed there is a possibility of fluorescent particles remaining at the measuring area, resulting in a non-zero measurement at t=0. A decrease in the measured curve can take place after this non-zero concentration because of the decrease in emission energy per particle in time by photo bleaching as described in Chapter 2.

Large time delay before diffusion Some measurements have a time to diffusion that is longer than expected. This is presumably due to human inaccuracy. At the beginning of every test, the device is filled with DI water from the bottom channel. When stops are placed in the end of the in- and outlet of the bottom channel too fast, extra pressure is built up causing a water flow towards or in the upper channel, creating a bigger volume with a small concentration of particles.

Shift in curve In the last measurement set in the analysis (Appendix G), the fit is proved to perform better whenever the measurement curve is shifted towards a zero value at t=0. The shift in the curve is mostly because of a time delay and/or a non-zero concentration at t=0. Both are explained above.

In summary Based on the description in the foregoing paragraph, the boundaries to include experiments in the analysis are 0-3 for the a value, 0.1-10 for the b value and a residual norm of maximally 0.5. All phenomena described in the paragraphs before are summarized in Table 3.3. In the first set of columns each experiment is specified. The second set of columns specifies whether the experiment is included in further analysis based on its values for a, b and the weighted resnorm. The ✓indicates that the value is within the range, ×indicates that the value is not valid and the * indicates that the value is a case of doubt. The test is not included in the analysis if one or more ×or two or more * are given and is marked with a bold font. The third set of columns outlines the frequency of earlier described phenomena, in which ✓indicates present, ×indicates absent, * indicates slightly present and ∼indicates that the fitting error has a sinusoidal shape.

Correlations between follow-up measurements Looking at the graphs composed out of the Glycine experiments, each set of up-following measurements shows an increase of b over each cycle. As stated earlier, an increase of b can be an indicator of a decrease in porosity, so a sign of fouling. This, however, can only be

Table 3.3: Overview of the validity of each test and occurring phenomena. In the first set of columns each experiment is specified. The second set of columns specifies whether the experiment is included in further analysis based on its values for a, b and the weighted resnorm. The ✓indicates that the value is within the range, ×indicates that the value is not valid and the * indicates that the value is a case of doubt. The test is not included in the analysis if one or more ×or two or more * are given and is marked with a bold font. The third set of columns outlines the frequency of earlier described phenomena, in which ✓indicates present, ×indicates absent, * indicates slightly present and ∼indicates that the fitting error has a sinusoidal shape

Feed	Membrane	Test	a	b	W. resnorm	Noise peaks	$C_0 \neq 0$	Time delay	fitting error
Glycine	0.4 µm	P1	✓	✓	✓	✓	×	×	∼
		P2	✓	✓	✓	✓	×	×	∼
		P3	✓	✓	✓	✓	×	×	∼
		P4	✓	✓	×	✓	×	×	
	1 µm	P1	✓	✓	*	✓	×	×	∼
		P2	✓	×	*	✓	✓	×	
		P3	✓	✓	×	✓	×	×	
	3 µm	**P1**	×	✓	✓	✓	×	✓	
		P2	✓	✓	✓	✓	✓	×	
		P3	✓	✓	✓	✓	✓	×	
		P4	✓	×	×	✓	✓	✓	
		P5	×	✓	✓	×	✓	×	∼
	5 µm	**P1**	✓	×	×	✓	×	×	
		P2	✓	✓	✓	*	✓	×	∼
		P3	✓	✓	✓	✓	×	×	
		P4	*	*	✓	✓	✓	✓	
		P5	*	✓	*	*	×	×	
BSA	0.4 µm	P1	✓	✓	✓	*	×	×	
		P2	✓	✓	✓	×	✓	×	∼
		P3	✓	✓	✓	✓	×	×	
		P4	×	✓	✓	✓	×	×	
		P5	✓	✓	✓	*	*	×	
	1 µm	P1	✓	✓	✓	✓	×	×	∼
		P2	✓	✓	✓	*	✓	✓	
		P3	×	×	×	✓	✓	×	
		P4	×	✓	✓	*	×	×	∼
		P5	✓	✓	*	×	×	×	
	3 µm	P1	✓	✓	✓	✓	×	×	∼
		P2	✓	✓	✓	*	✓	×	∼
		P3	✓	✓	✓	*	✓	×	∼
	5 µm	**P1**	×	✓	✓	✓	×	✓	
		P2	×	*	✓	*	×	×	
		P3	✓	✓	✓	*	✓	×	
		P4	✓	*	*	×	✓	×	
		P4 S	✓	✓	✓	×	×	×	∼

Table 3.4: Overview of the change in *a* and *b* value

Feed	Membrane	variable	1-2	factor	2-3	factor	3-4	factor	4-5	factor
Glycine	0.4 µm	*a*	↗	1.08	↗	2.08				
		b	↗	1.46	↗	1.87				
	1 µm	*a*								
		b								
	3 µm	*a*			↗	3.80				
		b			↗	7.14				
	5 µm	*a*			↘	0.43				
		b			↗	1.45				
BSA	0.4 µm	*a*	↗	1.88	↘	0.52	[		↘]	0.53
		b	↗	1.91	↘	0.62	[		↘]	0.74
	1 µm	*a*	↗	4.89						
		b	↘	0.75						
	3 µm	*a*	↘	0.21	↗	2.77				
		b	↘	0.54	↗	1.74				
	5 µm	*a*					↘	0.39		
		b					↗	0.50		

stated when *a* has a constant value, which is not the case. A decreasing *a* value can indicate that particles do not permeate through the membrane, but the combination of decreasing *a* and increasing *b* is only seen in the set of measurement cycles of a test-device with a 5 µm pore size membrane. When looking at the graphs of the BSA measurements, there is not any distinguishable pattern in up-following measurements. Table 3.4 is composed to create an oversight on possible patterns regarding cycle number and factor of increase. Also this graph does not result in any discovered patterns. Comparing the propagation of *a* and *b* for each pore size and type of feed, no distinct patterns are observed for follow up measurements. Therefore no correlations can be drawn for *a* and *b* with cycle number. This physically means that it is not possible to distinguish fouling using multiple measurement cycles. It is possible that any effect of fouling is flushed away during a cleaning cycle.

Uncertainty The dynamic experiments are repeated with the test devices for maximally 5 times. Testing for one flow cell with five test cycles had a duration of five days. For this reason, only one flow cell containing each specific membrane for diffusion with each specific particle type is tested and the production and testing is not repeated to check for repeatability. Therefore, the repeatability and accuracy of these tests is not known and it is uncertain whether the different measurements are a case of standard deviation or a significant pattern.

A

Initial qualitative test

The quantitative test was planned to arise as follows:

1. Bottom channel is injected with water at a flow rate of 1 μl/ min.
2. After 1 hour, an injection is added in the the top channel. This is injected with a specific solution at a flow rate of 1 μl/ min.
   At this point, both the channels will be experiencing a flow rate.
3. Microfluidic device is placed on the inverted fluorescent microscope.

The following assumptions are done on beforehand:

- There is no liquid flux through the membrane; pure diffusion
- The membrane pores foul after a period of time.

The diffusional pattern that was expected to show during the measurements is visualised in 6 situations in Figure A.1. It is not clear whether and when the sixth situation and thus total fouling would appear, this would become clear during the tests.

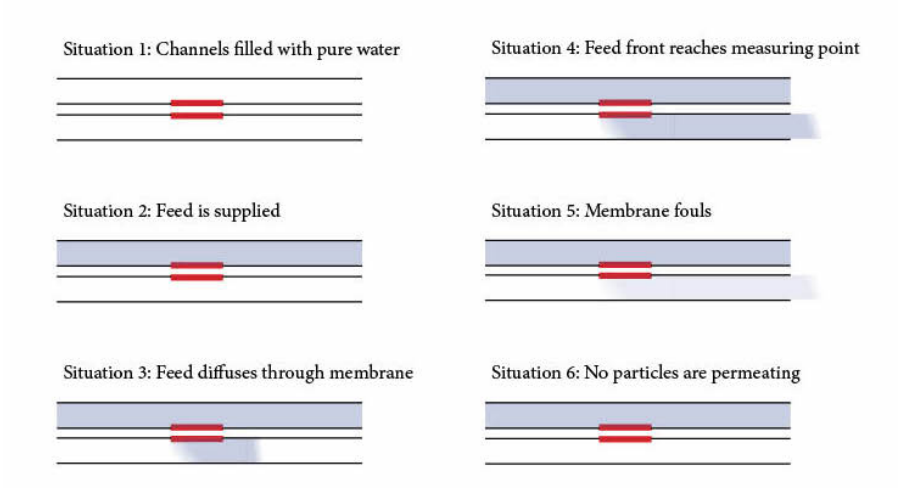

Figure A.1: The expected situations during the test.

The intensity graph of the measurement was expected to be similar to Figure A.2.

In filtering systems feed is applied with a certain pressure and the volume permeated through the membrane is measured [14], [19]. In this case the permeating concentration is constant when fouling does not

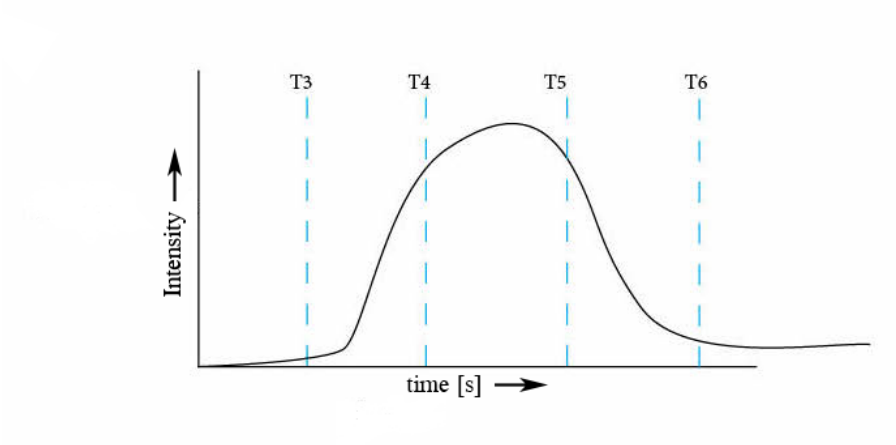

Figure A.2: The expected situations during the test.

occur and decreases when fouling occurs. The most important area's to look at are the duration of the maximum intensity value and the slope with which this intensity decreases in between situation 5 and 6. Now, 6 is defined as the point where the membrane is clogged, but due to the cross-flow applied there could also be an equilibrium between fouling forming and removal, so the permeation of particles through the membrane does not become zero.

As the assumption is done that there will be no flux through the membrane, diffusion of particles can be measured by comparison with a zero diffusion image at t=0.

A.1. Problems

Unfortunately, the microfluidic system did not behave perfectly: liquid follows the path of least resistance and therefore most of the time there was an outflow at only one of the two outlets. This resulted in the fact that either all of the liquid was flowing through the measurement channel or all was flowing out of the upper outlet. For this reason, the decision is made to apply a flowrate at only one channel at a time.

B

Schematic drawings

Dimensions and details are important to have clearly documented for reproduction of devices. Therefore, this chapter contains all dimensional drawings of the test devices produced.

B.1. Molds for PDMS test device

The molds are 3D printed with the high resolution 3D printer of Envisiontech. The CAD models have dimensions visible in Figures B.1 and B.2.

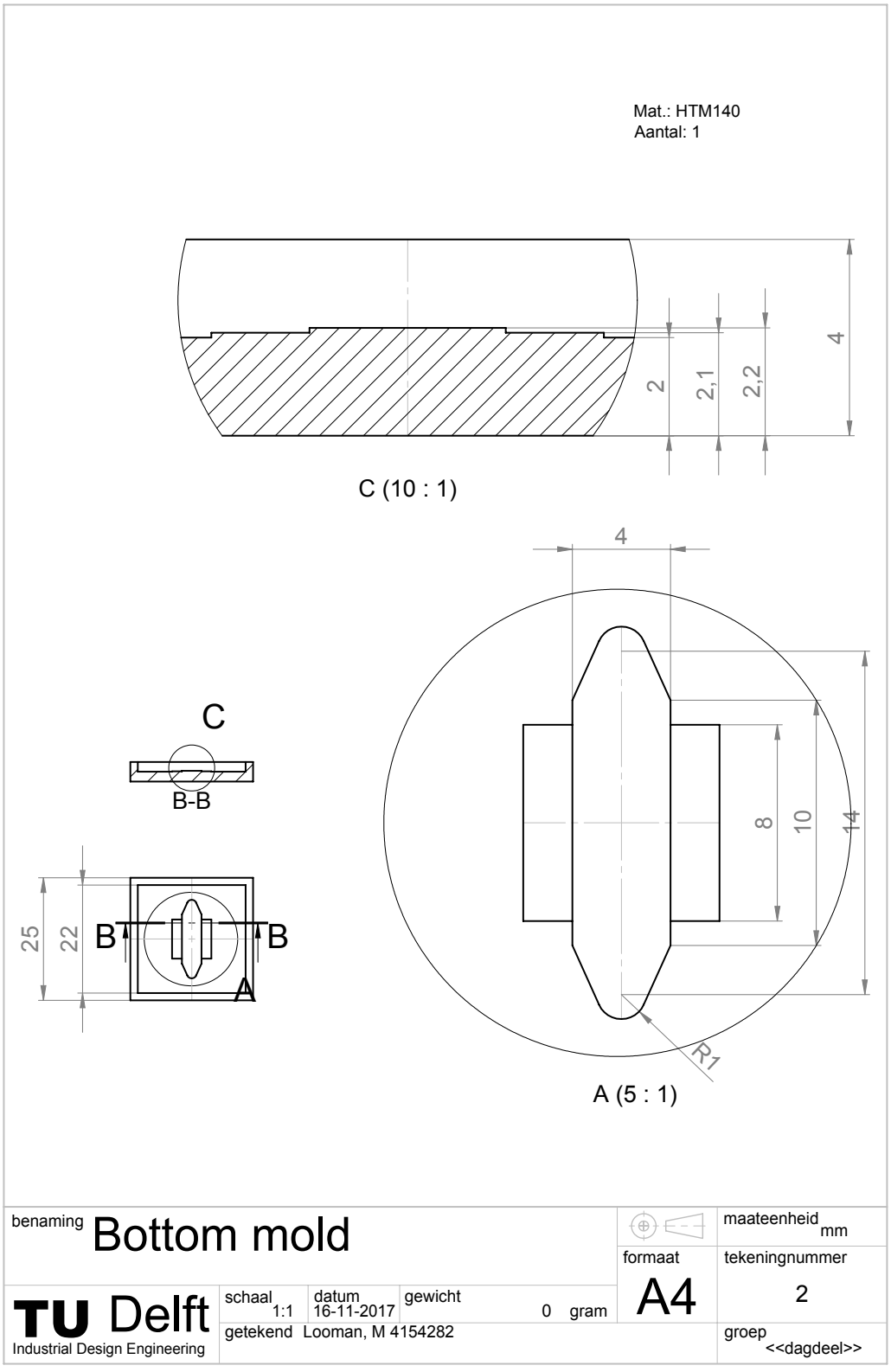

Figure B.1: Dimensional drawing of the bottom mold.

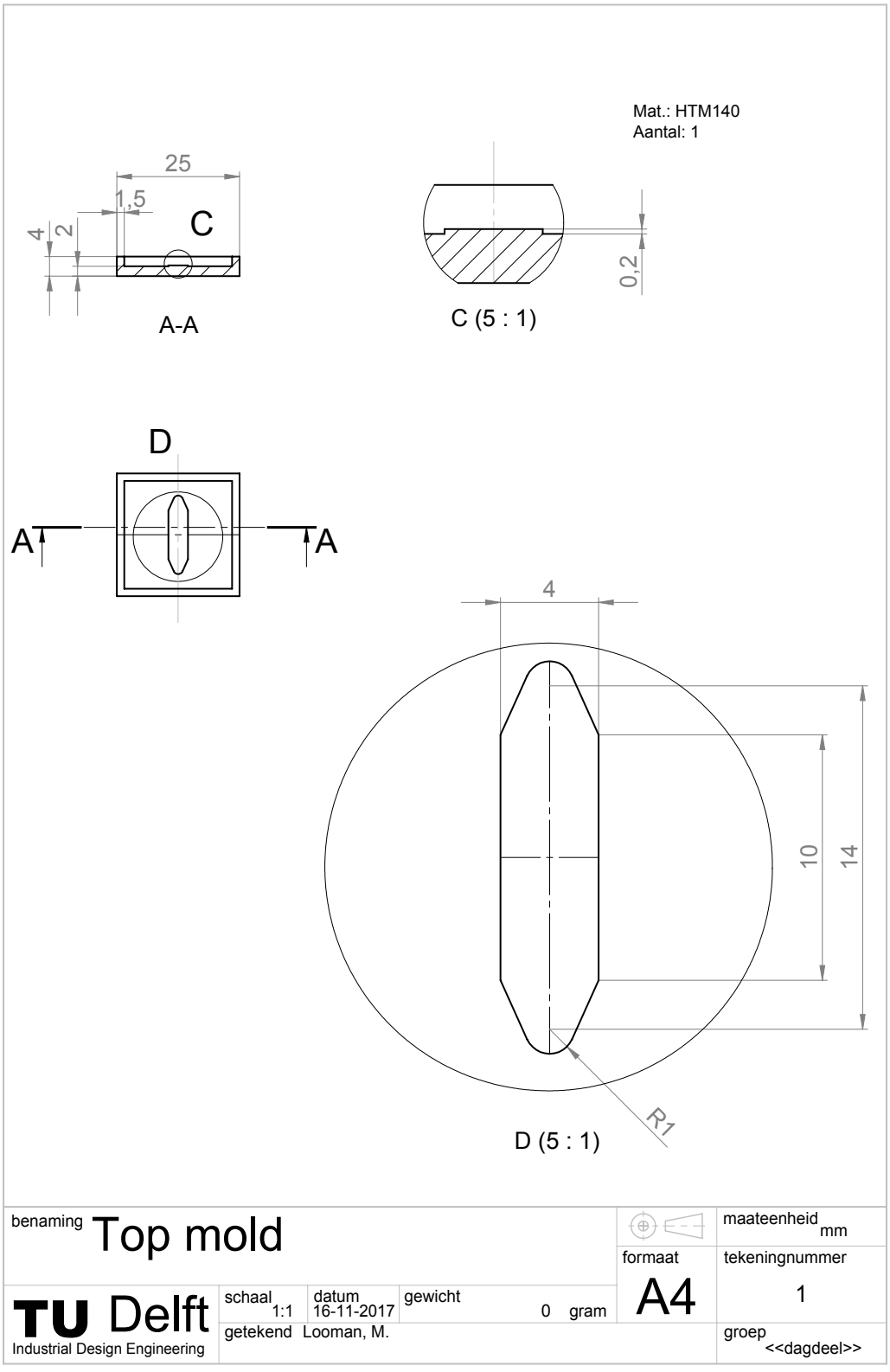

Figure B.2: Dimensional drawing of the top mold.

C

Operation and protocols

Protocols are composed to increase the repeatability of an experiment, analysis or production process. During this research a method is developed to produce a microfluidic device clamping a membrane. This appendix is meant for knowledge transfer and therefore contains every protocol that is needed to produce a microfluidic flow cell and to re-execute the experiments described throughout the thesis work. This Chapter is ordered chronologically and follows several production steps before describing the final testing protocols. Every protocol begins with a list of materials that are required for execution of the protocol. Then every step is explained and the protocol ends with tips and tricks during the process.

C.1. Step 1: Production of Components

First of all the components need to be produced before the microfluidic system can be assembled.

C.1.1. Adhesive layer production

The adhesive layer needs high precision in cutting and is therefore cut with a laser cutter of OPTEC. As the adhesive layer must be cut in rectangular forms, the forms are drawn in Autocad and can be uploaded to the laser. The settings are optimised for lasercutting the adhesive layer and are given in Table C.1.

Tip Make sure that the adhesive layer is clean/dust free before and after cutting: clean the laser-cut shapes with a cleanroom wipe with ethanol

C.1.2. Membrane cutting (straight cut)

Membranes are delivered in patches and have to be cut in the right dimensions. This is done by hand with a rectangular tool that is produced with the Envisiontech 3D printer as described in the section below. The dimensions of the cutting tool are 40x40x10 mm.

List of tooling The following items are required for membrane cutting:

- Piece of plastic with desired 2D shape (in my case 3D printed)
- Straight knife

Table C.1: Settings used for lasercutting the adhesive layer.

Laser		**Process**	
Diode current (A)	6.44	Drill numbers	4
Speed (mm/s)	20	Drilling Step (um)	20
Jump Speed	200	Number of levels	1
Laser Firing Rate (KHz)	50	Z Step (um)	60
Laser Power (%)	20	Repetitions	75

- Membrane material
- Clean cutting plate

Steps of execution The steps are as follows:

- Place the membrane on the cutting plate
- Place the shaped piece of plastic on the membrane as if it is a mold
- Side by side cut the membrane along the sides of the plastic piece.

Tip Only use the shaping piece as a folding ruler and do not press on the membrane. This is prone to deform or damage.

C.1.3. Mold production

The production of the mold is executed with a high resolution stereo-lithography 3D printer of Envisiontech. A CAD model must be imported in Magics, placed at a position within the possible printing area and supports must be generated. The maximal dimensions of the surface on which objects can be printed are 25x40 mm. Then, the part and supports are saved and must be edited in Perfactory RP software to create a folder with images of all separate consecutive layers. The resolution of the 3D printer is 25, 50 or 100 μm depending on the chosen resin and layer thickness. The mold for the test device is printed with HTM140 with 25 μm thick layers. Because the Envisiontech uses inverted 3D printing, bubbles are more easily trapped within a structure. Two ways to diminish bubble forming that are applied during this research are to fill the reservoir of the resin until 1/3 to 1/2 (not less) and to pipet bubbles existing before printing out of the resin.

After 3D printing, the resin is removed through desiccating the print in isopropanol for two minutes and curing the resin with 2 light sources in the UV curing machine for two minutes.

Tip The minimum distance of a channel to the edge of the mold must be 5 millimetres. When this becomes smaller, there will be a big chance of cutting of the channel when removing the PDMS from the mold.

C.1.4. PDMS production

Once the mold is completed, PDMS casting can take place. The proportion PDMS:curing agent is 10:1 and per mold 2 gram of PDMS is sufficient to produce a good cast. After degassing for half an hour to remove bubbles in the PDMS, the molds are baked at 70 °C for 1 hour to cure the PDMS. Detaching the PDMS of the mold becomes harder as the amount of relief in the mold increases. As a solution for PDMS sticking on the mold, a few droplets of Ethanol are added. The in- and outlet holes are created with a 0.58/0.97 inner/outer diameter hollow needle. The needle needs to be pushed in gently, because the risks of cracks in the PDMS is high. To enlarge the reproducibility, a guide has been made with crosses indicating the location of punching (Figure C.1).

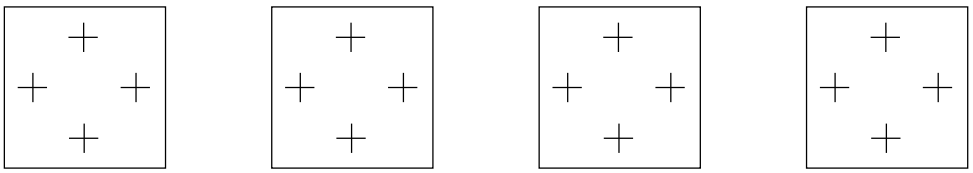

Figure C.1: Guidelines for punching in- and outlets.

List of tooling The following items are required for PDMS production:

- Mold with inverted form of the desired channel

- Big petri glass
- Rearing stick
- Timer (set for 5 minutes)
- Pipette
- PDMS and curing agent
- Weighing machine
- Desiccator
- Oven
- Ethanol
- Hollow needle 0.58/0.97 mm inner-/outer diameter

Steps of execution The steps are as follows:

- Make sure the mold is properly cleaned. Otherwise execute the mold cleaning protocol.
- Mix PDMS and curing agent in proportion 10:1 (about 2:0.2 gr per mold) for 5 minutes with a rearing stick
- Poor the PDMS inside the mold
- Degas in the desiccator for 30 minutes

  Stop the pump and release pressure after 10 and 20 minutes. This fastens the degassing process.
- Bake at 70°C for 1 hour
- Cut the sides of the PDMS loose from the mold

  Add a few droplets of Ethanol under the loose PDMS to enhance loosening.
- Create in- and outlets in the PDMS with a hollow needle

Tip Make sure that the mold is properly filled. This way, the PDMS layer will be most probably the most straight.

C.1.5. Cleaning of HTM140 molds

In order to be able to use the HTM140 molds multiple times, the molds can be cleaned after use.

List of tooling The following items are required for mold cleaning:

- A glass beaker
- Tweezers
- Ethanol
- Aceton
- IPA
- ultrasonicator
- Drying pistol
- Dastex cleanroom wipes

Steps of execution The procedure that is needed for cleaning is as follows:

- Remove all big pieces of PDMS with tweezers
- Cleaning step 1

  Place the mold inside a beaker

  Fill the beaker with Ethanol

  Place the beaker in the ultrasonicator for 2 minutes

  Dry the mold with towels and a drying pistol
- Repeat *Cleaning step 1* with Aceton
- Repeat *Cleaning step 1* with IPA

C.2. Step 2: Composition of microfluidic system

List of tooling The following items are required for PDMS production:

- Tweezers with sharp tips
- Tweezers with blunt tips
- PDMS layers
- Lasercut adhesive layers
- Membrane in the desired shape

Steps of execution The steps are as follows:

- Execute oxygen plasma treatment on the PDMS
- Remove one of the non-sticking sides around the adhesive layer (sharp tip tweezers)
- Place the adhesive layer very accurately on both PDMS sides (sharp tip tweezers)
- Remove the non-sticking layer from the other side of the adhesive layer (sharp tip tweezers)
- Press the membrane on the bottom layer of PDMS (blunt tip tweezers)
- Attach 2 PDMS layers on each other

Tip Try to attach the membrane as tight as possible to prevent membrane bending.

C.3. Step 3: Testing

List of tooling The following items are required for testing:

- Deionized water
- Labeled feed, mixed in the right concentration
- Syringe pump
- Tubing set with an inner- and outer diameter of 0.58 and 0.97 mm respectively
- Fluorescence microscope

Steps of execution The steps are as follows:

- Connect tubing set to device
- Let the DI water fill the microfluidic device and flow through for 60 minutes
- Connect tubing to test liquid
- Put on fluorescence microscope
- Place the microfluidic device on the microscope and focus on the lower channel on the point in the middle, right after the membrane
- Inject test device for 4 hours
- Take snapshots of the measuring spot at desired time frames
- After tests cut loose the membrane and analyse with an SEM

C.4. Static fouling analysis

The static fouling analysis contains only few steps. As this is done to test all of the membranes on fouling with a certain foulant, one needs to be sure to have the same concentration everywhere.

List of tooling The following items are required for the analysis:

- Deionized water
- Labeled feed, mixed in the right concentration
- A pipette, able to suspend 50 microliter.
- Membranes that need to be tested
- 2 plastic boxes, divided in compartments.

Steps of execution The steps are as follows:

- Make sure the pipette is adjusted to suspend 50 microliter.
- Dispense a pattern of 3 droplets of DI water inside 6 compartments in one of the boxes (6 types of membrane to be tested)
- Place 3 membranes of one type of membrane in one of the compartments; one membrane on each droplet
- Dispense 50 micro litre of dissolved feed over every membrane
- After 1 hour take one membrane per compartment out of the box and let it dry in the other plastic box
- After 1 day take one membrane per compartment out of the box and let it dry in the other plastic box
- After 1 week take one membrane per compartment out of the box and let it dry in the other plastic box

Tip Be sure to classify the first as well as the second box and write down the membrane type and time of 'soaking' per compartment

C.5. Step 4: SEM Analysis and image processing

List of tooling Both the SEM analysis and image processing do not need a lot of hardware, but more software. That is why software is also included in this list:

- Sputtercoater
- SEM
- Supportive programme to image with the SEM
- FIJI (also known as ImageJ)

Steps of execution The steps are as follows:

- Sputter-coat the membrane with a 2nm layer of Gold
- Image the membranes with SEM
- Pore sizes can be analysed with FIJI:
- Open the desired image in FIJI
- Select line drawing and draw a horizontal line over the length of the scale bar
- Analyze –> Set Scale...
- Use the value under the scale bar to fill in *Known distance* and *Unit of length*
- Image –> Adjust –> Treshold...
- Set the values for treshold so that the pores are distinguished from the membrane surface and press *Apply*
- Analyze –> Analyze particles...
- Fill in the range of area of the particles that you expect to see in *Size* and the circularity in *circularity* (this last one is mostly trial and error) and press *Ok*.
- Fiji will provide a table with measured particles/pores

Tip Be smart and cut the membrane in half before use. Whenever it gets lost or broken, there will be another part of the membrane left.

Tip Try to image the pores perpendicularly and not under an angle: otherwise the measurements are not valid.

Tip If there is a process which is the same for multiple images, a Macro can be written in FIJI.

D

Calibration of measured intensities and particle concentrations

The settings used for imaging with the fluorescence microscope in combination with the light exposure and filter influence the intensity values imaged with the microscope and measured with ImageJ. For this reason, calibrations are done both for Glycine and BSA. Preceding to the calibration, test tubes are prepared with a range of concentrations of Glycine and BSA in deionized water. The calibration is done with a calibration device, shown schematically in Figure D.1a, which consists of a glass plate and a PDMS layer with a channel of the same dimensions as the test device. The calibration itself is done by injecting a certain concentration of fluids into the calibration channel and after injection imaging the light emission with the microscope.

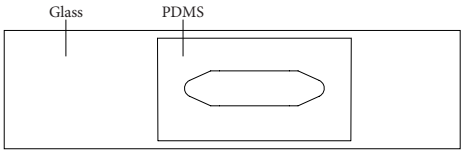

(a) Illustration of the calibration device.

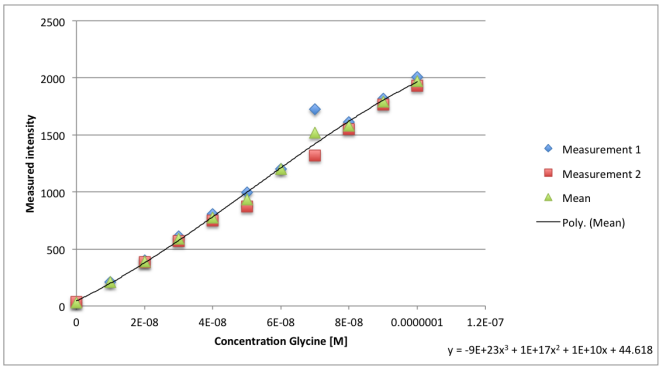

(b) Calibration graph for Glycine measured and fitted with a 3rd degree polynomial

The measurements are started at zero concentration and are measured in increasing concentration. After imaging, the mean intensity per frame is determined with ImageJ and feed concentrations can be coupled to intensity values. The obtained values are fitted with polynomial curve fitting as the detection limits of the microscope give a restriction in measurable concentration. Fitting gives Equation D.1 for calibration with Glycine and Equation D.2 for calibration with BSA. In these equations, C is the dimensionless concentration of fluorescent particles in the solution, calculated by dividing the calibration concentration, $C_{\text{calibration}}$ with the concentration of particles used during the experiments, C_{exp}.

$$I_G = 945.99C_G^3 + 1450C_G^2 + 1415.7C_G + 44.618 \tag{D.1}$$

$$I_{BSA} = -445.51C_{BSA}^3 + 721.17C_{BSA}^2 + 1151.3C_{BSA} + 29.757 \tag{D.2}$$

The calibration is executed for concentrations up to 10^{-7} [M] and because is not known whether a curve fit with polynomials is correct, the curve progression for larger concentrations cannot be predicted by the fitted equation. Therefore, during this research only interpolation will take place within the calibrated window and extrapolation or predictions are not done.

Limit of detection Every fluorescence microscope has its detection limits. With a determined light source and frame time settings, the intensity of light emitted by the fluorescent medium reaches a point where the recorded image does not change when increasing particle concentration. This detection limit causes a asymptote in the calibration curve. During the experiments, the upper limit of detection is not reached and the lower limit of detection is considered to be of minimal impact.

E

Problem solving: plasma cleaner

The plasma cleaner did not bond with the treatments that are normally used for PDMS. Bonding inside a plasma cleaner is affected by three factors:

- PDMS
- Settings
- Plasma cleaner

During the production of a PDMS device, the PDMS is, in this process, casted and cured at 70 °C for 1 hour. It could be that the PDMS is not completely cured then and that this causes problems in the bonding. Therefore several curing processes are executed and tested for bonding after plasma treatment.

Further, the settings of the machine could be different for the specific PDMS casts. Therefore, the plasma cleaning time, pressure and power are variated and tested for amount of bonding. Table E.1 shows the different values that are tested for the PDMS curing process and the bonding settings. the different settings and processes are combined, but none of the combinations resulted in proper bonding.

Table E.1: Variables used for bonding check

PDMS curing process		**Bonding settings**		
Temperature [°C]	Time [h]	Power [Watt]	Time [min]	Pressure [mbar]
60	1	60	1	0.4
70	3	90	1	0.4
70, 150	3, 12	60	3	0.4
		60	1	0.6

Because both the settings and the curing process of the PDMS shown in Table E.1 did not result in good bonding, I have tried to bond the PDMS layers in another plasma bonder available at the applied labs of the Technical University of Delft. Here, one plasma cleaner is used only to bond PDMS. The settings that are used to bond with this machine are maximum power (Wim van Oordt did not know what was exactly this power), bonding for 2:20 min at a pressure of 7 mbar, followed by baking in the oven at 70 °C for 15 minutes. The machine was perfectly able to bond our PDMS samples and in consultation with Bhattacharya et al. [10] the conclusion is drawn that the previous bonding trials with the machine at the faculty of 3mE did not reach a high enough pressure to effectively bond.

In order to use the plasma cleaner available at the faculty, one must make sure to bond for **3 minutes** with a power of **60 Watt** at **4 mbar**. This pressure can be reached by first pumping down to a pressure of 0.3 mbar and then almost fully open the gas valve to increase the pressure.

F

Static analysis

During the stationary experiment, membranes are put into a solution of Glycine, BSA and λ-DNA for an hour, a day and a week to verify whether the feed particles adhere to the membrane in a stationary situation.

The membranes are dried and imaged with the SEM and afterwards analysed with Fiji to distinguish the remaining pore size and amount of pores. This is described more in depth in Chapter 3.1.

In this chapter, the data assembled with Fiji is presented and described. Further, interpretations are done on the applying fouling principles and a discussion is included. Correlations of pore size and feed particle with fouling are analysed in the last section.

F.1. Data processing

Every treated membrane is imaged nine times, thus the pore size is averaged and contains a standard deviation over nine measurements for each prepared membrane. The amount of pores is first summed for the three magnifications at one position and the average and standard deviation over the three measurement positions is displayed. In the graphs, the values for pore area and amount of pores are normalised with the mean value of the reference membrane: A_{meas}/A_{ref} and N_{meas}/N_{ref}. To keep a good oversight, the axes for duration of fouling are not shown in proportion of hours. Therefore with the eye only a conclusion can be drawn on whether a correlation is positive or negative and not whether the correlation is linear, quadratically or exponentially. The static fouling experiments are not repeated, so the standard error of the mean cannot be calculated for each pore size. However, to check for a correlation of pore size and area over track-etched membranes in general, the measurements on the membranes with different pore sizes can be taken together and each membrane can be seen as a sample. This way, the error of the mean is calculated.
A measure for pore area and amount of pores could not be identified for the SEM images of the PVDF and MCE membranes, so these are omitted from the analysis. An important note for the next subsections is that every graph shows data of 9 images from which multiple pores are analysed. The data points in the graphs are mean values of the measurements and the error bars indicate a standard deviation of this mean, unless explained otherwise in the subsection. The mean values are connected by a dashed line to guide the eye.

F.1.1. Glycine fouling, 0.4 µm pore size

Figure F.1a and F.1b show the change in pore area and amount of pores respectively after fouling for 1 hour, 1 day and 1 week. When looking at Glycine fouling at a membrane with a 0.4 µm pore size, no significant pore size decrease is measured. For the amount of pores measured, the standard deviation is too high to draw a conclusion on the change over fouling time.

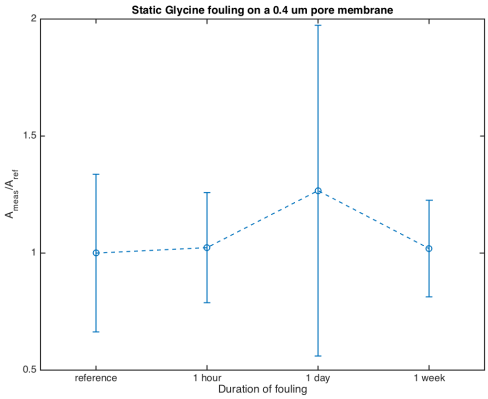

(a)

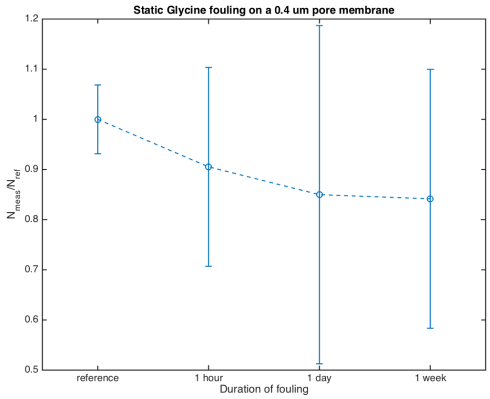

(b)

Figure F.1: Fouling of a 0.4 µm pore size membrane with Glycine over time: mean values of a) pore area and b) number of pores measured for fouling with Glycine. The values are normalised with values measured for a reference membrane. The error bars indicate the standard deviation of the mean and the dashed line is meant to guide the eye.

F.1.2. Glycine fouling, 1 µm pore size

Figure F.2a and F.2b show the change in pore area and amount of pores respectively after fouling for 1 hour, 1 day and 1 week. When looking at Glycine fouling at a membrane with a 1 µm pore size, no conclusion can be drawn on the change of pore area in fouling time because of the high standard deviation. However, a significant decrease in measured amount of pores is visible after 1 hour of fouling. This physically means that a cake layer of Glycine has covered the pores of the membrane.

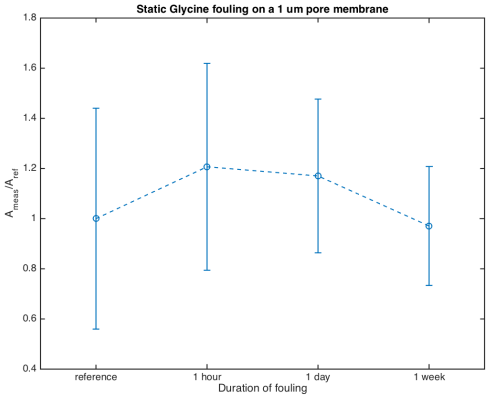

(a)

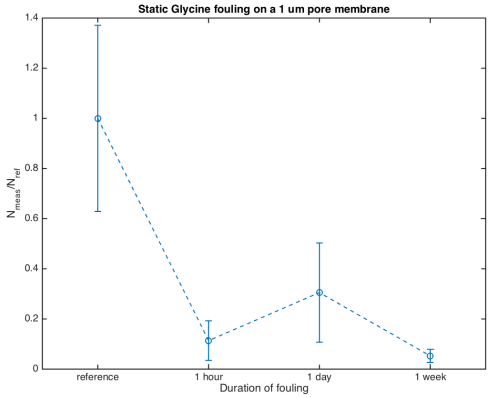

(b)

Figure F.2: Fouling of a 1 µm pore size membrane with Glycine over time: mean values of a) pore area and b) number of pores measured for fouling with Glycine. The values are normalised with values measured for a reference membrane. The error bars indicate the standard deviation of the mean and the dashed line is meant to guide the eye.

F.1.3. Glycine fouling, 3 µm pore size

Figure F.3a and F.3b show the change in pore area and amount of pores respectively after fouling for 1 hour, 1 day and 1 week. When looking at Glycine fouling at a membrane with a 3 µm pore size, pore area has a negative correlation with the period of fouling. If looking at the measured amount of pores over duration of fouling, the Graph does also show a negative correlation. However both graphs show a relatively large standard deviation.

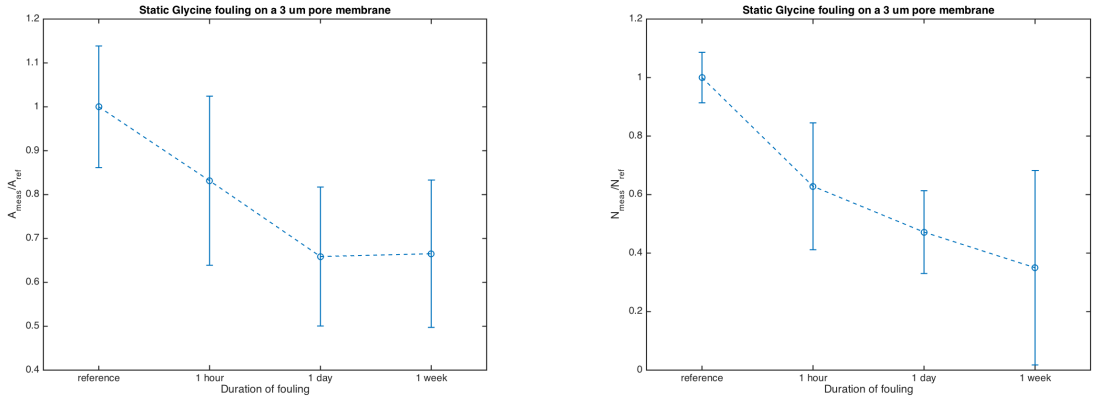

(a) (b)

Figure F.3: Fouling of a 3 µm pore size membrane with Glycine over time: mean values of a) pore area and b) number of pores measured for fouling with Glycine. The values are normalised with values measured for a reference membrane. The error bars indicate the standard deviation of the mean and the dashed line is meant to guide the eye.

F.1.4. Glycine fouling, 5 µm pore size

Figure F.4a and F.4b show the change in pore area and amount of pores respectively after fouling for 1 hour, 1 day and 1 week. When looking at Glycine fouling at a membrane with a 5 µm pore size, no significant correlations are distinguishable for either pore area or amount of pores measured over duration of fouling.

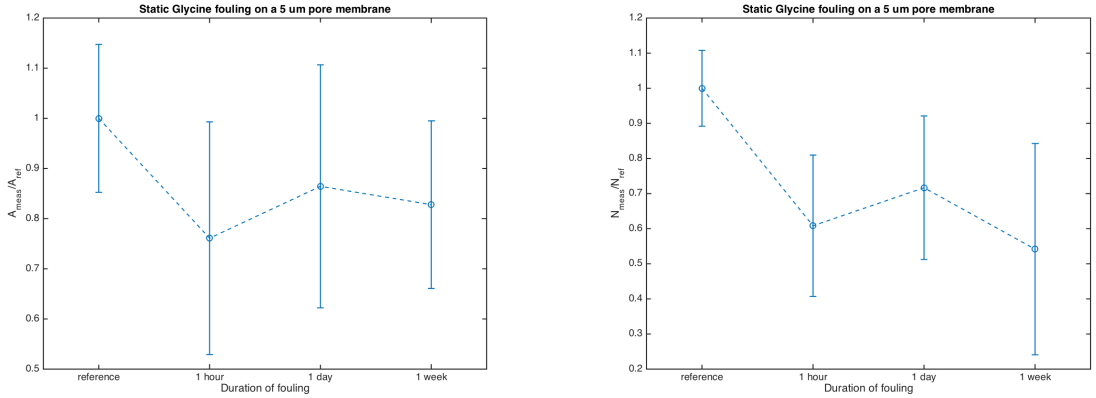

(a) (b)

Figure F.4: Fouling of a 5 µm pore size membrane with Glycine over time: mean values of a) pore area and b) number of pores measured for fouling with Glycine. The values are normalised with values measured for a reference membrane. The error bars indicate the standard deviation of the mean and the dashed line is meant to guide the eye.

F.1.5. BSA fouling, 0.4 µm pore size

Figure F.5a and F.5b show the change in pore area and amount of pores respectively after fouling for 1 hour, 1 day and 1 week. When looking at BSA fouling at a membrane with a 0.4 µm pore size, the standard deviation of the data is too high to draw a conclusion on the correlation of pore area with the duration of fouling.

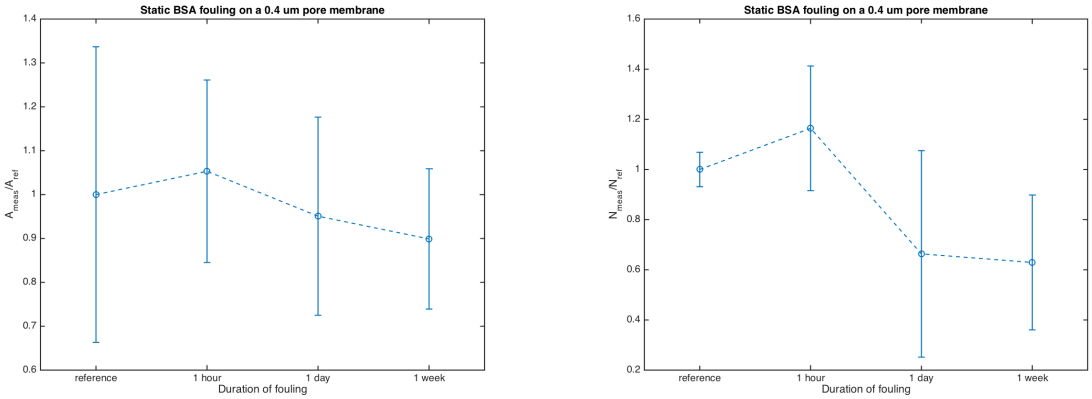

(a) (b)

Figure F.5: Fouling of a 0.4 µm pore size membrane with BSA over time: mean values of a) pore area and b) number of pores measured for fouling with BSA. The values are normalised with values measured for a reference membrane. The error bars indicate the standard deviation of the mean and the dashed line is meant to guide the eye.

F.1.6. BSA fouling, 1 µm pore size

Figure F.6a and F.6b show the change in pore area and amount of pores respectively after fouling for 1 hour, 1 day and 1 week. The mean pore area is decreasing with fouling duration, but the relatively large standard deviation leads to an invalid conclusion about the correlation of pore area and duration of fouling. Further, the measured amount of pores does not show a logical or consistent behaviour and no conclusions can be drawn due to the large standard deviation.

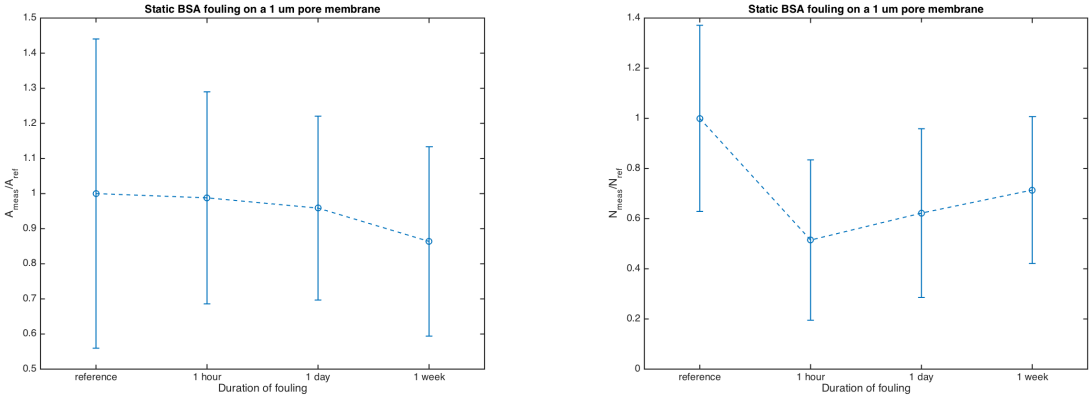

(a) (b)

Figure F.6: Fouling of a 1 µm pore size membrane with BSA over time: mean values of a) pore area and b) number of pores measured for fouling with BSA. The values are normalised with values measured for a reference membrane. The error bars indicate the standard deviation of the mean and the dashed line is meant to guide the eye.

F.1.7. BSA fouling, 3 µm pore size

Figure F.7a and F.7b show the change in pore area and amount of pores respectively after fouling for 1 hour, 1 day and 1 week. For BSA fouling on a membrane with a 3 µm pore size, a negative correlation between pore area and duration of fouling is possible. However, the standard deviation is high, so conclusions on the correlation can not be drawn with certainty. Further the mean amount of pores decreases with fouling time, but the decrease in pore area is only significant after 1 day.

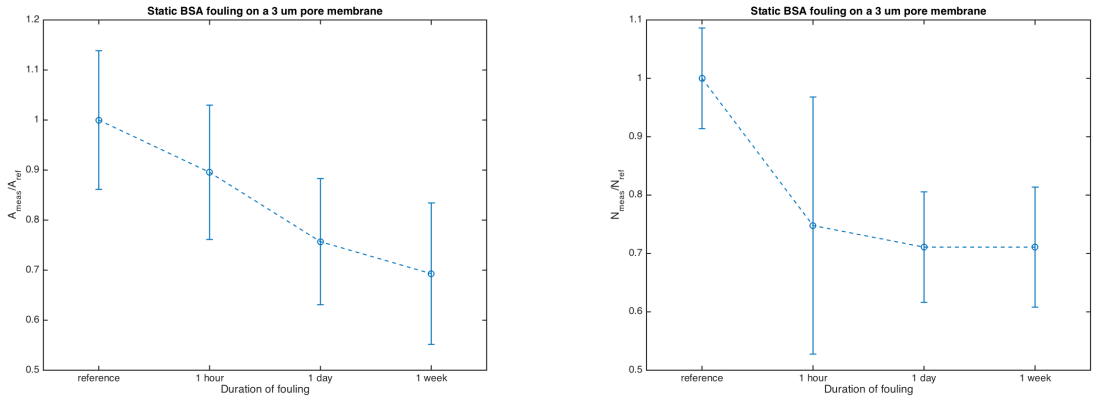

(a) (b)

Figure F.7: Fouling of a 3 µm pore size membrane with BSA over time: mean values of a) pore area and b) number of pores measured for fouling with BSA. The values are normalised with values measured for a reference membrane. The error bars indicate the standard deviation of the mean and the dashed line is meant to guide the eye.

F.1.8. BSA fouling, 5 µm pore size

Figure F.8a and F.8b show the change in pore area and amount of pores respectively after fouling for 1 hour, 1 day and 1 week. For both the measured pore area and amount of pores, the standard deviation is too high to draw a conclusion on the correlation with the duration of fouling.

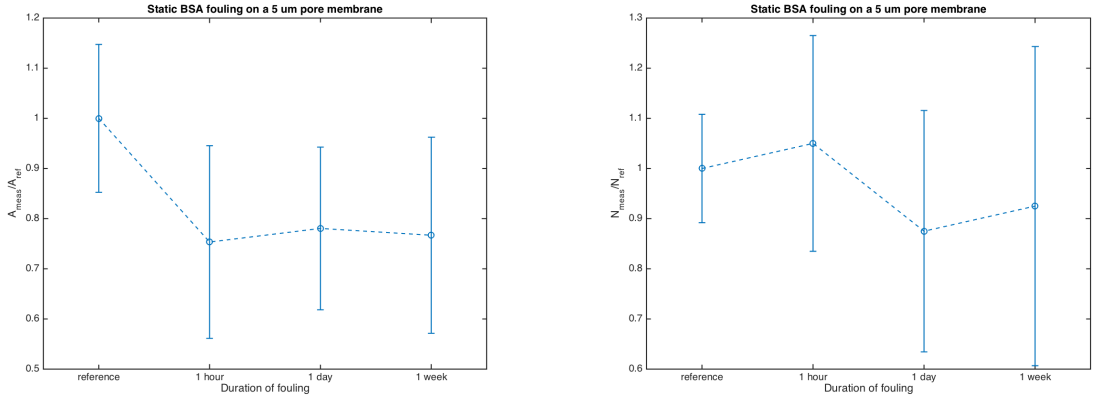

(a) (b)

Figure F.8: Fouling of a 5 µm pore size membrane with BSA over time: mean values of a) pore area and b) number of pores measured for fouling with BSA. The values are normalised with values measured for a reference membrane. The error bars indicate the standard deviation of the mean and the dashed line is meant to guide the eye.

F.1.9. λ-DNA fouling, 0.4 µm pore size

Figure F.9a and F.9b show the change in pore area and amount of pores respectively after fouling for 1 hour, 1 day and 1 week. There is no significant measured change in pore area over fouling duration, but when looking at the correlation of amount of pores with duration of fouling, a negative correlation is seen during the first day of fouling. It is not clear whether the amount of particles forming a cake layer increases after the first day as the total area of the membrane could already be covered with a cake layer (normalised amount of pores is close to zero).

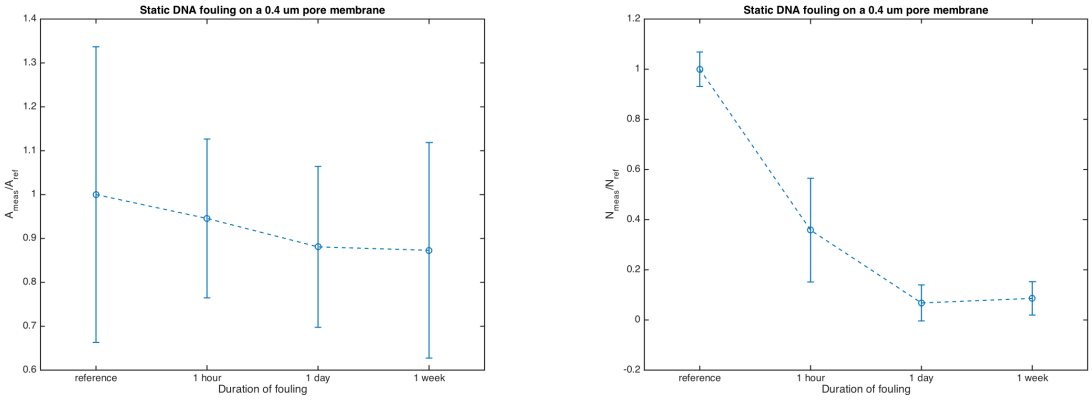

(a) (b)

Figure F.9: Fouling of a 0.4 µm pore size membrane with DNA over time: mean values of a) pore area and b) number of pores measured for fouling with DNA. The values are normalised with values measured for a reference membrane. The error bars indicate the standard deviation of the mean and the dashed line is meant to guide the eye.

F.1.10. λ-DNA fouling, 1 µm pore size

Figure F.10a and F.10b show the change in normalised pore area and amount of pores respectively after fouling for 1 hour, 1 day and 1 week. The mean normalised pore area is decreasing, but the standard deviation of the mean is too high to draw a significant conclusion on a correlation. Further, the mean normalised amount of pores decreases significantly with duration of fouling. Thus can be concluded that the counted amount of pores has a negative correlation with the duration of fouling over the whole testing period. This is an indicator of cake layer formation.

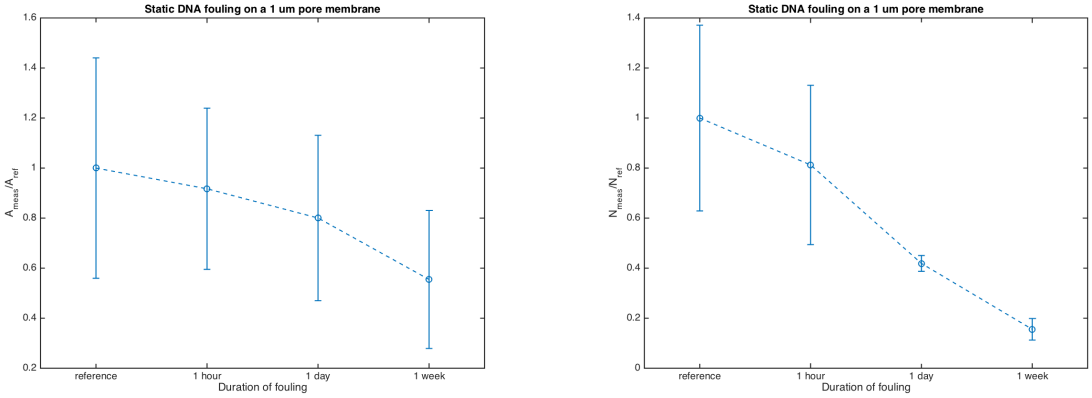

(a) (b)

Figure F.10: Fouling of a 1 µm pore size membrane with DNA over time: mean values of a) pore area and b) number of pores measured for fouling with DNA. The values are normalised with values measured for a reference membrane. The error bars indicate the standard deviation of the mean and the dashed line is meant to guide the eye.

F.1.11. λ-DNA fouling, 3 µm pore size

Figure F.11a and F.11b show the change in normalised pore area and amount of pores respectively after fouling for 1 hour, 1 day and 1 week. As can be seen at many other measurements for pore area, the mean normalised pore area decreases, but the standard deviation is too high to draw a significant conclusion. The same holds for the normalised mean amount of pores. A mean decrease is seen with duration of fouling, but the high standard deviation is obstructing a valid conclusion.

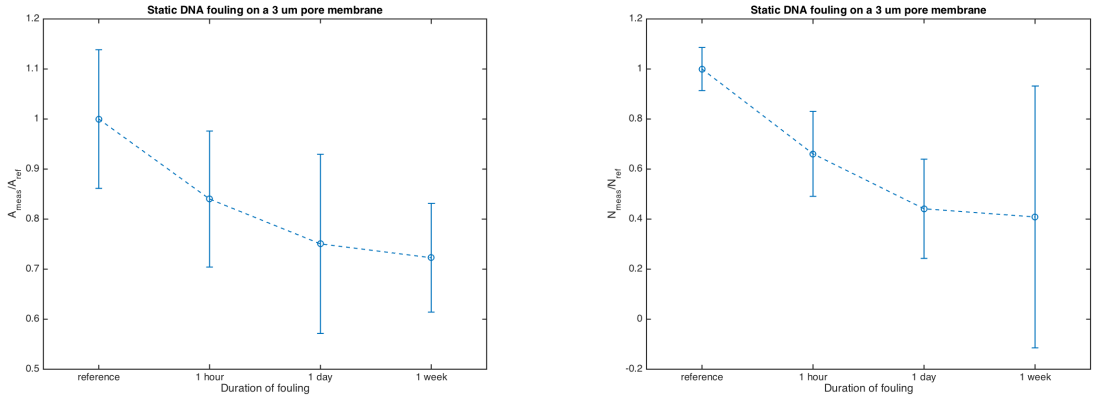

(a) (b)

Figure F.11: Fouling of a 3 µm pore size membrane with DNA over time: mean values of a) pore area and b) number of pores measured for fouling with DNA. The values are normalised with values measured for a reference membrane. The error bars indicate the standard deviation of the mean and the dashed line is meant to guide the eye.

F.1.12. λ-DNA fouling, 5 µm pore size

Figure F.12a and F.12b show the change in normalised pore area and amount of pores respectively after fouling for 1 hour, 1 day and 1 week. Both graphs show a descending mean with time. When looking at the correlation of normalised pore area with duration of fouling, the standard deviation is too high to predict the correlation over a fouling duration until one day. One can say that the mean is significantly decreased after a fouling duration of one week of fouling. Further, the normalised mean for pore count decreases significantly with a duration of fouling from one day to one week.

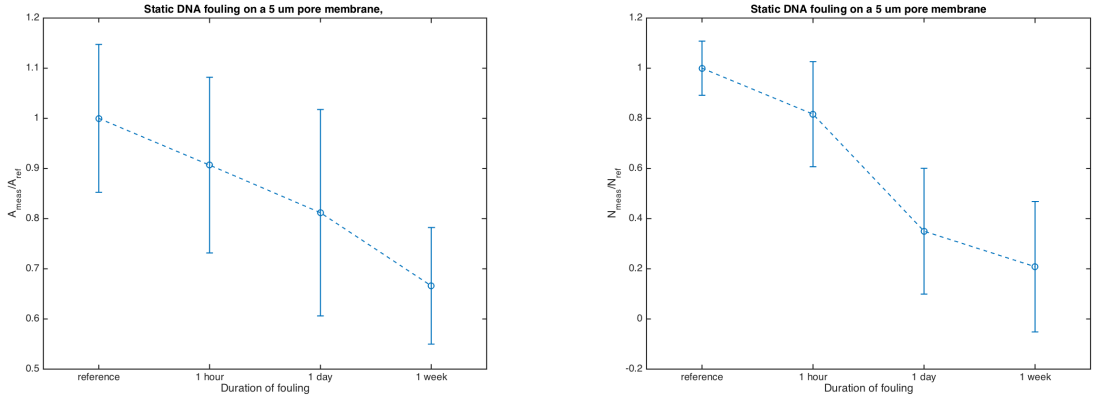

(a) (b)

Figure F.12: Fouling of a 5 µm pore size membrane with DNA over time: mean values of a) pore area and b) number of pores measured for fouling with DNA. The values are normalised with values measured for a reference membrane. The error bars indicate the standard deviation of the mean and the dashed line is meant to guide the eye.

F.2. Correlation of membrane properties with fouling

F.2.1. Fouling by Glycine

When looking at the graphs showing the change in mean normalised pore area and amount of pores for one day, one hour and one week, a significant decrease in measured amount of pores is visible for a membrane with a pore size of 1 µm.

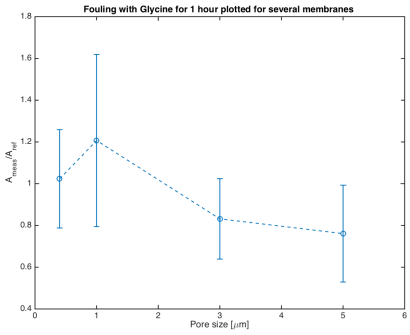

(a)

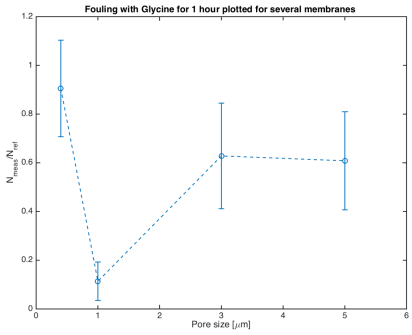

(b)

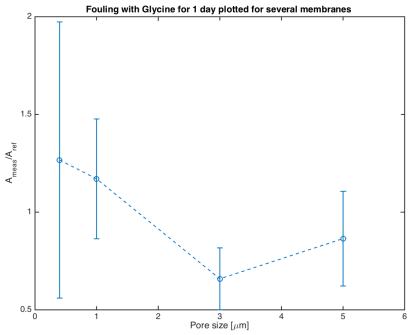

(a)

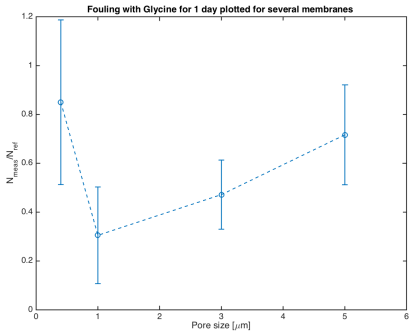

(b)

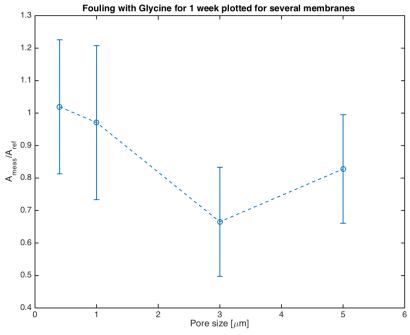

(a)

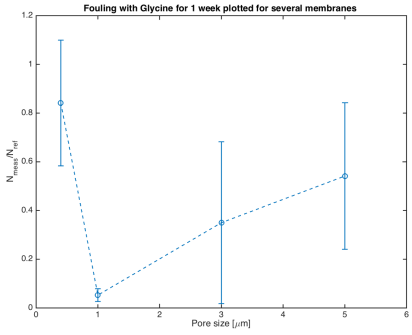

(b)

F.2.2. Fouling by BSA

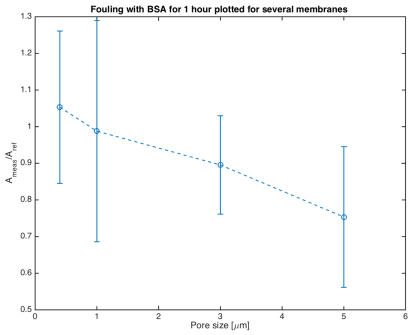

(a)

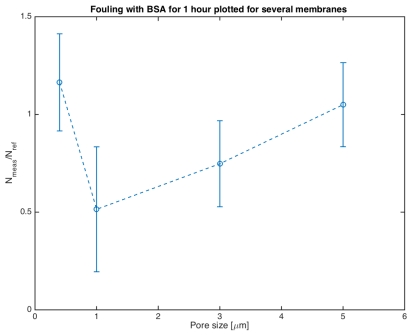

(b)

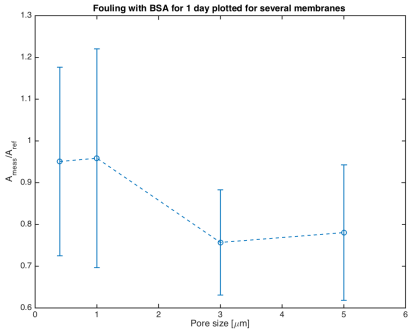

(a)

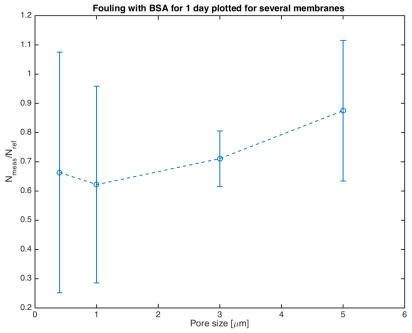

(b)

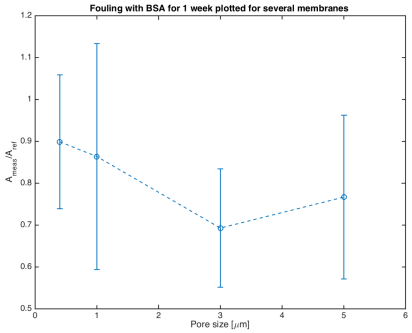

(a)

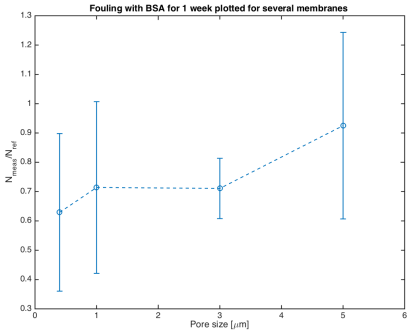

(b)

F.2.3. Fouling by λ-DNA

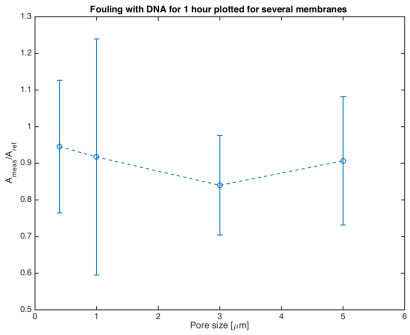

(a)

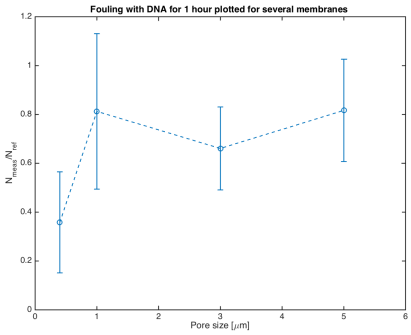

(b)

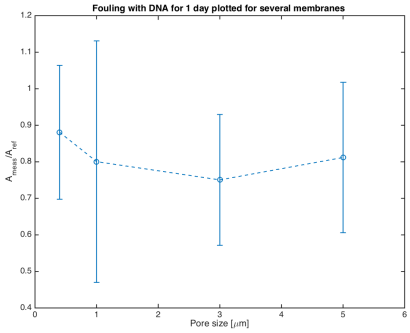

(a)

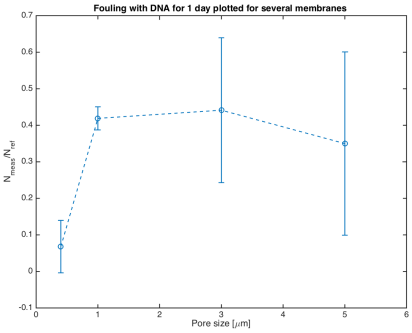

(b)

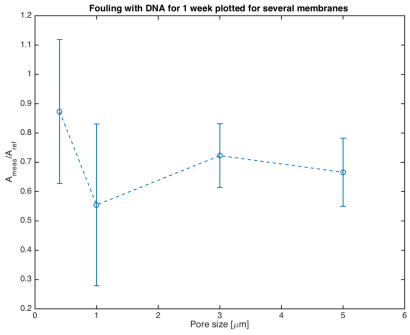

(a)

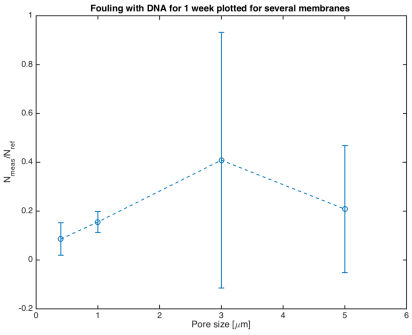

(b)

F.2.4. Fouling over all feed particles

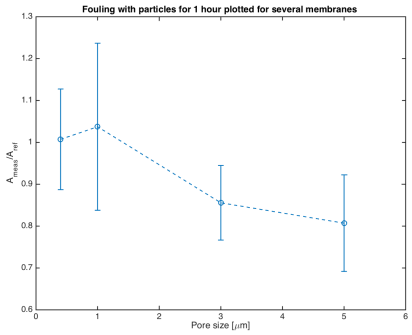

(a)

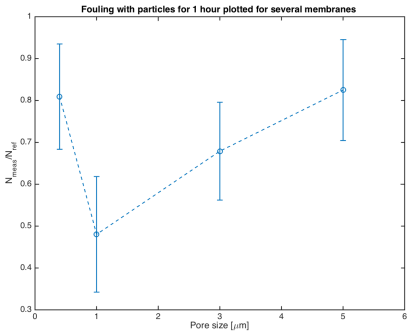

(b)

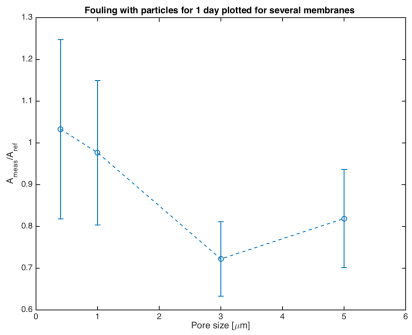

(a)

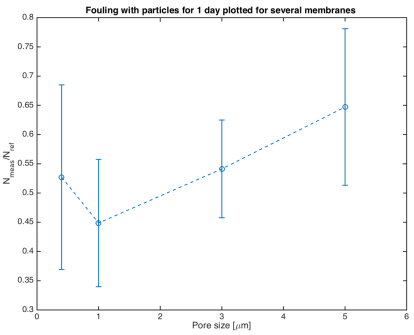

(b)

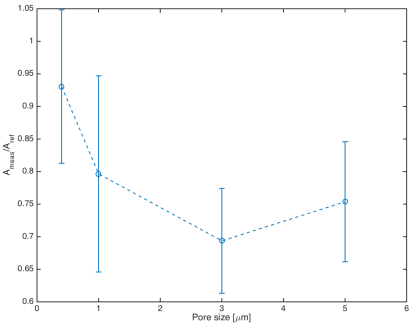

(a)

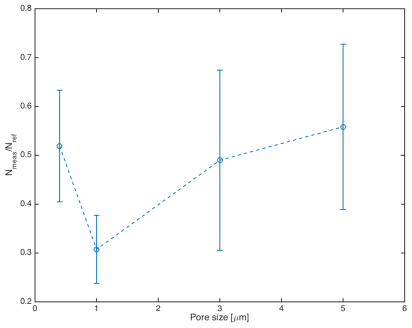

(b)

F.3. Correlation of feed properties with fouling

F.3.1. Fouling on a 0.4 µm membrane

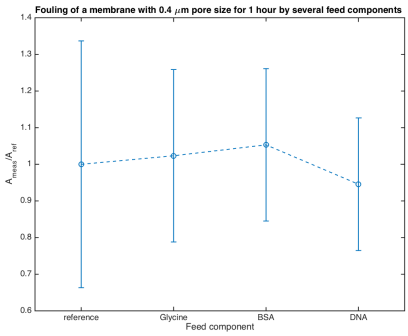

(a)

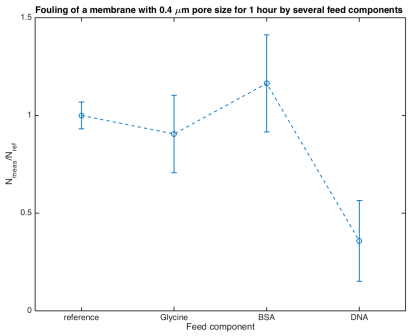

(b)

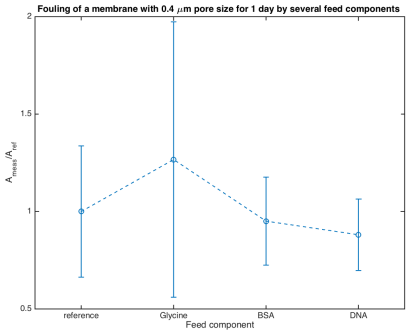

(a)

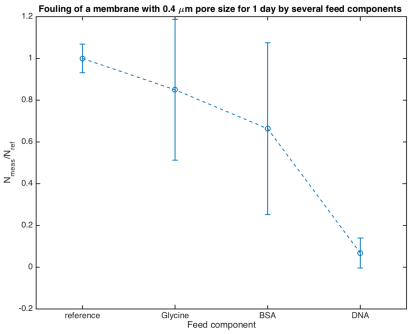

(b)

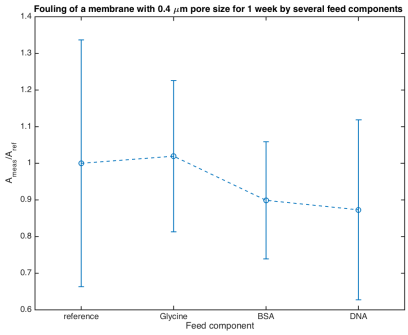

(a)

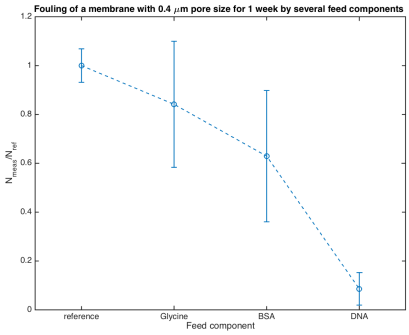

(b)

F.3.2. Fouling by a 1 µm membrane

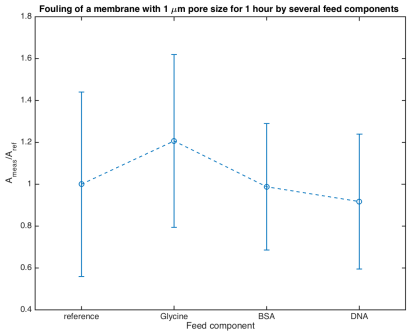

(a)

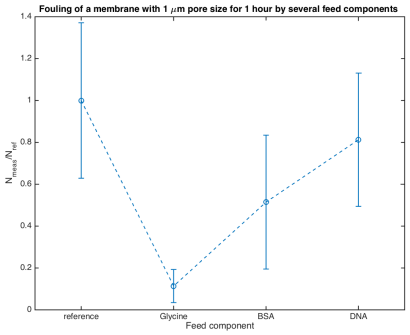

(b)

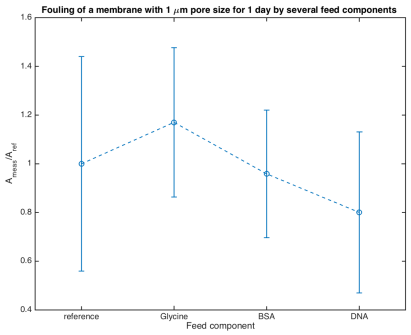

(a)

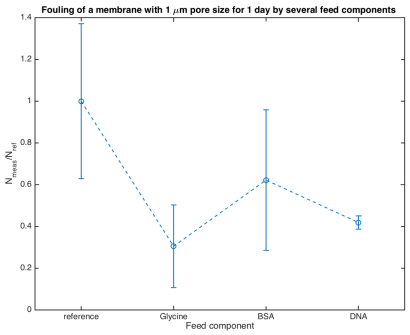

(b)

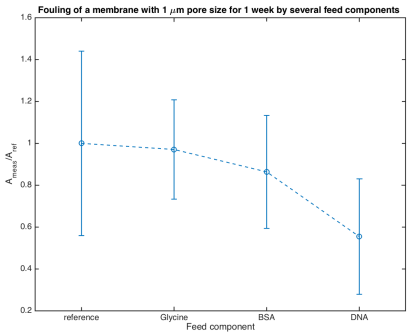

(a)

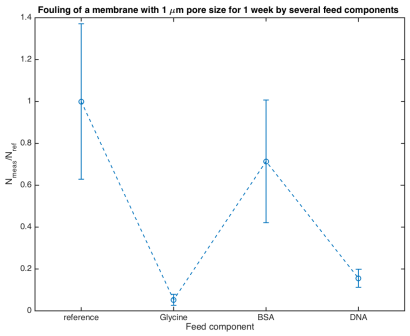

(b)

F.3.3. Fouling by a 3 µm membrane

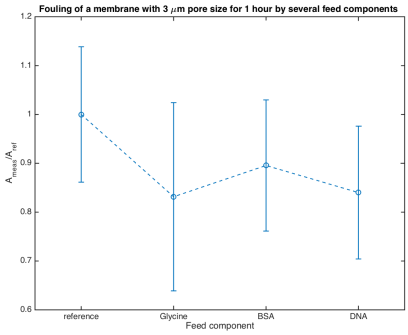

(a)

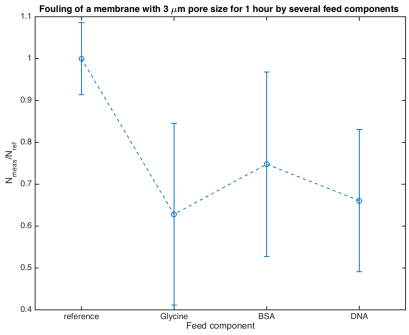

(b)

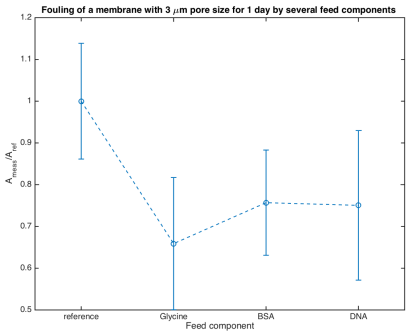

(a)

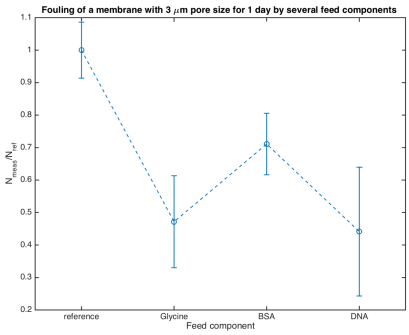

(b)

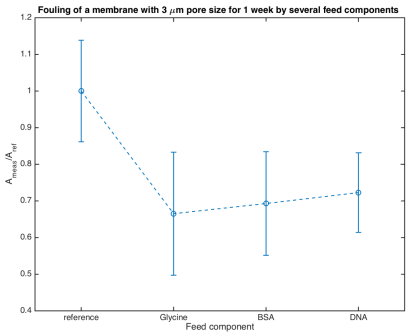

(a)

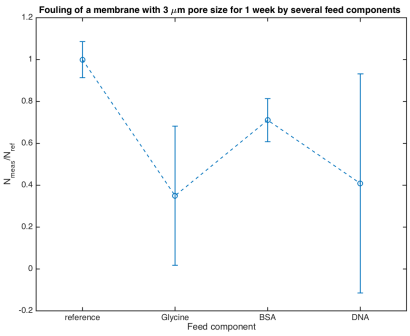

(b)

F.3.4. Fouling by a 5 µm membrane

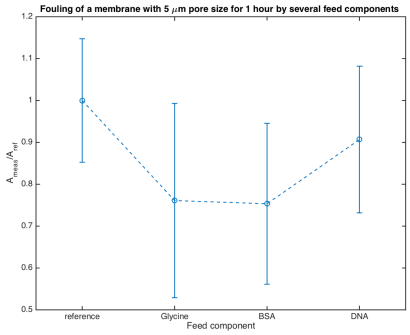

(a)

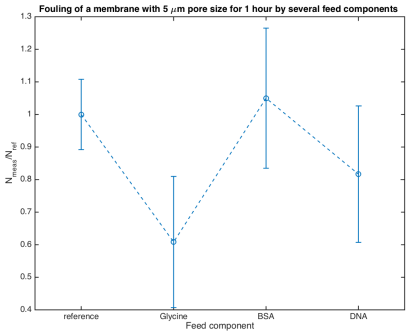

(b)

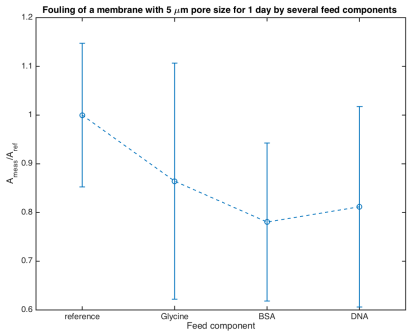

(a)

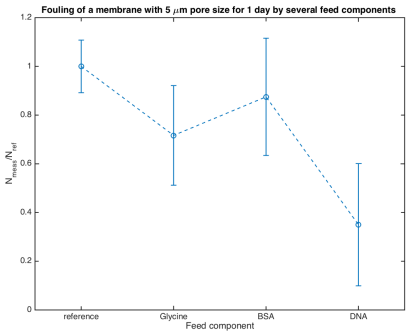

(b)

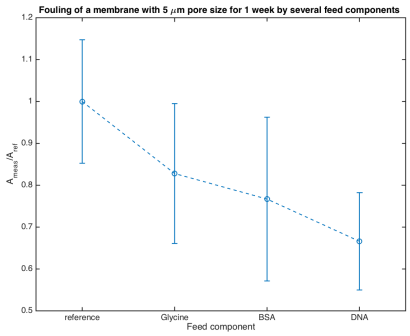

(a)

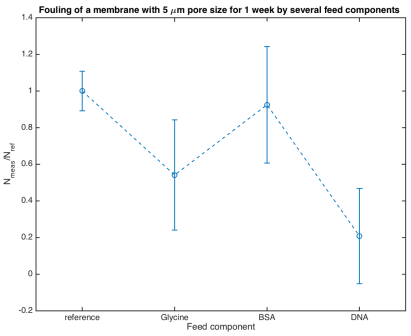

(b)

F.3.5. Fouling over all track-etched membranes

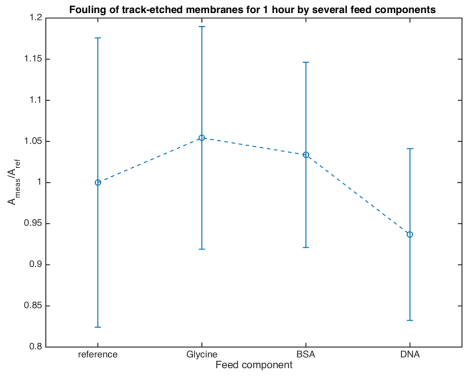

(a)

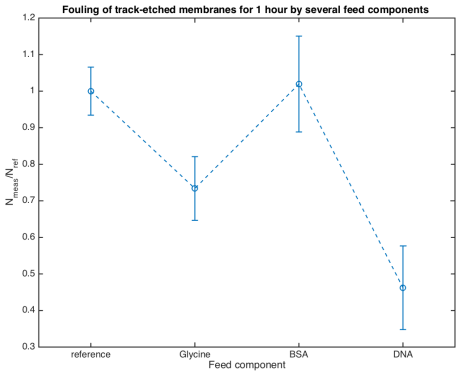

(b)

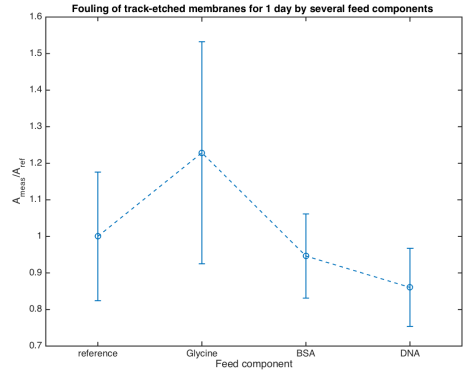

(a)

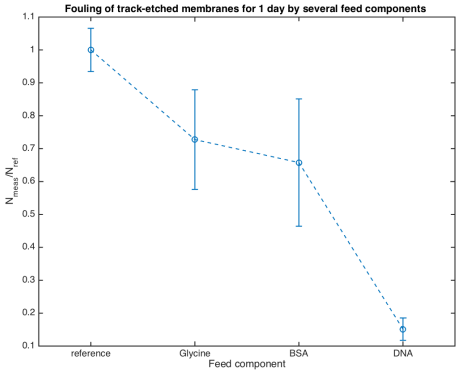

(b)

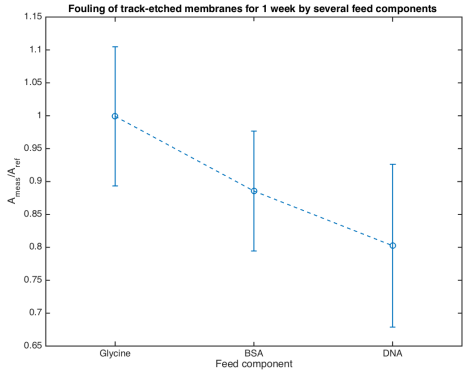

(a)

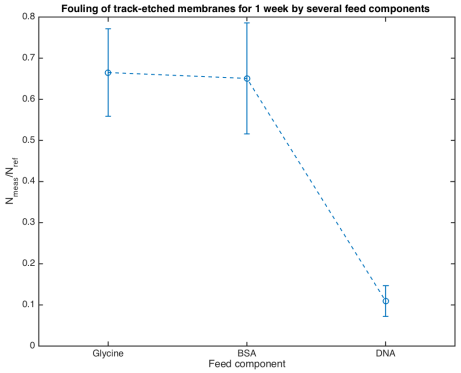

(b)

G

Dynamic analysis

Eight test devices are created to test the diffusion of two types of particles through four porous membranes with a defined pore size. Measurements are executed 3 to 5 times successively (P1-P5) with a cycle of 'flushing' after each test cycle. During the measurement, the light intensity created by excited fluorescent particles is captured with a fluorescence microscope and converted to a value for concentration. In this chapter, the experimental values for concentration are fitted to the fitting equation defined in Appendix 3.2.2. Further, the values of a and b are examined for correlations with respect to consequent tests with one device and with respect to pore size and feed. All of the fitting data are described piece by piece before verifying for correlations.

G.1. Experimental data fitting

The next subsections envision the fitting of the experimental data and provide a table with the obtained values for a and b. The resnorm, the squared 2-norm of the residual, which can be seen as a measure for significance of the curve fit, is added in each table. Because a certain deviation pattern is visible in multiple fitting graphs, a deviation plot is included in each subsection. To decide which of the fitting values are included in further analysis, only a values within the range 0-3 are accepted and b values within the range 0.1-2. A weighted resnorm up to 2 is accepted. The explanation for the boundaries is given in Section 3.2.4.

G.1.1. Glycine, 0.4 µm pore size

Four subsequent measurements on Glycine diffusion are done with a microfluidic system including a membrane with a 0.4 µm pore size.

P1 Figure G.1a shows the fit of the experimental data with the model. Comparing the fitting curve with the experimental data, there is a sinusoidal difference. This is considered as the error of the fit. Interpretations on the error of the fit and a physical explanation are given in Section 3.2.4.

Table G.1: Fitting values for dynamic measurement cycle 1 for diffusion of Glycine through a flow cell with a 0.4 µm pore size membrane.

	Value
a	0.1669
b	0.3412
resnorm	0.0024
weighted resnorm	0.08616

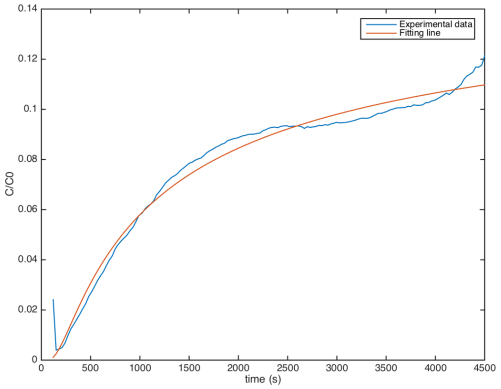

(a) A plot of the measurement data and the curve fit calculated by fitting the data to Equation **??** by minimizing the sum of squares

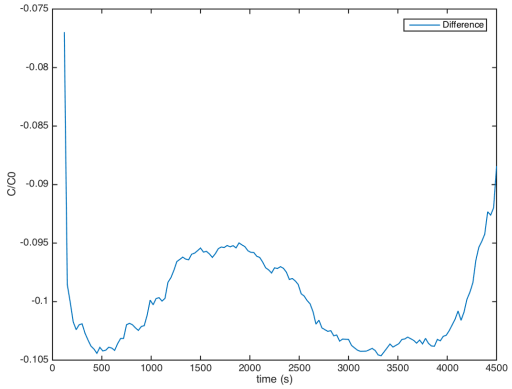

(b) Error of the fit with the measurement data

Figure G.1: Dynamic measurement cycle 1 for diffusion of Glycine through a flow cell with a 0.4 µm pore size membrane.

P2 The second data set can be fitted with the fitting line with an acceptable weighted resnorm. Figure G.2b shows again a sinusoidal error graph.

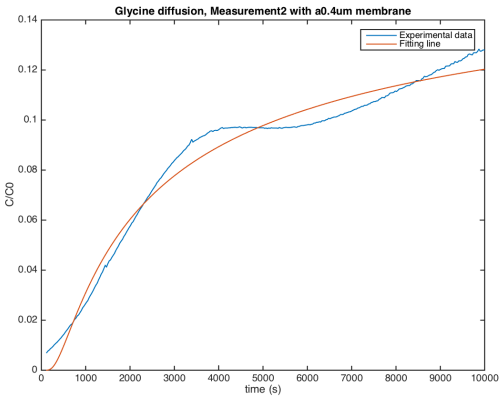

(a) A plot of the measurement data and the curve fit calculated by fitting the data to Equation **??** by minimizing the sum of squares

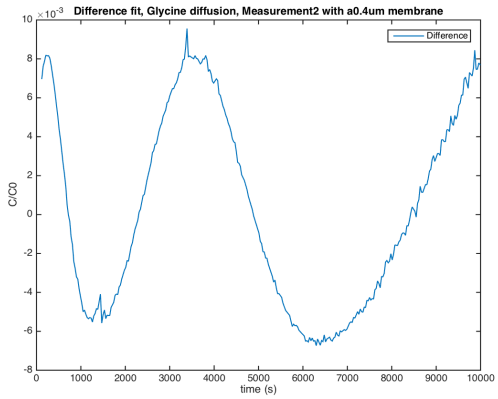

(b) Error of the fit with the measurement data

Figure G.2: Dynamic measurement cycle 2 for diffusion of Glycine through a flow cell with a 0.4 µm pore size membrane.

Table G.2: Fitting values for dynamic measurement cycle 2 for diffusion of Glycine through a flow cell with a 0.4 µm pore size membrane.

	Value
a	0.1809
b	0.4968
resnorm	0.0082
weighted resnorm	0.2506

P3 The third set of measurements shows a relatively good fit with a weighted resnorm of 3.1% and in Figure G.3b a non-constant sinusoidal error term is visible.

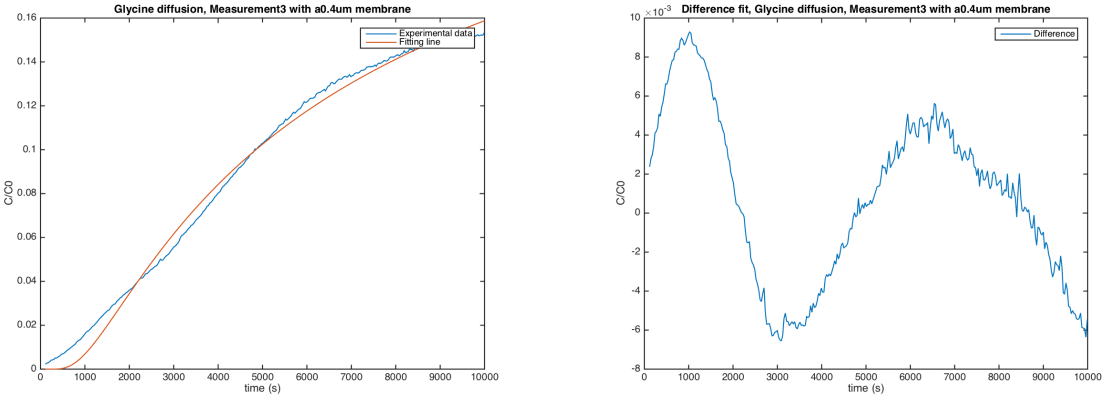

(a) A plot of the measurement data and the curve fit calculated by fitting the data to Equation **??** by minimizing the sum of squares

(b) Error of the fit with the measurement data

Figure G.3: Dynamic measurement cycle 3 for diffusion of Glycine through a flow cell with a 0.4 µm pore size membrane.

Table G.3: Fitting values for dynamic measurement cycle 3 for diffusion of Glycine through a flow cell with a 0.4 µm pore size membrane.

	Value
a	0.3938
b	0.9289
resnorm	0.0048
weighted resnorm	0.0310

P4 The fourth set of measurements shows behaviour that is not expected when analysing diffusion. The Matlab programme is able to fit the experimental data with a curve, but the weighted resnorm of 4.474 shows that the squared fitting error is over 400%. This means that the fit cannot be used to represent the measured data.

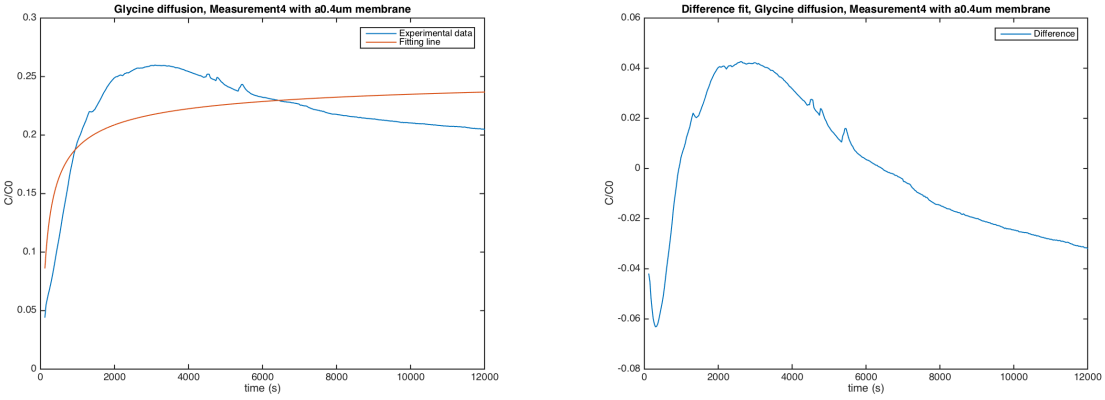

(a) A plot of the measurement data and the curve fit calculated by fitting the data to Equation **??** by minimizing the sum of squares

(b) Error of the fit with the measurement data

Figure G.4: Dynamic measurement cycle 4 for diffusion of Glycine through a flow cell with a 0.4 µm pore size membrane.

Table G.4: Fitting values

	Value
a	0.2563
b	0.1207
resnorm	0.2939
weighted resnorm	4.474

G.1.2. Glycine, 1 µm pore size

Three subsequent measurements with Glycine diffusion are done with a microfluidic system including a membrane with 1 µm pore size.

P1 The first set of measurements shows behaviour that can be compared with the fitting line. Anyhow, Figure G.5a shows a non-smooth measurement curve with a lot of peaks and dales, which cause a raise in the weighted resnorm. The interpretation of the peaks is given in Section 3.2.4. Further, the error of the fit visualised in Figure G.5b also has a periodic progression.

As the hypothesis is that the resnorm is raised because of the non-smooth behaviour, this measurement and curve fit are included in the rest of the analysis.

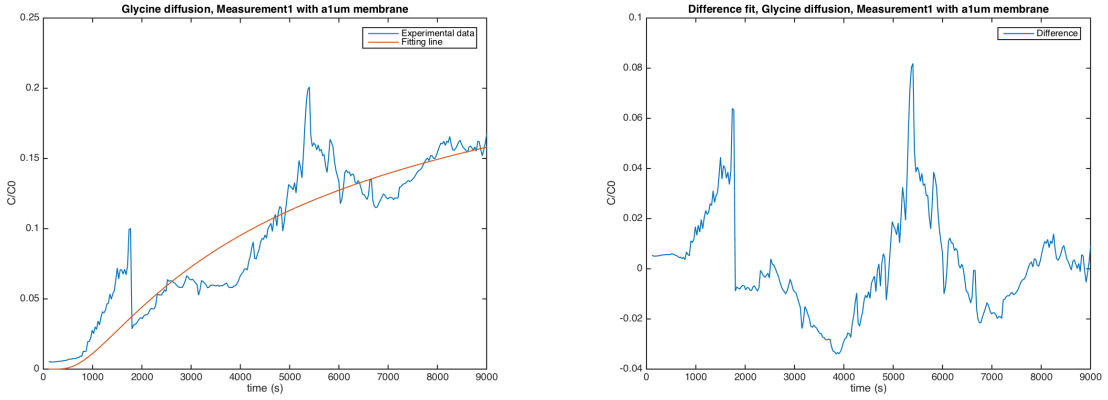

(a) A plot of the measurement data and the curve fit calculated by fitting the data to Equation **??** by minimizing the sum of squares

(b) Error of the fit with the measurement data

Figure G.5: Dynamic measurement cycle 1 for diffusion of Glycine through a flow cell with a 1 µm pore size membrane.

Table G.5: Fitting values

	Value
a	0.3294
b	0.7699
resnorm	0.1187
weighted resnorm	1.094

P2 The second set of data shows a curve fit with a very low b value. The interpretation of a low b value is given in Section 3.2.4. Because the value for b is too low to be accepted as a valid fit and because the weighted resnorm is over 10000%, this measurement is not included in the rest of the analysis.

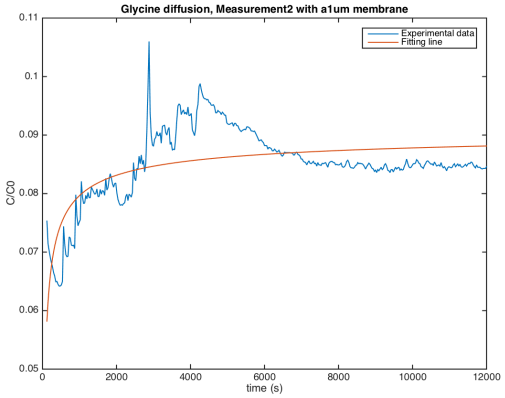

(a) A plot of the measurement data and the curve fit calculated by fitting the data to Equation **??** by minimizing the sum of squares

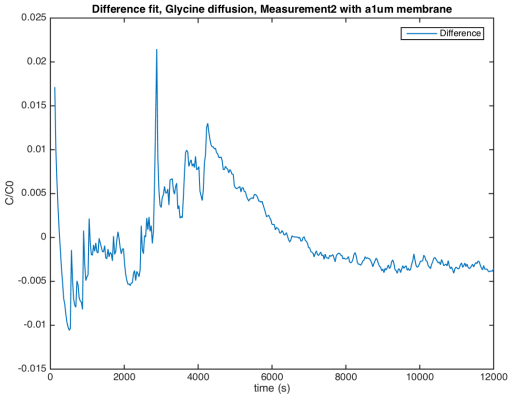

(b) Error of the fit with the measurement data

Figure G.6: Dynamic measurement cycle 2 for diffusion of Glycine through a flow cell with a 1 µm pore size membrane.

Table G.6: Fitting values

	Value
a	0.0916
b	0.0596
resnorm	1.0726
weighted resnorm	127.83

P3 One thing that is conspicuous about the third measurement is its high value for weighted resnorm. This is mostly due to an intensity/concentration peak around 4000 seconds. Because the weighted resnorm is too high to fit the experimental measurements correctly, this fit is omitted.

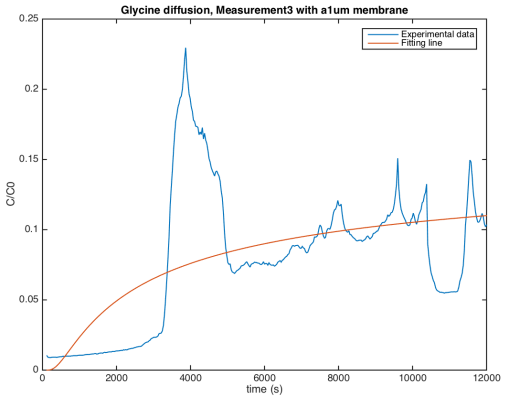

(a) A plot of the measurement data and the curve fit calculated by fitting the data to Equation **??** by minimizing the sum of squares

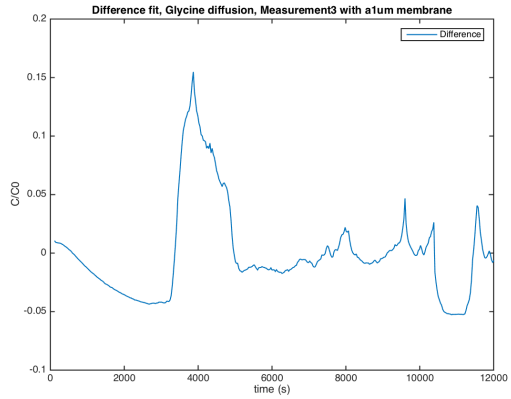

(b) Error of the fit with the measurement data

Figure G.7: Dynamic measurement cycle 3 for diffusion of Glycine through a flow cell with a 1 µm pore size membrane.

Table G.7: Fitting values

	Value
a	0.1635
b	0.5309
resnorm	0.6369
weighted resnorm	23.825

G.1.3. Glycine, 3 µm pore size

Five subsequent measurements with Glycine diffusion are done with the microfluidic system including a membrane with a 3 µm pore size.

P1 The measurement curve shows a sudden peak at 2500 sec (around 40 min) with a progression that is constant nor predictable. The curve fit shows an a value bigger than 1 which is caused by the sudden ascend. The interpretation of a high a value in combination with this sudden increase is given in Section 3.2.4.

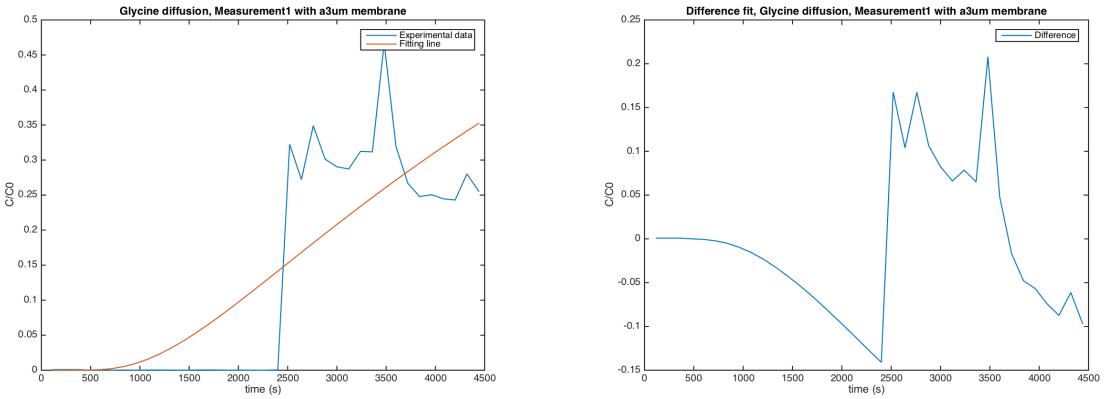

(a) A plot of the measurement data and the curve fit calculated by fitting the data to Equation **??** by minimizing the sum of squares

(b) Error of the fit with the measurement data

Figure G.8: Dynamic measurement cycle 1 for diffusion of Glycine through a flow cell with a 3 µm pore size membrane.

Table G.8: Fitting values

	Value
a	1.5471
b	0.9488
resnorm	0.2806
weighted resnorm	0.1172

P2 The measurement curve seems to be fitted well. However the b value is a little low, so possibly not only diffusion is playing part in this measurement.

Table G.9: Fitting values

	Value
a	0.2308
b	0.1447
resnorm	0.0114
weighted resnorm	0.2140

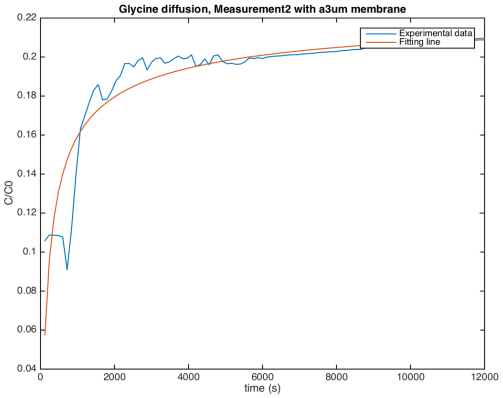

(a) A plot of the measurement data and the curve fit calculated by fitting the data to Equation **??** by minimizing the sum of squares

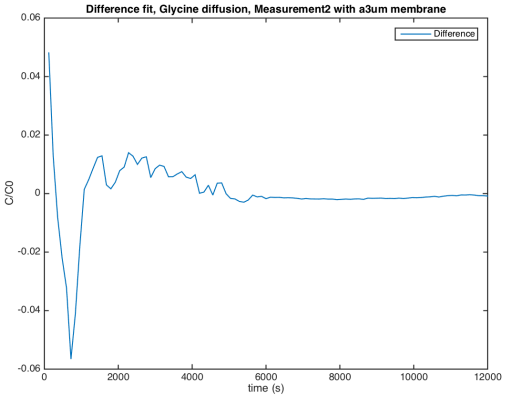

(b) Error of the fit with the measurement data

Figure G.9: Dynamic measurement cycle 2 for diffusion of Glycine through a flow cell with a 3 µm pore size membrane.

P3 The third measurement initiates with a small peak with slight concentration decrease and then propagates with a curve that can be fitted. The interpretation of a small peak at t=0 is given in Section 3.2.4.

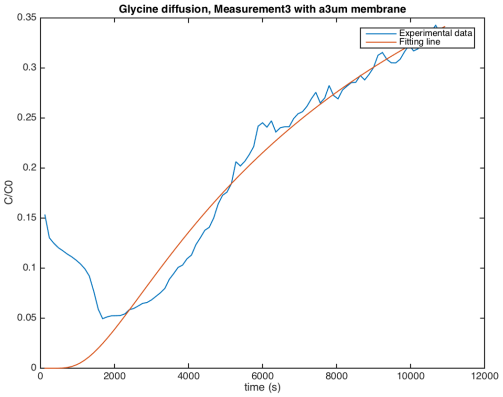

(a) A plot of the measurement data and the curve fit calculated by fitting the data to Equation **??** by minimizing the sum of squares

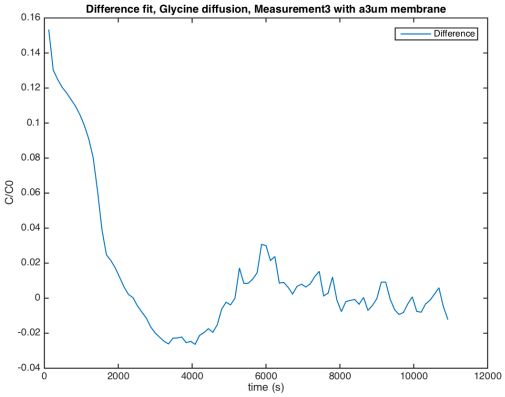

(b) Error of the fit with the measurement data

Figure G.10: Dynamic measurement cycle 3 for diffusion of Glycine through a flow cell with a 3 µm pore size membrane.

Table G.10: Fitting values

	Value
a	0.8767
b	1.0330
resnorm	0.1650
weighted resnorm	0.2147

P4 The experimental data in this case show a peak at the beginning and a decrease in concentration in time. Matlab is able to fit this data with a negative value for b, which physically means that the concentration is at maximum at t=0 and that the particles diffuse away from the measuring spot. Further interpretation is given in Section 3.2.4.

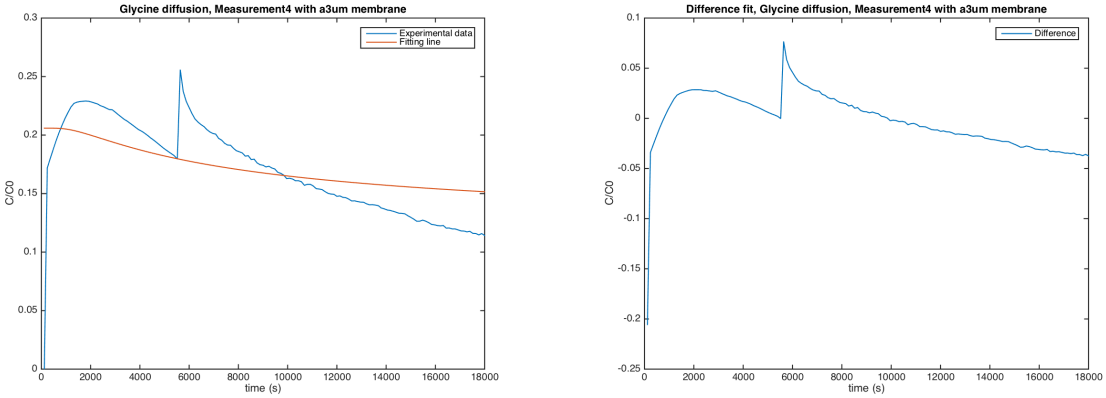

(a) A plot of the measurement data and the curve fit calculated by fitting the data to Equation **??** by minimizing the sum of squares

(b) Error of the fit with the measurement data

Figure G.11: Dynamic measurement cycle 4 for diffusion of Glycine through a flow cell with a 3 µm pore size membrane.

Table G.11: Fitting values

	Value
a	0.1029
b	-0.9734
resnorm	0.1256
weighted resnorm	11.862

P5 The high value for a indicates that diffusion was not the only factor playing a role in the distribution of fluorescent particles. More about the interpretation of a high a value can be read in Section 3.2.4. Because of the high value of a, this measurement will be omitted.

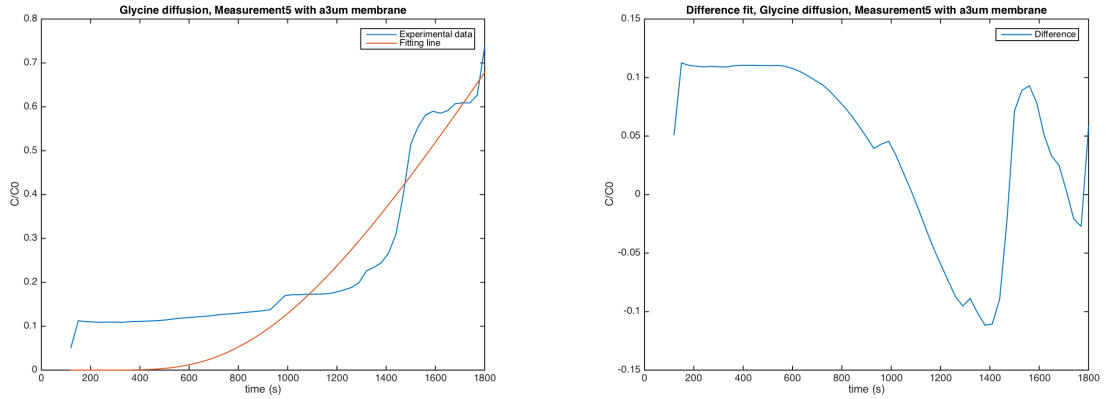

(a) A plot of the measurement data and the curve fit calculated by fitting the data to Equation **??** by minimizing the sum of squares

(b) Error of the fit with the measurement data

Figure G.12: Dynamic measurement cycle 5 for diffusion of Glycine through a flow cell with a 3 µm pore size membrane.

Table G.12: Fitting values

	Value
a	11.5994
b	0.9219
resnorm	0.3896
weighted resnorm	0.0029

G.1.4. Glycine, 5 µm pore size

Five subsequent measurements with Glycine diffusion are done with the microfluidic system including a membrane with a 5 µm pore size.

P1 Again, the experimental data can be fitted with a negative b value. This is enough to omit the fitted values. Further, the experimental data shows a large amount of small peaks, which are interpreted in Section 3.2.4.

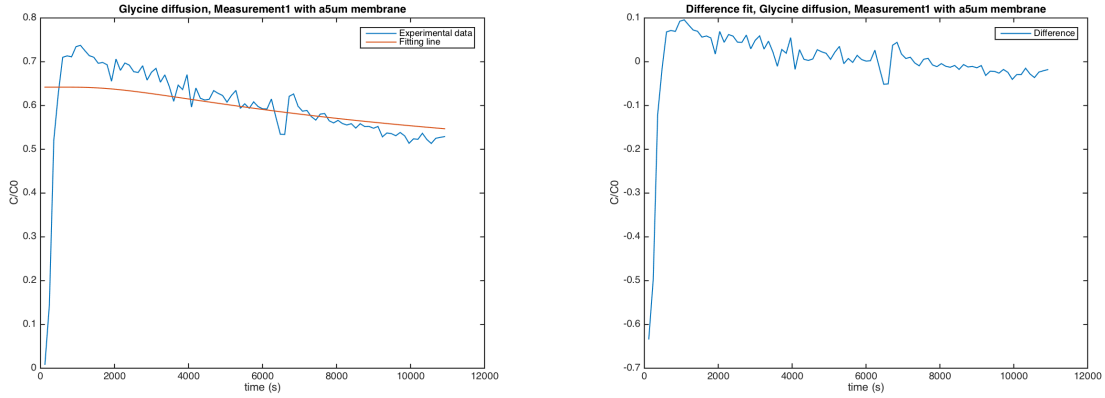

(a) A plot of the measurement data and the curve fit calculated by fitting the data to Equation **??** by minimizing the sum of squares

(b) Error of the fit with the measurement data

Figure G.13: Dynamic measurement cycle 1 for diffusion of Glycine through a flow cell with a 5 µm pore size membrane.

Table G.13: Fitting values

	Value
a	0.3210
b	-1.2541
resnorm	0.7858
weighted resnorm	7.626

P2 This set of measurements is fitted within reasonable values showing four small peaks. When looking at the error of the fit one can see a decreasing sinusoidal propagation.

Table G.14: Fitting values

	Value
a	0.7996
b	0.6641
resnorm	0.1521
weighted resnorm	0.2379

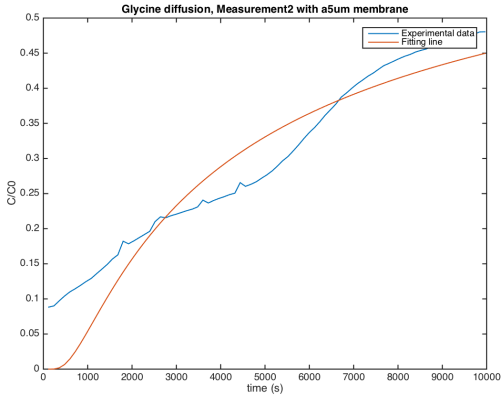

(a) A plot of the measurement data and the curve fit calculated by fitting the data to Equation **??** by minimizing the sum of squares

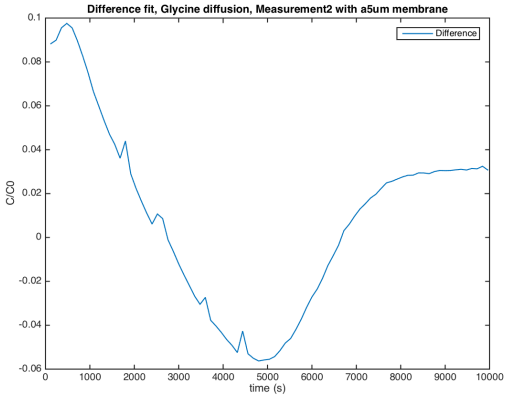

(b) Error of the fit with the measurement data

Figure G.14: Dynamic measurement cycle 2 for diffusion of Glycine through a flow cell with a 5 µm pore size membrane.

P3 The third measurement shows a relatively good curve fit with a small a value and a b value close to 1. Further, a lot of small peaks are visible in the error graph in Figure G.15b.

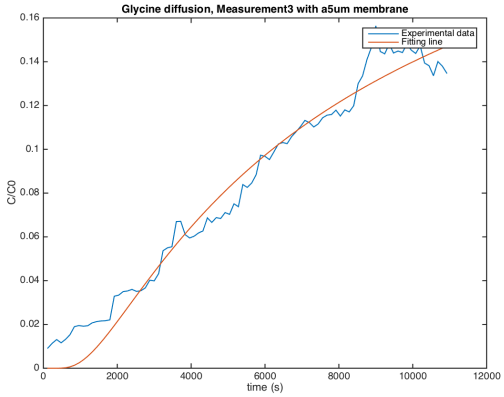

(a) A plot of the measurement data and the curve fit calculated by fitting the data to Equation **??** by minimizing the sum of squares

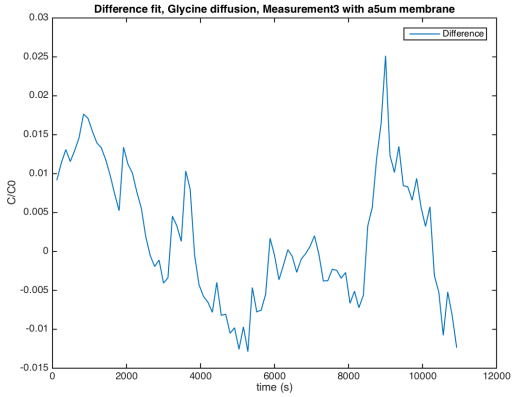

(b) Error of the fit with the measurement data

Figure G.15: Dynamic measurement cycle 3 for diffusion of Glycine through a flow cell with a 5 µm pore size membrane.

Table G.15: Fitting values

	Value
a	0.3476
b	0.9612
resnorm	0.0068
weighted resnorm	0.0563

P4 The fourth measurement begins to increase after 6000 seconds, which, compared to the other measurements, is relatively late. The fitted values for a and b are high, which would probably not have happened when being able to incorporate time to diffusion (Appendix 3.2.2). An explanation for the large time delay is given in Section 3.2.4.

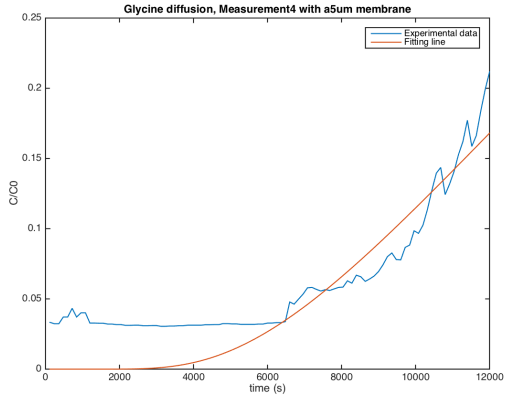

(a) A plot of the measurement data and the curve fit calculated by fitting the data to Equation **??** by minimizing the sum of squares

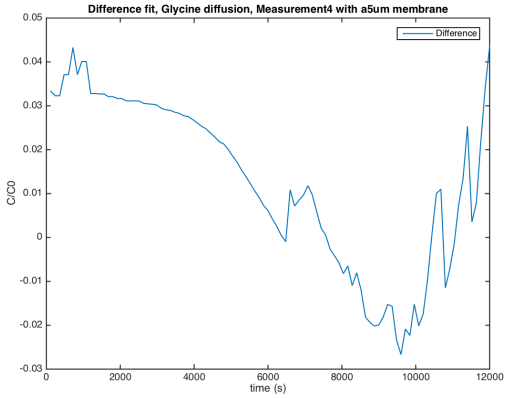

(b) Error of the fit with the measurement data

Figure G.16: Dynamic measurement cycle 4 for diffusion of Glycine through a flow cell with a 5 µm pore size membrane.

Table G.16: Fitting values

	Value
a	2.6134
b	2.3059
resnorm	0.0627
weighted resnorm	0.0092

P5 The graph visible in Figure G.17a shows a curve with a peak at the beginning and a decrease in measured concentration afterwards. The low value for *b* implies that there must have been an overpressure creating the first peak (Section 3.2.4). This is why this measurement is omitted.

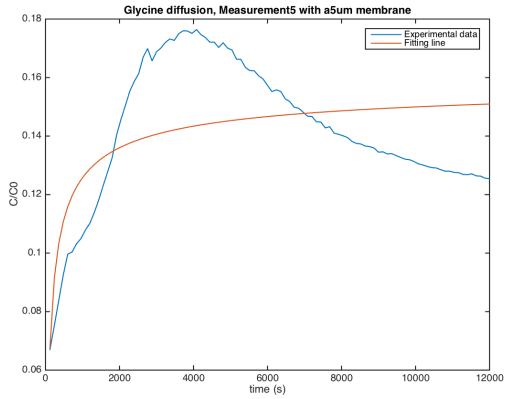

(a) A plot of the measurement data and the curve fit calculated by fitting the data to Equation **??** by minimizing the sum of squares

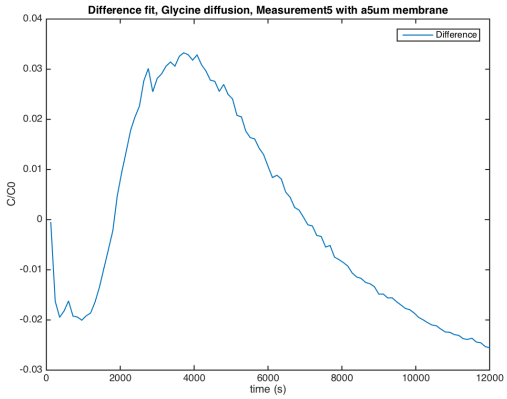

(b) Error of the fit with the measurement data

Figure G.17: Dynamic measurement cycle 5 for diffusion of Glycine through a flow cell with a 5 µm pore size membrane.

Table G.17: Material properties needed for the used feed

	Value
a	0.1654
b	0.1089
resnorm	0.0448
weighted resnorm	1.6376

G.1.5. BSA, 0.4 µm pore size

Five subsequent measurements with BSA diffusion are done with the microfluidic system including a membrane with a 0.4 µm pore size.

P1 The first measurement and fit, shown in Figure G.18a, show a very good consistency. Around 2500 seconds, a peak is visible and further only small errors are measured. The a value is bigger than 1, which means that the curve is ascending too much.

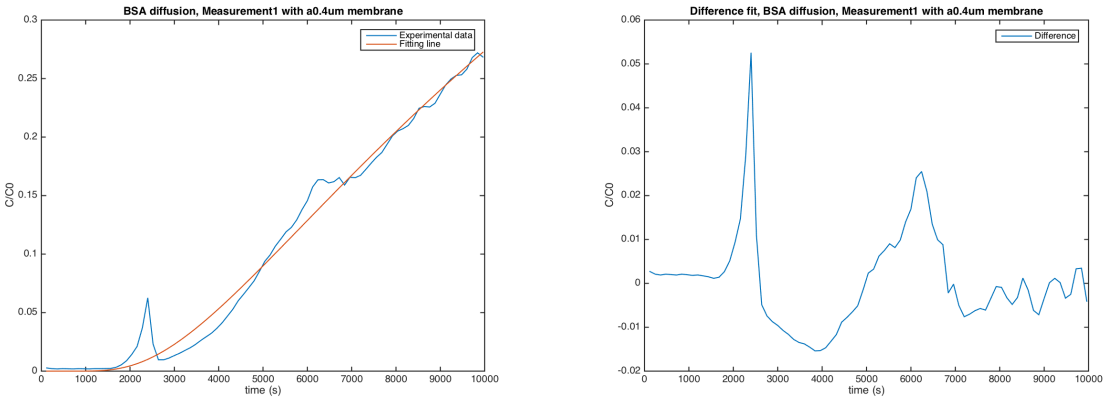

(a) A plot of the measurement data and the curve fit calculated by fitting the data to Equation **??** by minimizing the sum of squares

(b) Error of the fit with the measurement data

Figure G.18: Dynamic measurement cycle 1 for diffusion of BSA through a flow cell with a 0.4 µm pore size membrane.

Table G.18: Material properties needed for the used feed

	Value
a	1.4826
b	0.3853
resnorm	0.0099
weighted resnorm	0.0045

P2 The second set of measurements is also fitted with a relatively small weighted resnorm. A small peak appears around 1200 s and separate from the beginning, the error seems to be propagating sinusoidally. The a value is relatively high.

Table G.19: Material properties needed for the used feed

	Value
a	2.7934
b	0.7371
resnorm	0.0306
weighted resnorm	0.0039

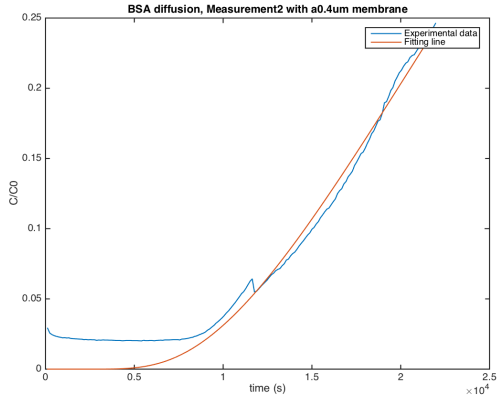

(a) A plot of the measurement data and the curve fit calculated by fitting the data to Equation **??** by minimizing the sum of squares

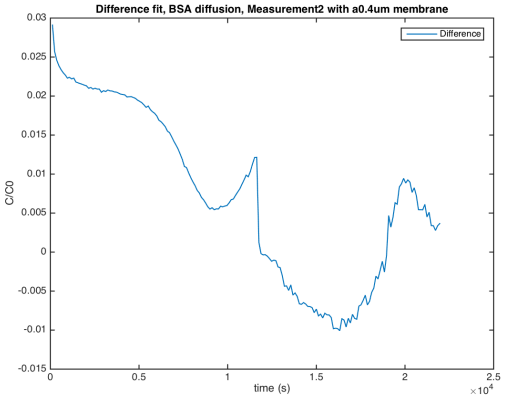

(b) Error of the fit with the measurement data

Figure G.19: Dynamic measurement cycle 2 for diffusion of BSA through a flow cell with a 0.4 µm pore size membrane.

P3 The third measurements are very concurrent at the start and as time passes, the tiny noise peaks become bigger (see Figure G.20b). The value for a is again relatively large.

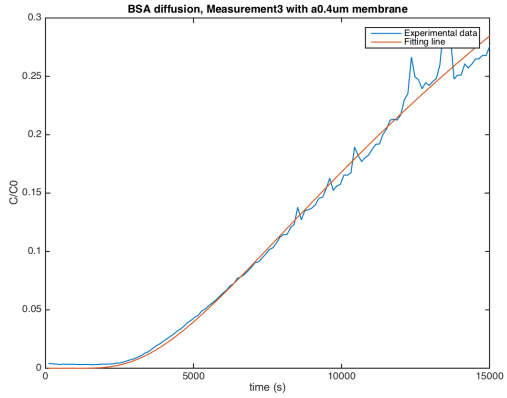

(a) A plot of the measurement data and the curve fit calculated by fitting the data to Equation **??** by minimizing the sum of squares

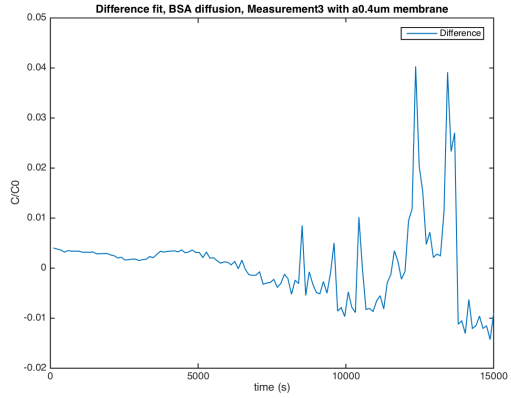

(b) Error of the fit with the measurement data

Figure G.20: Dynamic measurement cycle 3 for diffusion of BSA through a flow cell with a 0.4 µm pore size membrane.

Table G.20: Fitting values

	Value
a	1.4461
b	0.4560
resnorm	0.0141
weighted resnorm	0.0067

P4 The graph of the fourth measurement in Figure G.21a shows an exceptional small weighted resnorm, but is fitted with an a value that is out of proportion. Therefore, this measurement must be omitted.

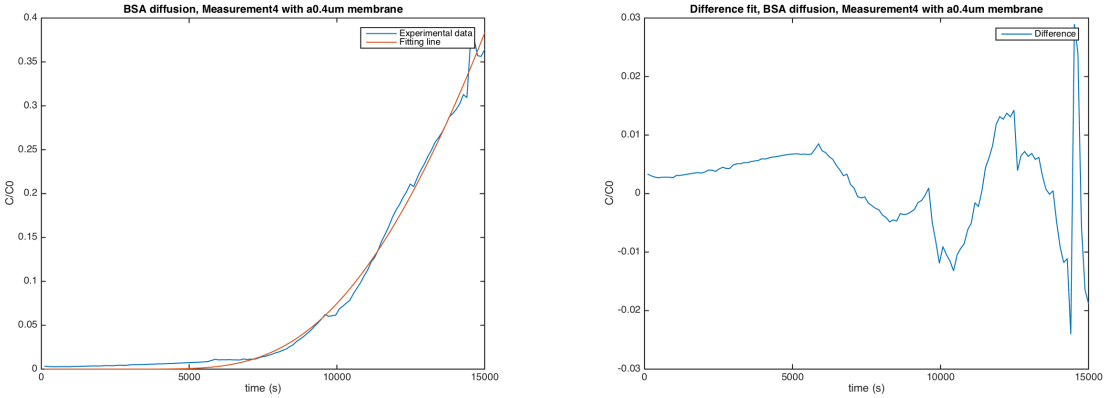

(a) A plot of the measurement data and the curve fit calculated by fitting the data to Equation **??** by minimizing the sum of squares

(b) Error of the fit with the measurement data

Figure G.21: Dynamic measurement cycle 4 for diffusion of BSA through a flow cell with a 0.4 µm pore size membrane.

Table G.21: Fitting values

	Value
a	24.8275
b	0.8617
resnorm	0.0072
weighted resnorm	1.168e-04

P5 The fifth measurement is again fitted with a relatively low weighted resnorm. In addition, the a and b value are within the accepted range.

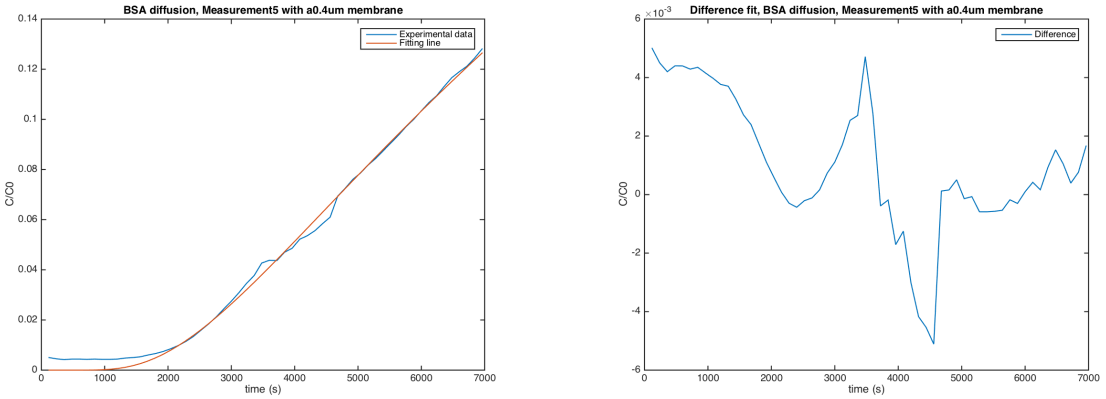

(a) A plot of the measurement data and the curve fit calculated by fitting the data to Equation **??** by minimizing the sum of squares

(b) Error of the fit with the measurement data

Figure G.22: Dynamic measurement cycle 5 for diffusion of BSA through a flow cell with a 0.4 µm pore size membrane.

Table G.22: Fitting values

	Value
a	0.7665
b	0.3365
resnorm	3.6476e-04
weighted resnorm	6.2084e-04

G.1.6. BSA, 1 µm pore size

Five subsequent measurements with BSA diffusion are done with the microfluidic system including a membrane with a 1μm µm pore size.

P1 The first measurement shows a curve fit with a sinusoidal error and small noise peaks. The values for a and b are relatively low, but within the accepted range.

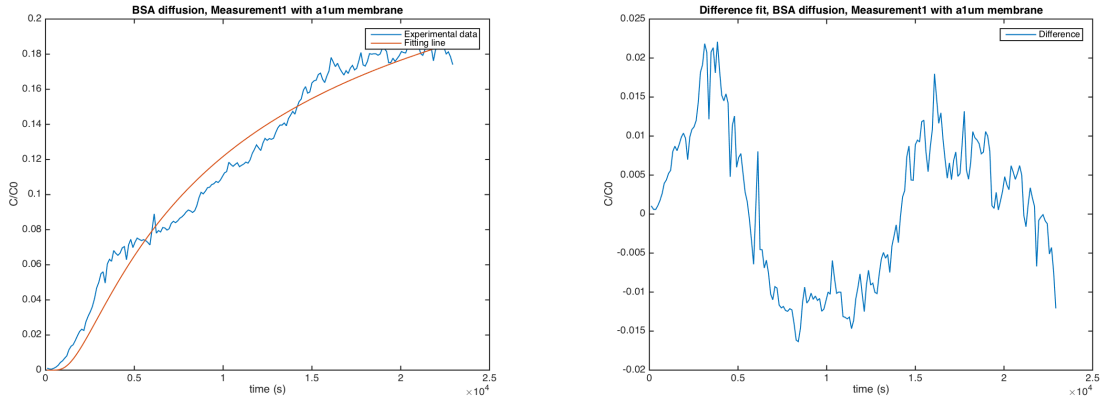

(a) A plot of the measurement data and the curve fit calculated by fitting the data to Equation **??** by minimizing the sum of squares

(b) Error of the fit with the measurement data

Figure G.23: Dynamic measurement cycle 1 for diffusion of BSA through a flow cell with a 1 µm pore size membrane.

Table G.23: Fitting values

	Value
a	0.3460
b	0.2704
resnorm	0.0177
weighted resnorm	0.1478

P2 The second set of measurements has a relatively larger offset or weighted resnorm and is fitted with a relatively high value for a. If a further propagation of the concentration in time was measured, the fit should in my opinion have a lower a and lower b value, because at t=16000 seconds the curve seems to have already flattened out. Then, however, the b would become very low.

Table G.24: Fitting values

	Value
a	1.6930
b	0.2034
resnorm	1.3582
weighted resnorm	0.4739

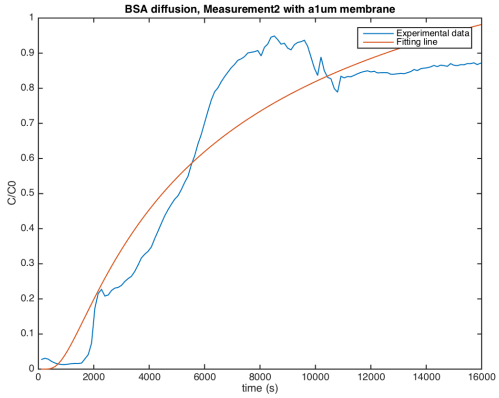

(a) A plot of the measurement data and the curve fit calculated by fitting the data to Equation **??** by minimizing the sum of squares

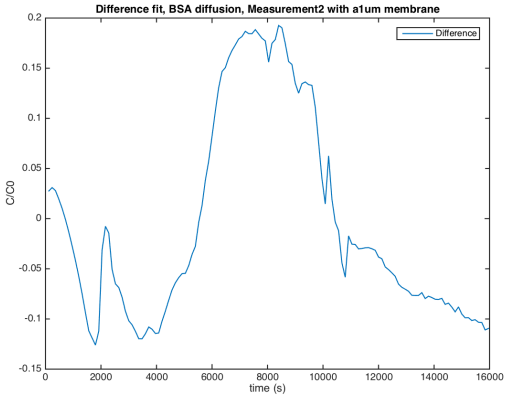

(b) Error of the fit with the measurement data

Figure G.24: Dynamic measurement cycle 2 for diffusion of BSA through a flow cell with a 1 µm pore size membrane.

P3 The third set of measurements is fitted with a small a value and a large negative b value. Additionally, the weighted resnorm is very high, so this measurement is omitted.

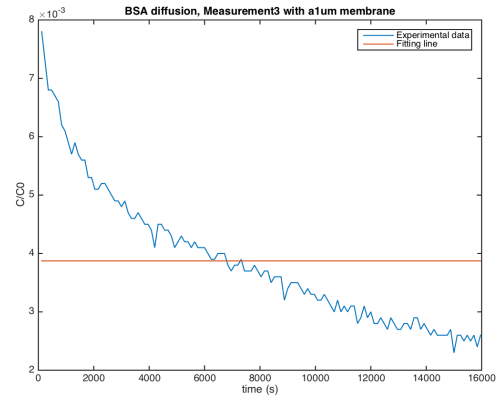

(a) A plot of the measurement data and the curve fit calculated by fitting the data to Equation **??** by minimizing the sum of squares

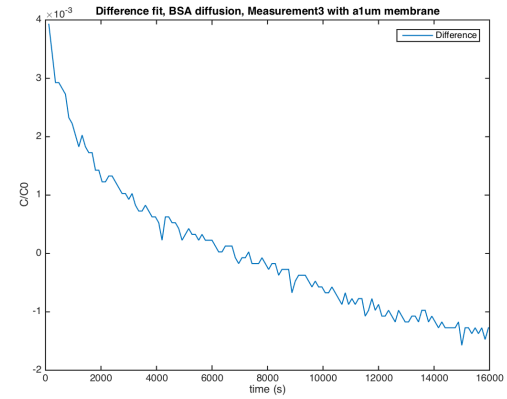

(b) Error of the fit with the measurement data

Figure G.25: Dynamic measurement cycle 3 for diffusion of BSA through a flow cell with a 1 µm pore size membrane.

Table G.25: Fitting values

	Value
a	0.0019
b	-9.0000
resnorm	1.7678e-04
weighted resnorm	48.970

P4 The fourth set of measurements shows a very rare phenomenon: the curve seems to reach an equilibrium around 7000 seconds, but afterwards starts increasing again. This happens again around 11000 seconds. This phenomenon results in measured values that are above the injected concentration. This is impossible and a possible cause is given in Section 3.2.4.

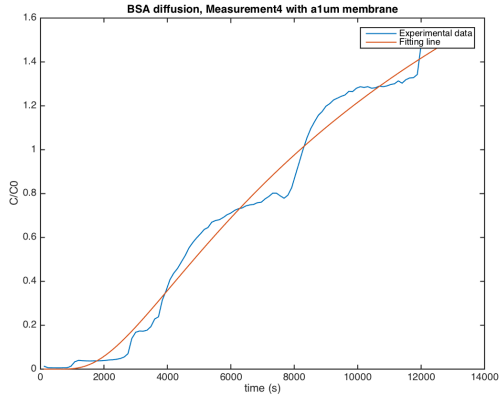

(a) A plot of the measurement data and the curve fit calculated by fitting the data to Equation **??** by minimizing the sum of squares

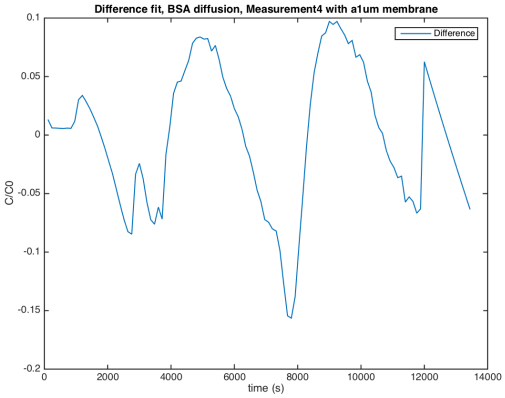

(b) Error of the fit with the measurement data

Figure G.26: Dynamic measurement cycle 4 for diffusion of BSA through a flow cell with a 1 µm pore size membrane.

Table G.26: Fitting values

	Value
a	4.5889
b	0.3238
resnorm	0.3990
weighted resnorm	0.0189

P5 The fifth set of measurements again shows measurements with a measured value for concentration that is higher than the injected concentration. Next to the resulting high value for a, the value for b is relatively low, thus this measurement must be omitted.

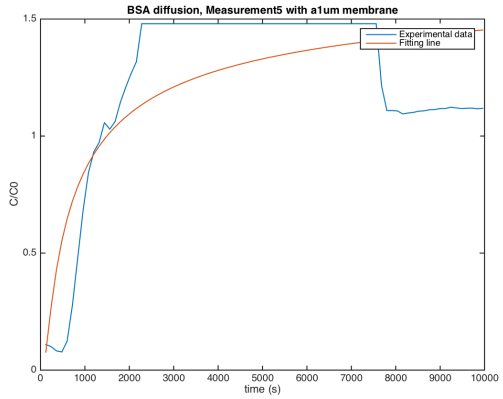

(a) A plot of the measurement data and the curve fit calculated by fitting the data to Equation **??** by minimizing the sum of squares

(b) Error of the fit with the measurement data

Figure G.27: Dynamic measurement cycle 5 for diffusion of BSA through a flow cell with a 1 µm pore size membrane.

Table G.27: Fitting values

	Value
a	1.7622
b	0.0642
resnorm	4.6650
weighted resnorm	1.5022

G.1.7. BSA, 3 µm pore size

Three subsequent measurements with BSA diffusion are done with the microfluidic system including a membrane with a 3 µm pore size.

P1 The first measurement corresponds well with the curve fit, resulting in a weighted resnorm of 0.11%. The value for a is again relatively high, but the experimental curve shows a less steep slope than the curve fit at 14000 seconds so whenever the measurement could have endured for a longer time period, the measurements and curve fit would have been propagating towards the right values. The error of the fit is sinusoidal and increases in time. Further, small noise peaks are visible and get bigger in time.

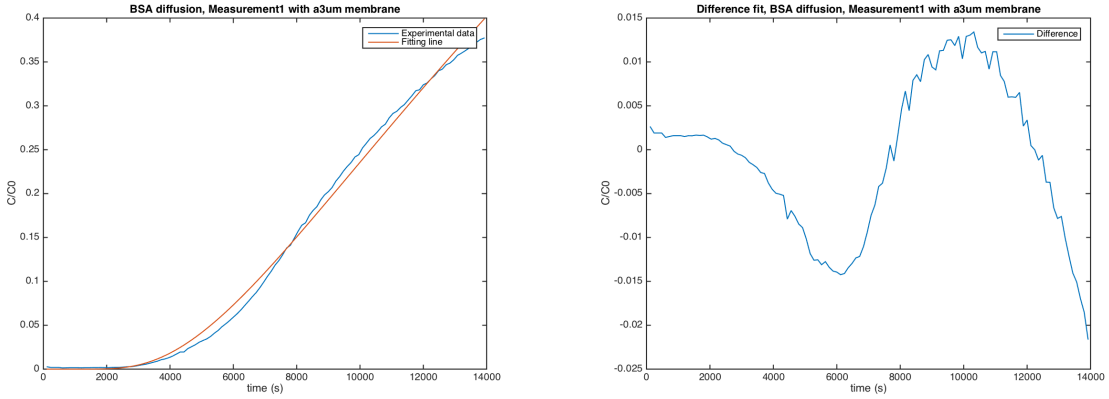

(a) A plot of the measurement data and the curve fit calculated by fitting the data to Equation **??** by minimizing the sum of squares

(b) Error of the fit with the measurement data

Figure G.28: Dynamic measurement cycle 1 for diffusion of BSA through a flow cell with a 3 µm pore size membrane.

Table G.28: Fitting values

	Value
a	2.7337
b	0.4984
resnorm	0.0085
weighted resnorm	0.0011

P2 The second set of measurements is fitted with a relatively big weighted resnorm of 30%. The values for a and b are within the accepted range. Optically seen, the fitting curve must be shifted up and slightly to the right to diminish the weighted resnorm and make the fit more significant. The error is sinusoidal and decreasing in time and gets bigger noise peaks in time.

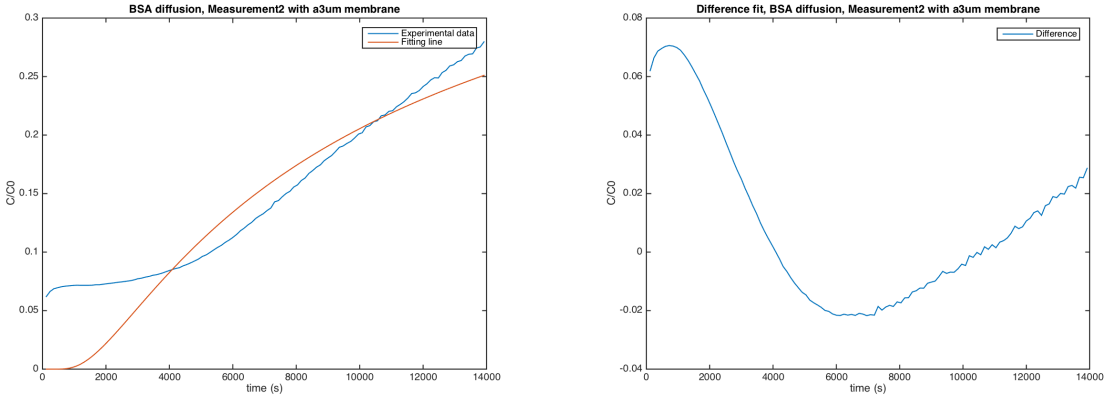

(a) A plot of the measurement data and the curve fit calculated by fitting the data to Equation **??** by minimizing the sum of squares

(b) Error of the fit with the measurement data

Figure G.29: Dynamic measurement cycle 2 for diffusion of BSA through a flow cell with a 3 µm pore size membrane.

Table G.29: Fitting values

	Value
a	0.5830
b	0.2701
resnorm	0.1021
weighted resnorm	0.3004

P3 The third set of measurements has similarities with the second one and the fit also seems to need a slight shift to reduce the resnorm. Nevertheless the values for a and b as well as the weighted resnorm are within the accepted range. Looking at the error of the fit in Figure G.30b, again a sinusoidal progression is visible and the formation of noise peaks over time can be distinguished.

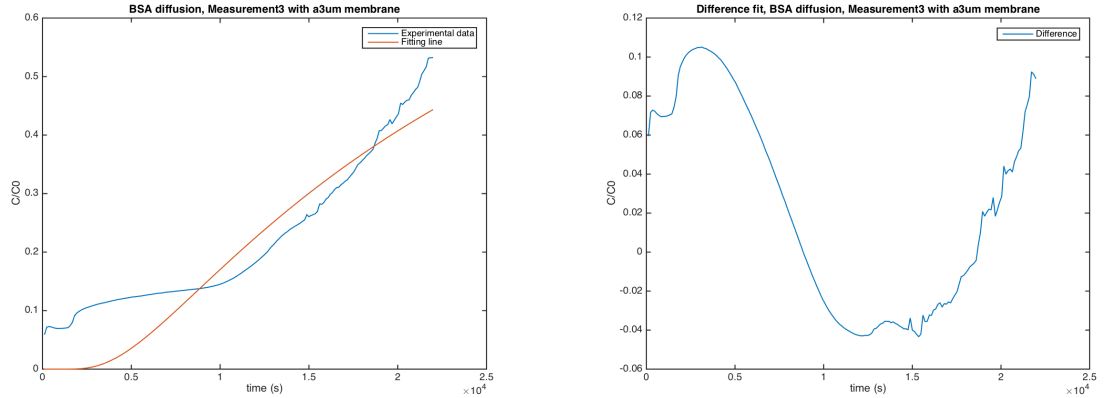

(a) A plot of the measurement data and the curve fit calculated by fitting the data to Equation **??** by minimizing the sum of squares

(b) Error of the fit with the measurement data

Figure G.30: Dynamic measurement cycle 3 for diffusion of BSA through a flow cell with a 3 µm pore size membrane.

Table G.30: Fitting values

	Value
a	1.6129
b	0.4702
resnorm	0.5849
weighted resnorm	0.2248

G.1.8. BSA, 5 µm pore size

Four subsequent measurements with BSA diffusion are done with the microfluidic system including a membrane with a 5µm pore size.

P1 The first set of measurements show a sudden steep increase around 13000 seconds followed by a decrease in concentration. This experimental value results in a very high value for a, which is not reasonable and therefore this measurement must be omitted.

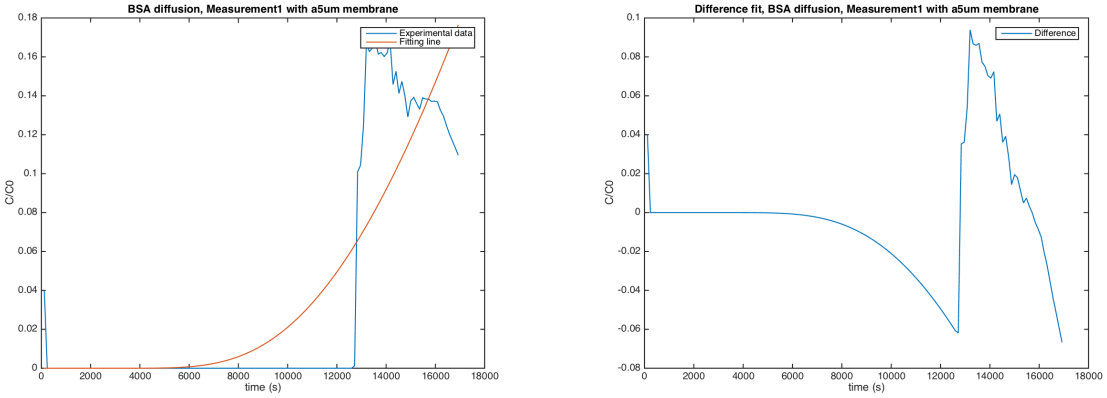

(a) A plot of the measurement data and the curve fit calculated by fitting the data to Equation **??** by minimizing the sum of squares

(b) Error of the fit with the measurement data

Figure G.31: Dynamic measurement cycle 1 for diffusion of BSA through a flow cell with a 5 µm pore size membrane.

Table G.31: Fitting values

	Value
a	9.3416
b	0.8873
resnorm	0.1340
weighted resnorm	0.0015

P2 The second set of measurements is of very low value and the Matlab script is not able to fit the measurements with values that are within the accepted range. As can be seen, the a value is negative, which is not possible because a a situation with a negative concentration is physically not possible. Further, the value for b is relatively large.

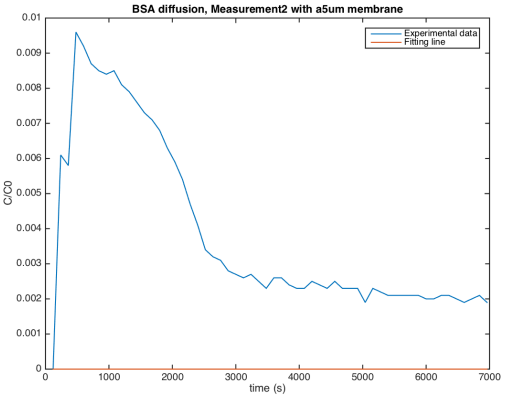

(a) A plot of the measurement data and the curve fit calculated by fitting the data to Equation **??** by minimizing the sum of squares

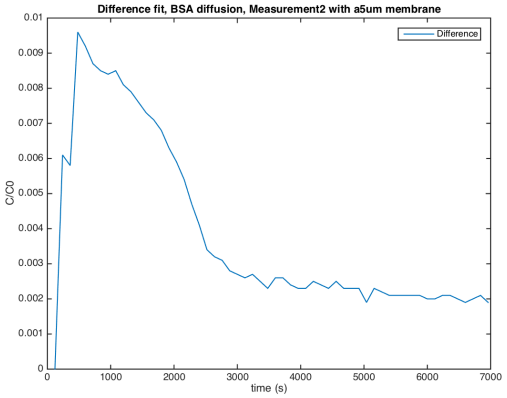

(b) Error of the fit with the measurement data

Figure G.32: Dynamic measurement cycle 2 for diffusion of BSA through a flow cell with a 5 µm pore size membrane.

Table G.32: Fitting values

	Value
a	-0.3693
b	8.1152
resnorm	0.0012
weighted resnorm	0.0088

P3 The third set of measurements starts with a non-zero concentration and propagates in a way that can be fitted properly. The fitting values are within the accepted range and the weighted resnorm is relatively high. Then looking at the fitting difference curve in Figure G.33b, one can see that the curve begins smoothly and higher noise peaks appear over time.

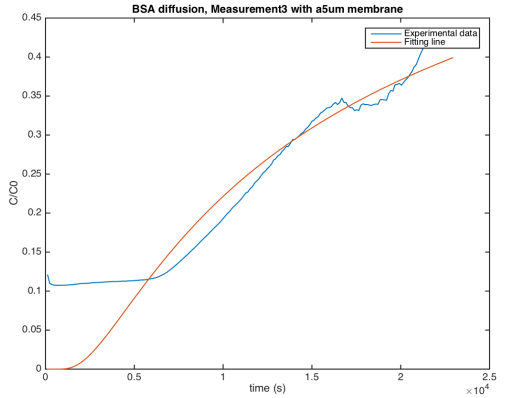

(a) A plot of the measurement data and the curve fit calculated by fitting the data to Equation **??** by minimizing the sum of squares

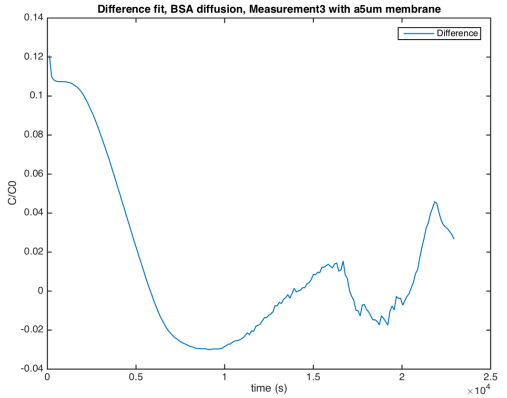

(b) Error of the fit with the measurement data

Figure G.33: Dynamic measurement cycle 3 for diffusion of BSA through a flow cell with a 5 µm pore size membrane.

Table G.33: Fitting values

	Value
a	0.8992
b	0.3368
resnorm	0.3661
weighted resnorm	0.4528

P4 The fourth set of measurements shows a phenomenon that is also visible in Figure G.29a and G.30a. When the fitting script would have allowed for a shift in the concentration, the weighted resnorm would be much lower. This is proved in the next paragraph

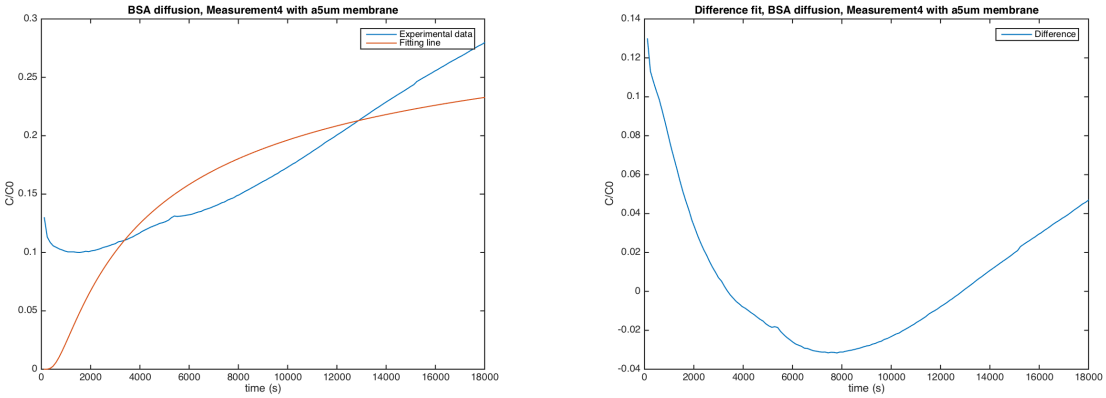

(a) A plot of the measurement data and the curve fit calculated by fitting the data to Equation **??** by minimizing the sum of squares

(b) Error of the fit with the measurement data

Figure G.34: Dynamic measurement cycle 4 for diffusion of BSA through a flow cell with a 5 µm pore size membrane.

Table G.34: Fitting values

	Value
a	0.3509
b	0.1696
resnorm	0.1847
weighted resnorm	1.5000

P4 shifted This paragraph is meant to prove that the fitting values can improve when shifting the measurement curve to a zero value at t=0. As can be seen, the fitted values for a and b are changed towards 1 and the weighted resnorm decreased with a factor 100. All values are within the desired range. When looking at the error of the fit, a sinusoidal error with a relatively small amplitude and small noise peaks are visible.

Table G.35: Fitting values

	Value
a	0.4701
b	0.4098
resnorm	0.0024
weighted resnorm	0.0109

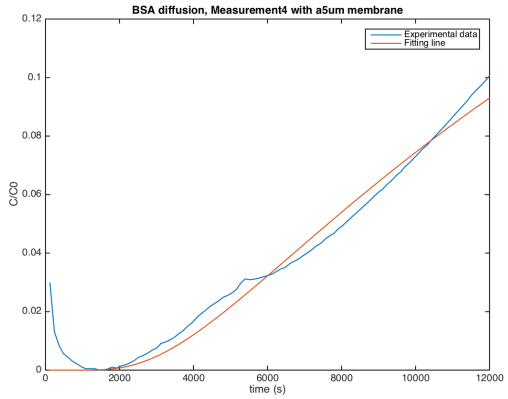

(a) A plot of the measurement data and the curve fit calculated by fitting the data to Equation **??** by minimizing the sum of squares

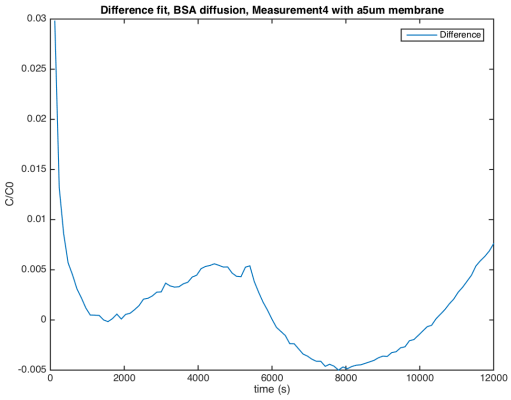

(b) Error of the fit with the measurement data

Figure G.35: Shifted dynamic measurement cycle 4 for diffusion of BSA through a flow cell with a 5 µm pore size membrane.

G.2. Comparison of the fitted a and b values in consecutive test cycles

In this section, all of the fitted a and b values are plotted in sequence of testing, to enable to see the correlation between the value and a potential fouling effect. For every membrane with every feed particle, the values are plotted as circles and the dashed lines are intended to guide the eye. After the sections in which the change in a and b value are plotted and described, a section follows in which the interpretations and conclusions for all plots is given.

G.2.1. Glycine

Membrane with 0.4 µm pore size In the plots of Figure G.36a and G.36b, the first test cycle has a low value for both a and b and these values rise slowly after the test cycles. The reason why the a value could become higher is that fluorescent particles adhere to the PDMS layers and are clotting together at the measuring point. However, the measurements with Glycine with the 0.4 µm membrane all started with a $C_0 = 0$ measurement.

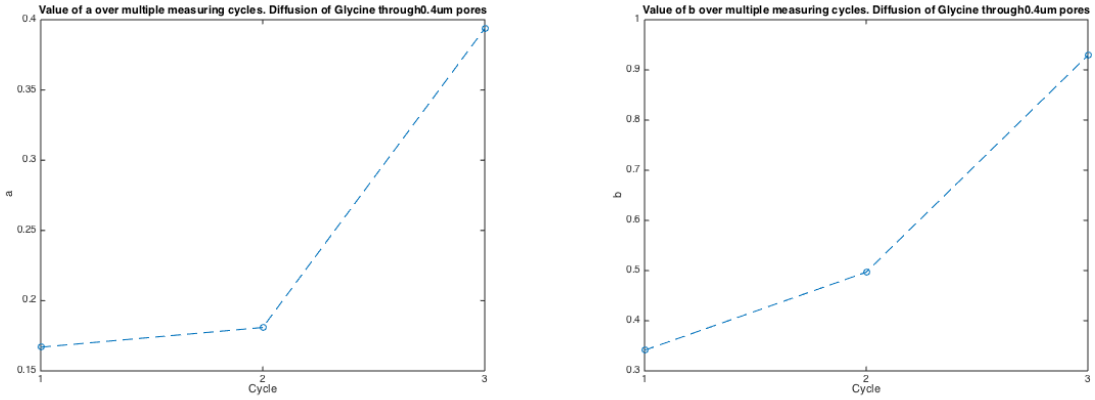

(a) (b)

Figure G.36: Plot of a and b value of follow-up measurements determined for a microfluidic system with a 0.4 µm pore membrane infused with Glycine.

Membrane with 1 µm pore size Because the values of a and b of the second and third test are not considered, only one value is shown in Figure G.37a and G.37b. This value cannot be compared so no conclusion can be drawn on dependency on consequent measurements.

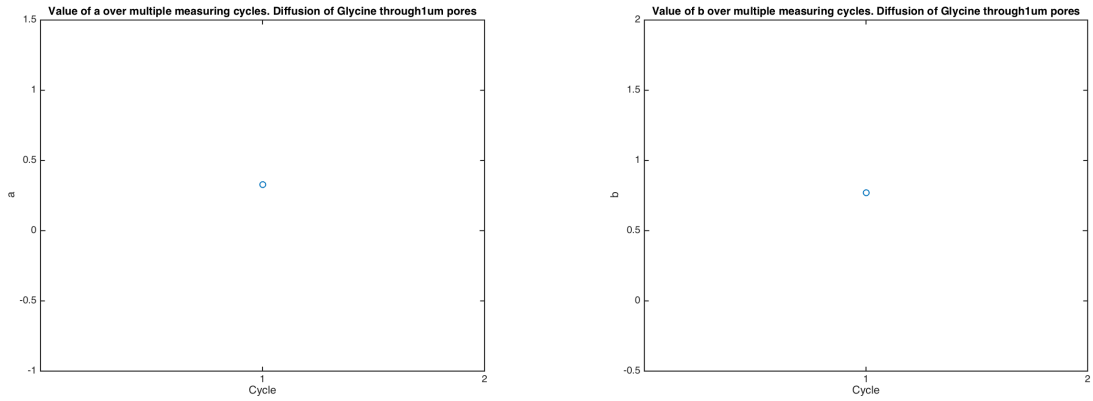

(a) (b)

Figure G.37: Plot of a and b value of follow-up measurements determined for a microfluidic system with a 1 µm pore membrane infused with Glycine.

Membrane with 3 µm pore size When comparing the valid measurements done with Glycine with the membrane with 3 µm pore size the values for a and b are increasing with a factor of 5-10, which seems to be a relatively large factor.

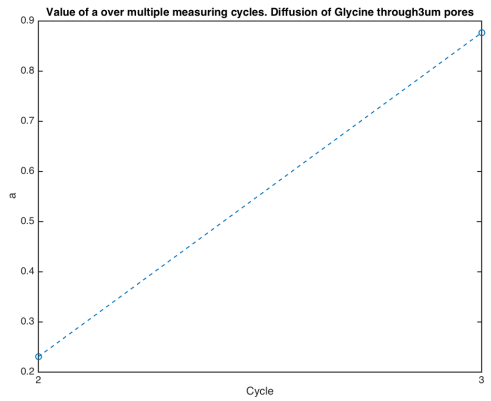

(a)

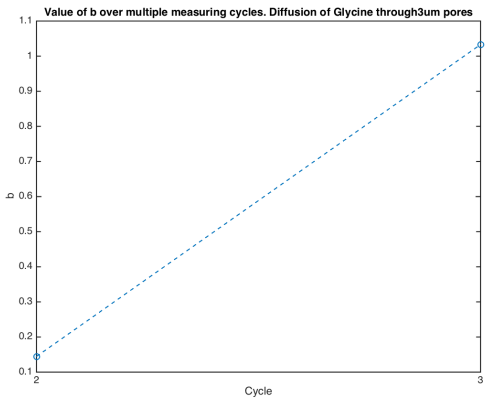

(b)

Figure G.38: Plot of a and b value of follow-up measurements determined for a microfluidic system with a 3 µm pore membrane infused with Glycine.

Membrane with 5 µm pore size When comparing the valid measurements done with Glycine with the membrane with 5 µm pore size, a new combination is seen: a is decreasing over the second to third cycle and b is decreasing over the same cycle.

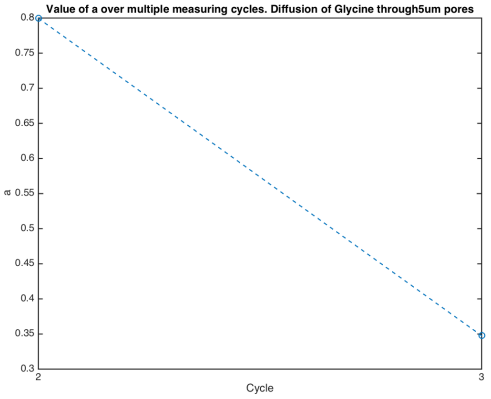

(a)

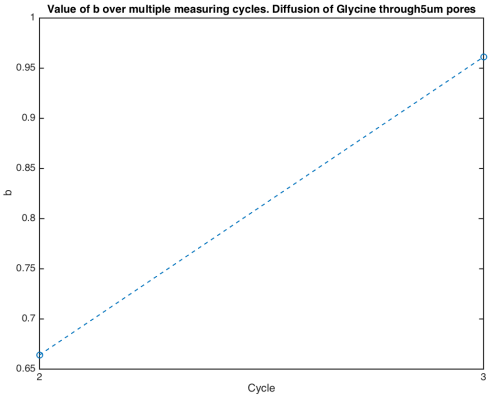

(b)

Figure G.39: Plot of a and b value of follow-up measurements determined for a microfluidic system with a 5 µm pore membrane infused with Glycine.

G.2.2. BSA

Membrane with 0.4 µm pore size In the plots of Figure G.40a and G.40b, the first test cycle has an inconspicuous value for both a and b and these values rises at the second test cycle and then at the third test cycle, the value for both a and b is comparable to the value of the first test cycle.

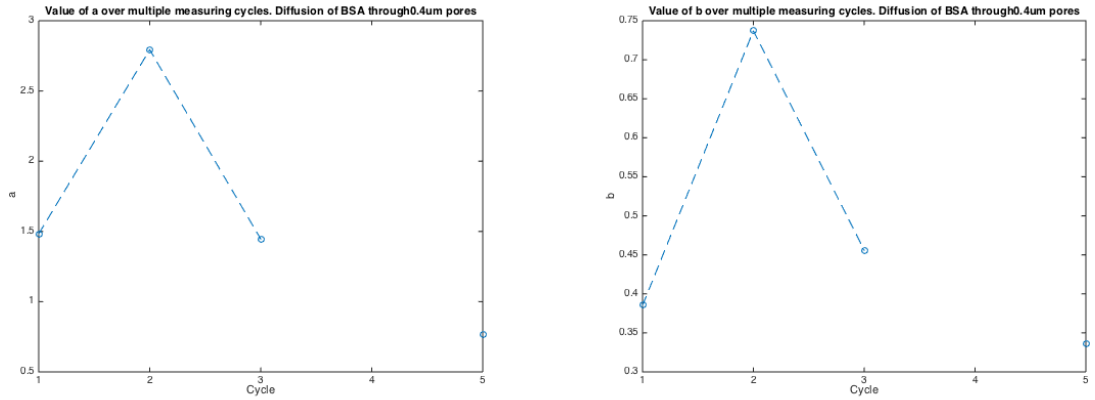

(a) (b)

Figure G.40: Plot of a and b value of follow-up measurements determined for a microfluidic system with a 0.4 µm pore membrane infused with BSA.

Membrane with 1 µm pore size In the plots of Figure G.41a and G.41b, the value of a increases a factor 3 from the first to the second measurement cycle and b decreases with a factor 0.3. This would physically mean that the permeability of the membrane increases after the first measurement.

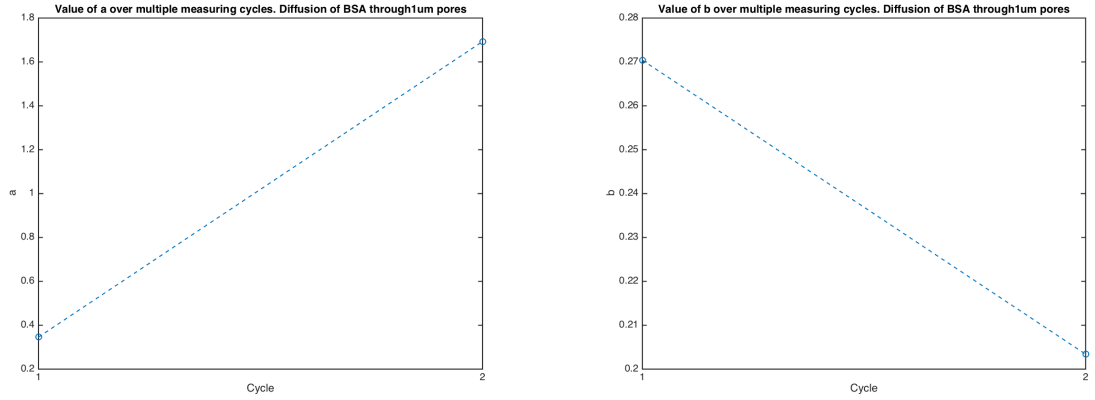

(a) (b)

Figure G.41: Plot of a and b value of follow-up measurements determined for a microfluidic system with a 1 µm pore membrane infused with BSA.

Membrane with 3 µm pore size In the plots of Figure G.42a and G.42b, the a and b value decrease in the second test cycle and increase again in the third test cycle.

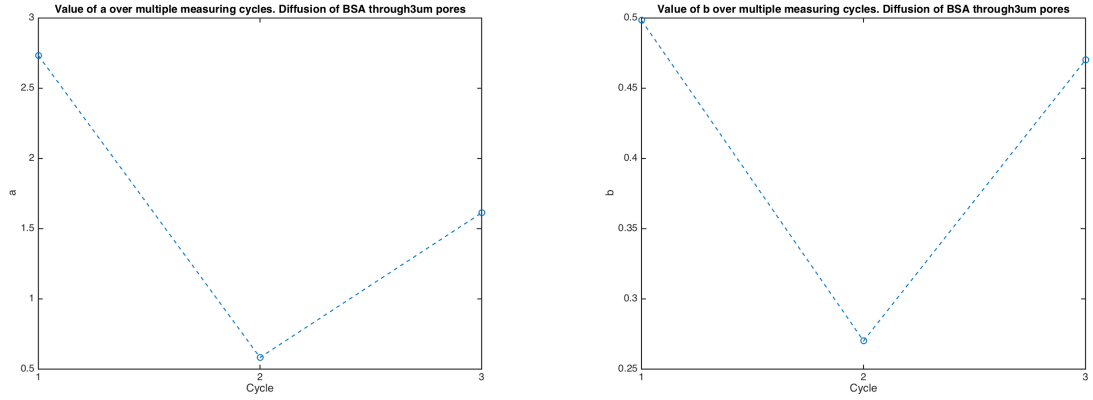

(a) (b)

Figure G.42: Plot of a and b value of follow-up measurements determined for a microfluidic system with a 3 µm pore membrane infused with BSA.

Membrane with 5 µm pore size In the plots of Figure G.43a and G.43b, a decreases with a factor 0.5 and b increases with a factor 1.2. This is possibly an indicator of fouling.

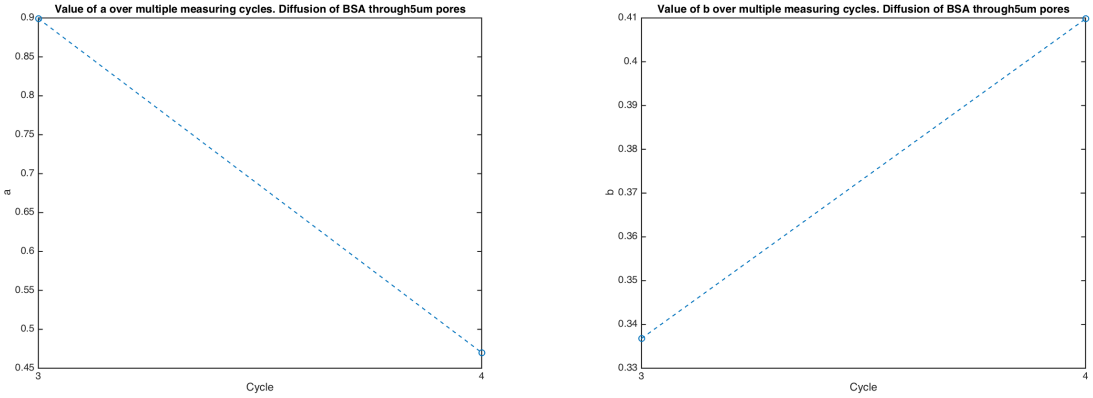

(a) (b)

Figure G.43: Plot of a and b value of follow-up measurements determined for a microfluidic system with a 5 µm pore membrane infused with BSA.

G.3. Dependence of a and b value on pore size

In order to verify whether the pore size of the membrane has a correlation with the measured data, mean a and b are calculated and plotted for membrane pore size (Figure G.44a to G.45b). The mean of the fitting values for each membrane is plotted and the error bars indicate the standard deviation of the fit. The dashed lines are intended to guide the eye.

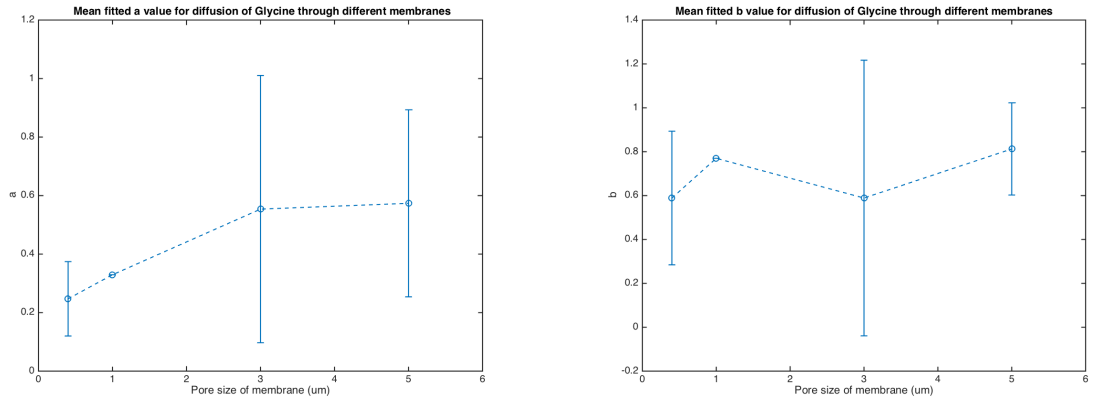

(a) (b)

Figure G.44: Dynamic diffusion analysis with Glycine: Plot of mean a and b value over pore size.

The a and b value for diffusion of Glycine through the membranes seems to have a positive correlation with pore size. Nevertheless, the relatively large bars for standard deviation designate that a conclusion cannot be drawn.

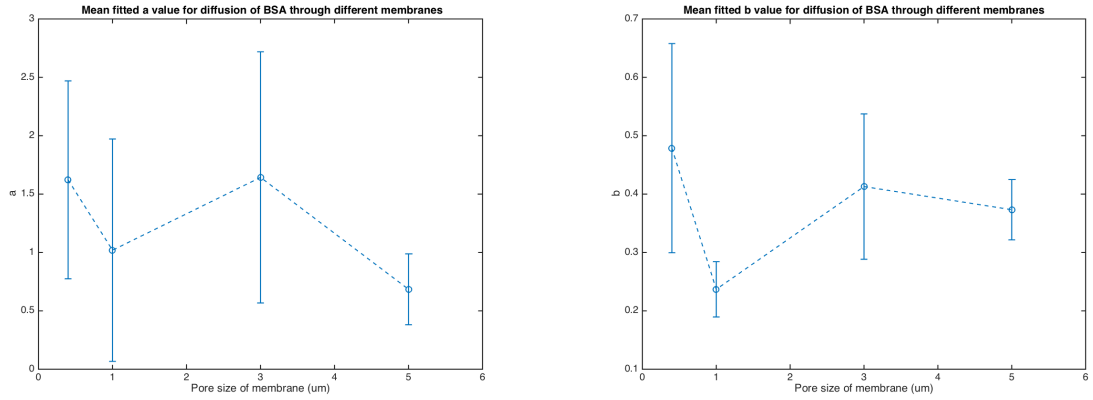

(a) (b)

Figure G.45: Dynamic diffusion analysis with BSA: Plot of mean a and b value over pore size.

The mean a and b value for diffusion of BSA through a measurement system cannot be described in only a positive or negative correlation with pore size. Either is the standard deviation small enough to draw a significant conclusion on the correlation of amount of value a and b and pore size of the membrane.

G.4. Dependence of a and b value on feed particles

The value of *a* already seemed to be higher when testing with BSA. In this chapter, the values for *a* and *b* for each system with a different membrane (thus pore size) are plotted against the tested feed particles. Because Glycine has a lower molecular weight than BSA, Glycine is plotted first in each graph.

G.4.1. 0.4 µm pore size

As can be seen in Figure G.46a and G.46b, the value of *a* increases significantly with increasing molecular weight. The mean value of *b* decreases with molecular weight, but unfortunately this is not significant.

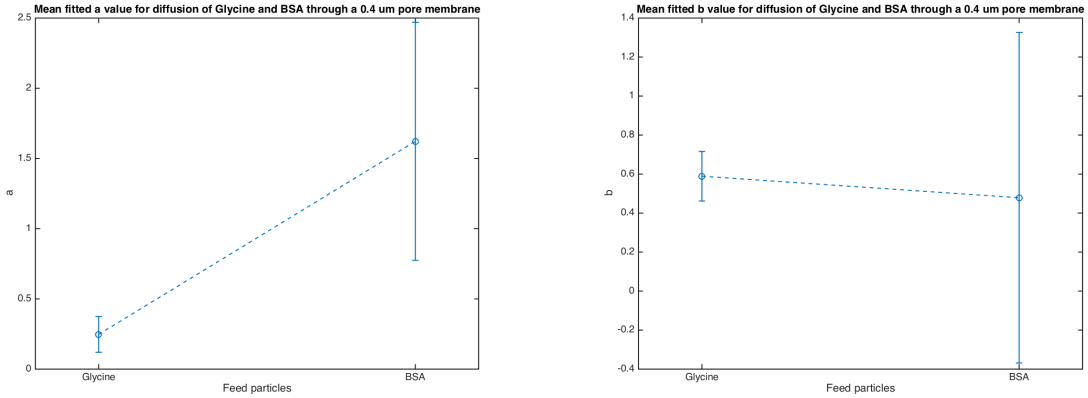

(a) (b)

Figure G.46: Dynamic diffusion analysis through a 0.4 µm pore size membrane: Plot of mean *a* and *b* value over feed particle.

G.4.2. 1 µm pore size

As can be seen in Figure G.47a and G.47b, the value of *a* increases with molecular weight and the value of *b* decreases with molecular weight. Both are non-significant.

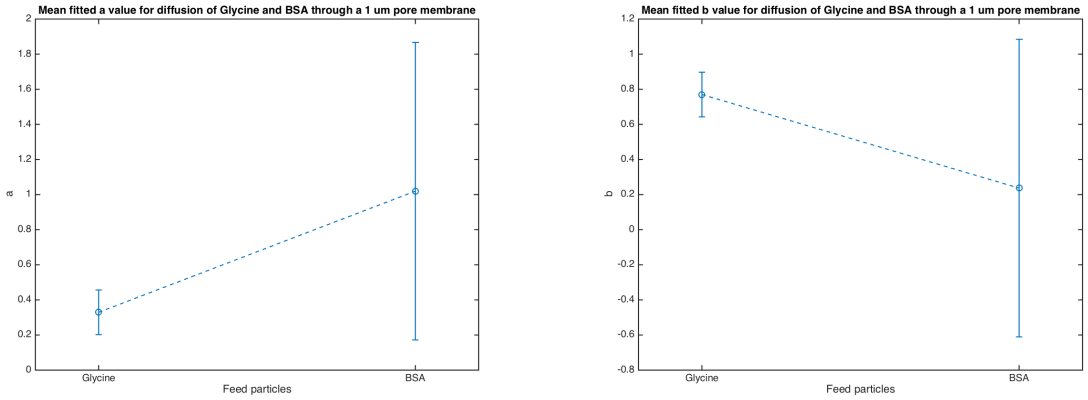

(a) (b)

Figure G.47: Dynamic diffusion analysis through a 1 µm pore size membrane: Plot of mean *a* and *b* value over feed particle.

G.4.3. 3 µm pore size

As can be seen in Figure G.48a and G.48b, the value of a increases with molecular weight and the value of b decreases with molecular weight. Both are non-significant.

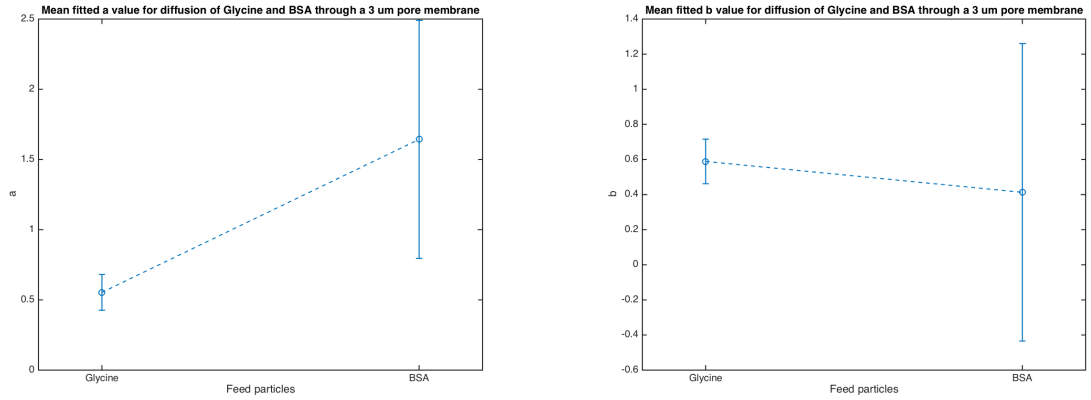

(a) (b)

Figure G.48: Dynamic diffusion analysis through a 3 µm pore size membrane: Plot of mean a and b value over feed particle.

G.4.4. 5 µm pore size

As can be seen in Figure G.49a and G.49b, the value of a increases with molecular weight and the value of b decreases with molecular weight. Both are non-significant.

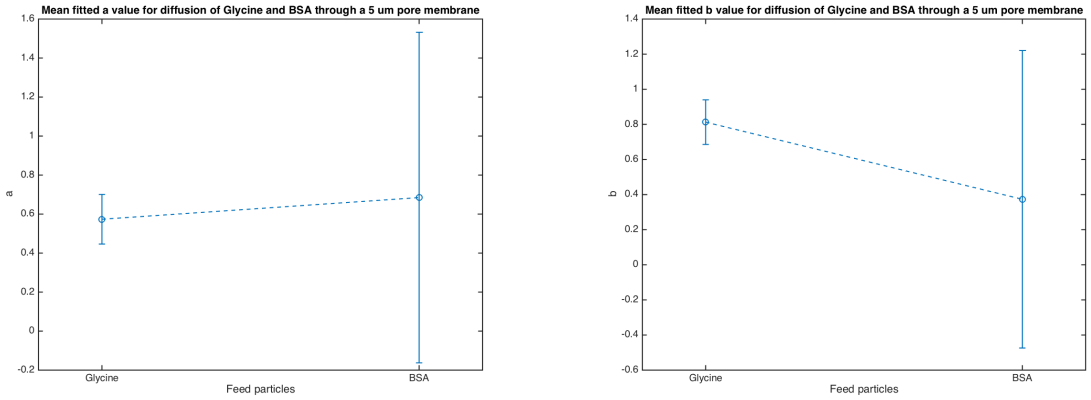

(a) (b)

Figure G.49: Dynamic diffusion analysis through a 5 µm pore size membrane: Plot of mean a and b value over feed particle.

G.4.5. All track-etched membranes

Looking at all tested membranes, there is a positive correlation for value a and a negative correlation for value b with molecular weight of the particle. Both the correlations are not significant because of the high standard deviation in the measurements. If the fouling effect on membranes is validated independent of pore size, all four fitting experiments for value a and b are taken together and a mean and error of the mean can be calculated. Figure G.50a and G.50b show the graphs with the mean of all fitting values for Glycine and BSA and the error bars indicate error of the mean.

With significance, the value of a is increasing over molecular weight. This is not an indication of fouling, but it can indicate that BSA particles agglomerate after the membrane. When looking at the a value of Glycine, which is significantly below 1 for all track-etched membranes, one could say that only part of the

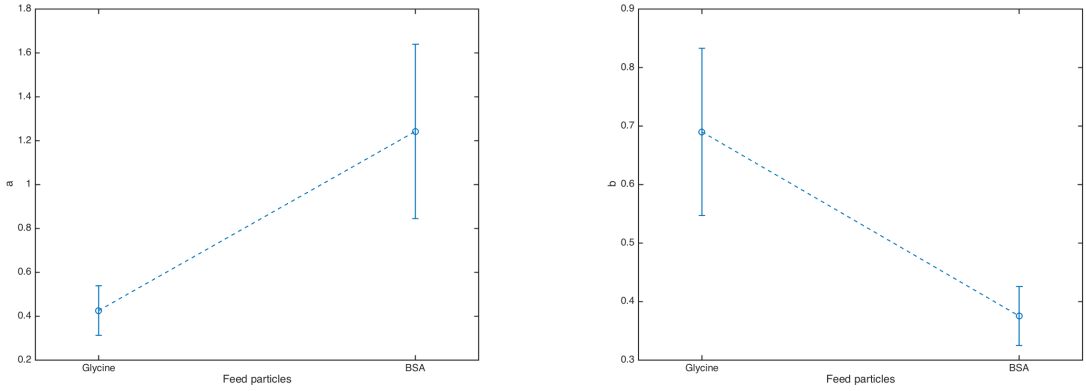

(a) (b)

Figure G.50: Dynamic diffusion analysis through several membranes: Plot of mean a and b value over feed particle.

feed particles diffuse through the membrane and there are particles adhering to the membrane. The values of b are not significantly correlated during this thesis. The b value for BSA has a large standard error and no conclusion can be drawn on this. The value of b for Glycine, is significantly lower than 1, so the diffusion term is higher than expected. No indication of fouling is distinguishable out of the results.

H

Planning

Before the start of a project, a planning is made as a guideline for each handling in time. Both the planning for the literature study and the thesis are given in this chapter.

H.1. Planning for the literature study

Week	10/10	17/10	24/10	31/10	7/11	14/11	21/11	28/11	5/12	12/12	19/12	26/12	2/1	9/1	16/1	23/1	30/1	6/2	13/2
Weeknr	41	2			3	4		5	6	7	8		9	10				11	12
Hours Lit study	16	16	16	16	16	16	16	16	16	16	16	0	16	16	16	0	0	30	26
280																			
Subject																			
Exploration																			
Current projects at TU																			
Wearable temperature sensors																			
Elaboration of sensors																			
Bubble trapping																			
Integration																			

H.2. Planning and milestones for the Thesis

In order to test every parameter well, a specific time frame is taken into account. The time frame with mile stones is visible in Table H.1. The milestone dates are marked in orange and the parts that need writing are marked in blue.

Table H.1: The planning for this thesis

Due date	What	Tasks
September 29	Literature study	☐ Finishing up Literature study
October 6	Research plan	☐ Test values ☐ Desired results ☐ Measurement devices ☐ Protocol for duration and execution of tests Research plan/planning
October 13	Device training	☐ High resolution 3D printer ☐ Chemical lab training ☐ PDMS casting ☐ Oxygen plasma treatment
October 27	Assemble every component for test	☐ Design in Solidworks ☐ Mold 3D printer fabricated ☐ Device casted in PDMS ☐ Tubing and syringes ☐ Pump ☐ Ordering of the missing components (membranes, test liquid)
November 3	Preparations for test	☐ Attaching the membrane ☐ Gluing parts together ☐ Installing the devices for a robust test setup
November 10	First test	☐ Checking and adjusting the protocol wherever needed Methods and materials
November 28	Test variable 1: Pore size	☐ Setting up and mark devices with different membranes Results: Pore size
December 15	Test variable 2: Pore tortuosity	☐ Setting up and mark devices with different membranes Results: Pore tortuosity
January 16	Test variable 3: Particle size	☐ Use 4 similar devices to test different feed Results: Particle nature/size
February 3	Test variable 4: Particle concentration	Use 4 similar devices to test different feed concentrations Results: Particle concentration
February 20	Test variable 5: Flowrate feed	☐ Use 4 similar devices to test different feed flow rates Results: Flow rate feed
March 2	Results & Analysis	☐ Calculating errors ☐ Comparing to literature Analysis
March 9	Conclusions	☐ Answering research questions Conclusion
March 9	Recommendations	☐ Other variables to test ☐ Other fields to explore with the results Recommendations
March 9	Planning of the defence	☐ Email Shannah Dokter to set a date
March 16	Submit pre-thesis	☐ Finalize report Abstract
March 30	Submit final thesis	☐ Compose presentation Corrections on thesis

H.3. Risk mitigation

There are four big milestones, which go with risks and are susceptible to not be completed within the given time when anything goes wrong. For every milestone a risk mitigation is done in which the risks are made clear and a 'plan B' is proposed.

H.3.1. Milestone 1: Production test set-up

The first milestone is incorporating every production step and ordering of components. As all of the production processes are executed in-house, much experience is apparent and there will probably not be a lot of unexpected problems concerning the production of the test set-up. A few components, however, must be ordered and can take time to arrive. Table H.2 shows the risk mitigation for milestone 1.

Table H.2: Risk table for Milestone 1

Process	**Risk**	**Possible solution**
3D printing	Bubbles	Degassing HTM140
PDMS casting	Bubbles	Degassing for a longer period
Membrane	Membrane does not stick well	Other adhesive

H.3.2. Milestone 2: Testing

The second milestone has to do with the testing phase and problems occuring during tests.

Table H.3 shows the risk mitigation for milestone 2.

Table H.3: Risk table for Milestone 2

Process	**Risk**	**Possible solution**
Testing	Leakages	sealing using a UV curable adhesive (Mukherjee) sealing with the silicon adhesive tape
PDMS	Channels collapse	Smaller dimensions
PDMS	Fouling on PDMS	Coating the PDMS channels Other material (Teflon)
Testing	Weak diffusion	Higher concentration of feed Larger membrane area
Fluorescent Microscope	Depth of focus	Changing height channels

H.3.3. Milestone 3: Writing thesis

The third milestone is about the results that need to be processed and analysed and the relations and conclusions that are drawn.

Table H.4 shows the risk mitigation for milestone 3. As can be seen, the risk analysis results in precautions that need to be done. Four measurements per setting will be the minimum, but the more measurements can be done, the more reliable the results are.

Table H.4: Risk table for Milestone 3

Process	**Risk**	**Precaution**
Analysis	Measurements that are outliers	Do at least 4 measurements with each setting

H.3.4. Milestone 4: Finalizing and presenting

The fourth milestone is related to the presentation of the work as a whole. Nothing has to be made and the tests must already be concluded at that point, but finalizing the report and writing the conclusions can give a lot of stress. Here, the best way to prevent stress is to listen to oneself and know when to take rest.

Bibliography

[1] Hasan Erbil Abaci, Karl Gledhill, Zongyou Guo, Angela M Christiano, and Michael L Shuler. Pumpless microfluidic platform for drug testing on human skin equivalents. *Lab on a Chip*, 15(3):882–888, 2015.

[2] Darryl R Absolom and A Wilhelm Neumann. Modification of substrate surface properties through protein adsorption. *Colloids and surfaces*, 30(1):25–45, 1987.

[3] MA Alam. Principles of electronic nanobiosensors. *Nanohub web course*, 2013.

[4] Wui Seng Ang, Sangyoup Lee, and Menachem Elimelech. Chemical and physical aspects of cleaning of organic-fouled reverse osmosis membranes. *Journal of Membrane Science*, 272(1):198–210, 2006.

[5] Ayse Asatekin, Elsa A Olivetti, and Anne M Mayes. Fouling resistant, high flux nanofiltration membranes from polyacrylonitrile-graft-poly (ethylene oxide). *Journal of Membrane Science*, 332(1):6–12, 2009.

[6] Richard W Baker. Membrane technology and applications. *John Wiley & Sons, Ltd*, pages 96–103, 2004.

[7] Stefan Balta, Arcadio Sotto, Patricia Luis, Lidia Benea, Bart Van der Bruggen, and Jeonghwan Kim. A new outlook on membrane enhancement with nanoparticles: the alternative of zno. *Journal of membrane science*, 389:155–161, 2012.

[8] Prity Bengani, Yangming Kou, and Ayse Asatekin. Zwitterionic copolymer self-assembly for fouling resistant, high flux membranes with size-based small molecule selectivity. *Journal of Membrane Science*, 493:755–765, 2015.

[9] Douglas M Benson, Joseph Bryan, Anne L Plant, Antonio M Gotto, and Louis C Smith. Digital imaging fluorescence microscopy: spatial heterogeneity of photobleaching rate constants in individual cells. *The Journal of cell biology*, 100(4):1309–1323, 1985.

[10] Shantanu Bhattacharya, Arindom Datta, Jordan M Berg, and Shubhra Gangopadhyay. Studies on surface wettability of poly (dimethyl) siloxane (pdms) and glass under oxygen-plasma treatment and correlation with bond strength. *Journal of microelectromechanical systems*, 14(3):590–597, 2005.

[11] Dhananjay Bodas and Chantal Khan-Malek. Hydrophilization and hydrophobic recovery of pdms by oxygen plasma and chemical treatment—an sem investigation. *Sensors and Actuators B: Chemical*, 123 (1):368–373, 2007.

[12] Glen R Bolton, Austin W Boesch, and Matthew J Lazzara. The effects of flow rate on membrane capacity: development and application of adsorptive membrane fouling models. *Journal of Membrane Science*, 279(1):625–634, 2006.

[13] Katleen Boussu, Carlo Vandecasteele, and Bart Van der Bruggen. Relation between membrane characteristics and performance in nanofiltration. *Journal of Membrane Science*, 310(1):51–65, 2008.

[14] WR Bowen, JI Calvo, and A Hernandez. Steps of membrane blocking in flux decline during protein microfiltration. *Journal of Membrane Science*, 101(1-2):153–165, 1995.

[15] LES Brink, SJG Elbers, T Robbertsen, and P Both. The anti-fouling action of polymers preadsorbed on ultrafiltration and microfiltration membranes. *Journal of membrane science*, 76(2-3):281–291, 1993.

[16] AD Britt and William B Moniz. Reactivity of first-singlet excited xanthene laser dyes in solution. *The Journal of Organic Chemistry*, 38(5):1057–1059, 1973.

[17] MG Buonomenna, LC Lopez, P Favia, R d'Agostino, A Gordano, and E Drioli. New pvdf membranes: the effect of plasma surface modification on retention in nanofiltration of aqueous solution containing organic compounds. *Water research*, 41(19):4309–4316, 2007.

[18] BD Cho and AG Fane. Fouling transients in nominally sub-critical flux operation of a membrane bioreactor. *Journal of membrane science*, 209(2):391–403, 2002.

[19] Dong-Chan Choi, Seon-Yeop Jung, Young-June Won, Jun Hee Jang, Jaewoo Lee, Hee-Ro Chae, Kyung Hyun Ahn, Sangho Lee, Pyung-Kyu Park, and Chung-Hak Lee. Three-dimensional hydraulic modeling of particle deposition on the patterned isopore membrane in crossflow microfiltration. *Journal of Membrane Science*, 492:156–163, 2015.

[20] Hyeok Choi, Kai Zhang, Dionysios D Dionysiou, Daniel B Oerther, and George A Sorial. Effect of permeate flux and tangential flow on membrane fouling for wastewater treatment. *Separation and Purification Technology*, 45(1):68–78, 2005.

[21] Hyeok Choi, Kai Zhang, Dionysios D Dionysiou, Daniel B Oerther, and George A Sorial. Influence of cross-flow velocity on membrane performance during filtration of biological suspension. *Journal of membrane science*, 248(1):189–199, 2005.

[22] Liang-Yin Chu, Yan Li, Jia-Hua Zhu, Hai-Dong Wang, and Yi-Jian Liang. Control of pore size and permeability of a glucose-responsive gating membrane for insulin delivery. *Journal of Controlled Release*, 97 (1):43–53, 2004.

[23] Michael W Chudacek and Anthony G Fane. The dynamics of polarisation in unstirred and stirred ultrafiltration. *Journal of membrane science*, 21(2):145–160, 1984.

[24] Christopher T Culbertson, Stephen C Jacobson, and J Michael Ramsey. Diffusion coefficient measurements in microfluidic devices. *Talanta*, 56(2):365–373, 2002.

[25] Yuan Dang, Miao Quan, Cheng-Mei Xing, Yan-Bing Wang, and Yong-Kuan Gong. Biocompatible and antifouling coating of cell membrane phosphorylcholine and mussel catechol modified multi-arm pegs. *Journal of Materials Chemistry B*, 3(11):2350–2361, 2015.

[26] Jianping Deng, Lifu Wang, Lianying Liu, and Wantai Yang. Developments and new applications of uv-induced surface graft polymerizations. *Progress in Polymer Science*, 34(2):156–193, 2009.

[27] MS El-Bourawi, Z Ding, R Ma, and Mohammed Khayet. A framework for better understanding membrane distillation separation process. *Journal of Membrane Science*, 285(1):4–29, 2006.

[28] Menachem Elimelech, Xiaohua Zhu, Amy E Childress, and Seungkwan Hong. Role of membrane surface morphology in colloidal fouling of cellulose acetate and composite aromatic polyamide reverse osmosis membranes. *Journal of membrane science*, 127(1):101–109, 1997.

[29] DC Elliott, RMC Dawson, WH Elliott, and KM Jones. Data for biochemical research. *Clarendon Press, Oxford*, page 221, 1959.

[30] Harold P Erickson. Size and shape of protein molecules at the nanometer level determined by sedimentation, gel filtration, and electron microscopy. *Biological procedures online*, 11(1):32, 2009.

[31] Milad Rabbani Esfahani, Holly A Stretz, and Martha JM Wells. Comparing humic acid and protein fouling on polysulfone ultrafiltration membranes: Adsorption and reversibility. *Journal of Water Process Engineering*, 6:83–92, 2015.

[32] M Ferrando, A Rŏžek, M Zator, F Lopez, and C Güell. An approach to membrane fouling characterization by confocal scanning laser microscopy. *Journal of Membrane Science*, 250(1):283–293, 2005.

[33] Robert W Field and Jun Jie Wu. Modelling of permeability loss in membrane filtration: Re-examination of fundamental fouling equations and their link to critical flux. *Desalination*, 283:68–74, 2011.

[34] Sal Giglia and Greg Straeffer. Combined mechanism fouling model and method for optimization of series microfiltration performance. *Journal of membrane science*, 417:144–153, 2012.

[35] Peter D Godfrey and Ronald D Brown. Shape of glycine. *Journal of The American Chemical Society*, 117 (7):2019–2023, 1995.

[36] Peter Grathwohl. *Diffusion in natural porous media: contaminant transport, sorption/desorption and dissolution kinetics*, volume 1. Springer Science & Business Media, 2012.

[37] N Awanis Hashim, Fu Liu, and K Li. A simplified method for preparation of hydrophilic pvdf membranes from an amphiphilic graft copolymer. *Journal of Membrane Science*, 345(1):134–141, 2009.

[38] ACJI Hernández, JI Calvo, P Prádanos, and F Tejerina. Pore size distributions in microporous membranes. a critical analysis of the bubble point extended method. *Journal of Membrane Science*, 112(1): 1–12, 1996.

[39] Chia-Chi Ho and Andrew L Zydney. A combined pore blockage and cake filtration model for protein fouling during microfiltration. *Journal of colloid and interface science*, 232(2):389–399, 2000.

[40] Ingmar H Huisman, Pedro Prádanos, and Antonio Hernández. The effect of protein–protein and protein–membrane interactions on membrane fouling in ultrafiltration. *Journal of Membrane Science*, 179(1-2):79–90, 2000.

[41] Luca Ianeselli, Fajun Zhang, Maximilian WA Skoda, Robert MJ Jacobs, Richard A Martin, Shirley Callow, Sylvain Prévost, and Frank Schreiber. Protein- protein interactions in ovalbumin solutions studied by small-angle scattering: effect of ionic strength and the chemical nature of cations. *The Journal of Physical Chemistry B*, 114(11):3776–3783, 2010.

[42] Yasunori Ichiki, Patrick SC Leung, Hiromi Ishibashi, Ross L Coppel, Aftab A Ansari, and M Eric Gershwin. Mitochondria and autoimmunity in primary biliary cirrhosis. *Mitochondrion*, 4(5):743–753, 2004.

[43] YL Jeyachandran, E Mielczarski, B Rai, and JA Mielczarski. Quantitative and qualitative evaluation of adsorption/desorption of bovine serum albumin on hydrophilic and hydrophobic surfaces. *Langmuir*, 25(19):11614–11620, 2009.

[44] B-H Jo, Linda M Van Lerberghe, Kathleen M Motsegood, and David J Beebe. Three-dimensional microchannel fabrication in polydimethylsiloxane (pdms) elastomer. *Journal of microelectromechanical systems*, 9(1):76–81, 2000.

[45] Seoktae Kang, Ayse Asatekin, Anne M Mayes, and Menachem Elimelech. Protein antifouling mechanisms of pan uf membranes incorporating pan-g-peo additive. *Journal of Membrane Science*, 296(1): 42–50, 2007.

[46] M Khayet and JI Mengual. Effect of salt concentration during the treatment of humic acid solutions by membrane distillation. *Desalination*, 168:373–381, 2004.

[47] Brian J Kirby. *Micro-and nanoscale fluid mechanics: transport in microfluidic devices*. Cambridge university press, 2010.

[48] Jong Kwan Koh, Yong Woo Kim, Sung Hoon Ahn, Byoung Ryul Min, and Jong Hak Kim. Antifouling poly (vinylidene fluoride) ultrafiltration membranes containing amphiphilic comb polymer additive. *Journal of Polymer Science Part B: Polymer Physics*, 48(2):183–189, 2010.

[49] Andrzej B Koltuniewicz, RW Field, and TC Arnot. Cross-flow and dead-end microfiltration of oily-water emulsion. part i: experimental study and analysis of flux decline. *Journal of Membrane Science*, 102: 193–207, 1995.

[50] NoHwa Lee, Gary Amy, Jean-Philippe Croue, and Herve Buisson. Identification and understanding of fouling in low-pressure membrane (mf/uf) filtration by natural organic matter (nom). *Water research*, 38(20):4511–4523, 2004.

[51] Jian-Hua Li, Mi-Zi Li, Jing Miao, Jia-Bin Wang, Xi-Sheng Shao, and Qi-Qing Zhang. Improved surface property of pvdf membrane with amphiphilic zwitterionic copolymer as membrane additive. *Applied Surface Science*, 258(17):6398–6405, 2012.

[52] Jie Liu, Xiang Shen, Yiping Zhao, and Li Chen. Acryloylmorpholine-grafted pvdf membrane with improved protein fouling resistance. *Industrial & Engineering Chemistry Research*, 52(51):18392–18400, 2013.

[53] Zhuang Liu, Wei Wang, Rui Xie, Xiao-Jie Ju, and Liang-Yin Chu. Stimuli-responsive smart gating membranes. *Chemical Society Reviews*, 45(3):460–475, 2016.

[54] ShyTyug Loh, Uwe Beuscher, Tarun K Poddar, Andrew G Porter, J Mark Wingard, Scott M Husson, and S Ranil Wickramasinghe. Interplay among membrane properties, protein properties and operating conditions on protein fouling during normal-flow microfiltration. *Journal of Membrane Science*, 332(1): 93–103, 2009.

[55] L Longsworth. Diffusion in liquids and the stokes–einstein relation, 1955.

[56] Alagarsamy Mathavan, Arumugam Ramdass, and Seenivasan Rajagopal. A spectroscopy approach for the study of the interaction of oxovanadium (iv)-salen complexes with proteins. *Journal of fluorescence*, 25(4):1141–1149, 2015.

[57] Tao Meng, Rui Xie, Yong-Chao Chen, Chang-Jing Cheng, Peng-Fei Li, Xiao-Jie Ju, and Liang-Yin Chu. A thermo-responsive affinity membrane with nano-structured pores and grafted poly (n-isopropylacrylamide) surface layer for hydrophobic adsorption. *Journal of Membrane Science*, 349(1-2): 258–267, 2010.

[58] Baoxia Mi and Menachem Elimelech. Organic fouling of forward osmosis membranes: fouling reversibility and cleaning without chemical reagents. *Journal of membrane science*, 348(1):337–345, 2010.

[59] Daniella B Mosqueda-Jimenez, Roberto M Narbaitz, and Takeshi Matsuura. Impact of membrane surface modification on the treatment of surface water. *Journal of environmental engineering*, 130(12): 1450–1459, 2004.

[60] Manisha Mukherjee, Nishanth V Menon, Xin Liu, Yuejun Kang, and Bin Cao. Confocal laser scanning microscopy-compatible microfluidic membrane flow cell as a nondestructive tool for studying biofouling dynamics on forward osmosis membranes. *Environmental Science & Technology Letters*, 3(8):303–309, 2016.

[61] Tejal M Patel and Kaushik Nath. Performance of polyamide and polyethersulfone membranes in the nanofiltration of reactive dye-salt mixtures on pilot scale. *Desalination and water treatment*, 52(37-39): 7026–7036, 2014.

[62] Fangshu Qu, Heng Liang, Zhaozhi Wang, Hui Wang, Huarong Yu, and Guibai Li. Ultrafiltration membrane fouling by extracellular organic matters (eom) of microcystis aeruginosa in stationary phase: influences of interfacial characteristics of foulants and fouling mechanisms. *Water research*, 46(5):1490–1500, 2012.

[63] D Rana and T Matsuura. Surface modifications for antifouling membranes. *Chemical reviews*, 110(4): 2448–2471, 2010.

[64] Amir Razmjou, Ellen Arifin, Guangxi Dong, Jaleh Mansouri, and Vicki Chen. Superhydrophobic modification of tio 2 nanocomposite pvdf membranes for applications in membrane distillation. *Journal of membrane science*, 415:850–863, 2012.

[65] Xueqin Ren, Mark Bachman, Christopher Sims, GP Li, and Nancy Allbritton. Electroosmotic properties of microfluidic channels composed of poly (dimethylsiloxane). *Journal of Chromatography B: Biomedical Sciences and Applications*, 762(2):117–125, 2001.

[66] Enrica Ricci, Roberto Sangiorgi, and Alberto Passerone. On the measurement of the surface tension of dna solutions. *Journal of colloid and interface science*, 102(1):295–297, 1984.

[67] Diana M Rodríguez and Carmen M Romero. Surface tension of glycine, alanine, aminobutyric acid, norvaline, and norleucine in water and in aqueous solutions of strong electrolytes at temperatures from (293.15 to 313.15) k. *Journal of Chemical & Engineering Data*, 62(11):3687–3696, 2017.

[68] Gianpaolo Sabia, Marco Ferraris, and Alessandro Spagni. Model-based analysis of the effect of different operating conditions on fouling mechanisms in a membrane bioreactor. *Environmental Science and Pollution Research*, 23(2):1598–1609, 2016.

[69] Florencia Saravia, Angela Klüpfel, Amadeu Zamora Richard, and Fritz H Frimmel. Identification of nanofiltration fouling layer constituents. *Desalination and Water Treatment*, 51(37-39):6921–6928, 2013.

[70] Qing Shi, Yanlei Su, Wenjuan Chen, Jinming Peng, Laiyin Nie, Lei Zhang, and Zhongyi Jiang. Grafting short-chain amino acids onto membrane surfaces to resist protein fouling. *Journal of membrane science*, 366(1-2):398–404, 2011.

[71] T Shimomura, M Hirakawa, I Murase, M Sasaki, and T Sano. Preparation of polyacrylonitrile reverse osmosis membrane by plasma treatment. *J. Appl. Polym. Sci*, 38:173–183, 1984.

[72] Rajindar Singh. *Hybrid Membrane Systems for Water Purification: Technology, Systems Design and Operations*. Elsevier, 2006.

[73] MK Sinha and MK Purkait. Preparation of a novel thermo responsive psf membrane, with cross linked pvcl-co-psf copolymer for protein separation and easy cleaning. *RSC Advances*, 5(29):22609–22619, 2015.

[74] Loling Song, EJ Hennink, I Ted Young, and Hans J Tanke. Photobleaching kinetics of fluorescein in quantitative fluorescence microscopy. *Biophysical journal*, 68(6):2588, 1995.

[75] Kvetoslav Spurny, James P Lodge, Evelyn R Frank, and David C Sheesley. Aerosol filtration by means of nuclepore filters: structural and filtration properties. *Environmental Science & Technology*, 3(5):453–464, 1969.

[76] Tim Steinhauer, Sabrina Hanély, Kerstin Bogendörfer, and Ulrich Kulozik. Temperature dependent membrane fouling during filtration of whey and whey proteins. *Journal of Membrane Science*, 492:364–370, 2015.

[77] Tatiane Almeida Drummond Tetzner, Naiara Zoccal Saraiva, Felipe Perecin, Simone Cristina Méo Niciura, Christina Ramires Ferreira, Clara Slade Oliveira, and Joaquim Mansano Garcia. The effects of ovalbumin as a protein source during the in vitro production of bovine embryos. *Revista Brasileira de Zootecnia*, 40(10):2135–2141, 2011.

[78] Bart Van der Bruggen, Leen Braeken, and Carlo Vandecasteele. Evaluation of parameters describing flux decline in nanofiltration of aqueous solutions containing organic compounds. *Desalination*, 147(1-3): 281–288, 2002.

[79] Eric M Vrijenhoek, Seungkwan Hong, and Menachem Elimelech. Influence of membrane surface properties on initial rate of colloidal fouling of reverse osmosis and nanofiltration membranes. *Journal of membrane science*, 188(1):115–128, 2001.

[80] Yao Wang, Zhi Wang, Xianglei Han, Jixiao Wang, and Shichang Wang. Improved flux and anti-biofouling performances of reverse osmosis membrane via surface layer-by-layer assembly. *Journal of Membrane Science*, 2017.

[81] Ya-jie XIE, Hai-yin YU, Shu-yuan WANG, and Zhi-kang XU. Improvement of antifouling characteristics in a bioreactor of polypropylene microporous membrane by the adsorption of tween 20. *Journal of Environmental Sciences*, 19(12):1461–1465, 2007.

[82] Jie Zhao, Qiang Shi, Shifang Luan, Lingjie Song, Huawei Yang, Hengchong Shi, Jing Jin, Xinglin Li, Jinghua Yin, and Paola Stagnaro. Improved biocompatibility and antifouling property of polypropylene nonwoven fabric membrane by surface grafting zwitterionic polymer. *Journal of membrane science*, 369(1): 5–12, 2011.

[83] Xiaoshan Zhu. Micro/nanoporous membrane based gas–water separation in microchannel. *Microsystem technologies*, 15(9):1459–1465, 2009.

[84] Katherine Zodrow, Lena Brunet, Shaily Mahendra, Dong Li, Anna Zhang, Qilin Li, and Pedro JJ Alvarez. Polysulfone ultrafiltration membranes impregnated with silver nanoparticles show improved biofouling resistance and virus removal. *Water research*, 43(3):715–723, 2009.